SCUOLA NORMALE SUPERIORE

Doctoral Thesis

An Eutherian-Specific MicroRNA Controls the Translation of *Satb2* in a Model of Cortical Differentiation

Scuola Normale Superiore di Pisa

PhD in Neuroscience

September 2021

Author: Manuella Mendes Martins

PhD supervisor: Federico Cremisi

"Nothing in life is to be feared, it is only to be understood.
Now is time to understand more, so that we fear less".

Marie Curie

TABLE OF CONTENTS

TABLE OF FIGURE

PRELUDE

The mammalian neocortex is a complex arrangement of neurons organized by a rigorous stratification into six layers (I-VI) following an inside-out mechanism that gives each of these layers specific morphology, physiological properties and local and long-distance axonal projections (Mcconnell, 1995). During mouse corticogenesis, neurons are originated from a common neuronal progenitor called radial glia (RG). Initially, RG cells form the ventricular zone (VZ) (Caviness et al., 1996) and undergo symmetric proliferative divisions in order to expand the progenitor pool. However, around E10.5, these cells start to divide asymmetrically and generate migrating neuronal precursor cells (NPCs) that eventually will give origin to neurons of all cortical layers through direct neurogenesis (Beattie & Hippenmeyer, 2017). Neurons can be generated as well by indirect neurogenesis. Neuronal precursor cells that migrate far from ventricular zone are called RG-derived basal progenitors (BP). BP cells organize themselves in the subventricular zone (SVZ) and then, a subclass called intermediate progenitors (IPs), migrate through the intermediate zone, reach the cortical plate and produce neurons for all the six layers in the neocortex (Greig et al, 2013; Lipin Loo, 2019). Deep pyramidal neurons (DPN) present in layer VI-V extend their projections subcortically while superficial pyramidal neurons (SPN) of layer III-II project intra-cortically and connect the two brain hemispheres through the *Corpus callosum*, which also receives fibers of a sub-population of layer V neurons. The layer IV neurons, receiving extra cortical inputs, are generated after DPN and before SPN formation. This correct organization into layers is due to the crucial role of genes coding for cell identity transcription factors (CITFs) that work regulating the capacity of cortical progenitor cells to produce several neuronal types along corticogenesis (Telley et al., 2019). For each subgroup of cells there are specific CITF. For instance, RGs are characterized by *Sox1, Sox2* and *Pax6*. The BPs present *Neurogenin2* and *Eomesodermin*. In the DPN the CITFs expressed are *Tbr1, Bcl11b* and *Fezf2* and in SPN *Cux1* and *Satb2* are crucial (Greig et al., 2013) (Figure 1A). Due to the fundamental role that these transcription factors exert during neuronal migration and positioning, appropriate regulation of cortical layering is fundamental and any impairment could lead to brain malformations or psychiatric disorders (Sun & Hevner, 2014). However, the mechanisms underlying the timing of activation of CITFs in specific progenitor cells at different developmental times during corticogenesis is still under scrutiny.

INTRODUCTION

THE BRAIN

The brain is composed by several groups of neurons with shared functions – neural pools – working together and integrating the information from input to output areas. With its hundreds of neural pools and trillions of synapses, the brain is the most complex and magnificent structure of the human body. It is capable to perform refined tasks afar from our present understanding. Even when other organs of the body are still healthy and functionally working, if brain activity has ceased, the patient is considered dead.

The development of the human brain is a long process that initiates in the third gestational week (GW) with formation of neural tube, the foundation of the whole central nervous system (CNS) (Stiles & Jernigan, 2010). Proliferation, migration and differentiation of neural progenitor cells together with temporally regulated factors through intrinsic (gene expression) and extrinsic (environmental conditions) features progressively define the fates and characterize specific classes of neurons. Indeed, a very wide range of neurons, each with specific dendritic morphology, local and long-distance axonal, neurotransmitter phenotypes and arrangements of gene expression, constitute the nervous system.

BRAIN STRUCTURES

A well-organized division splits the brain in three parts: the forebrain, midbrain and hindbrain. The forebrain is formed by the cerebrum, thalamus and hypothalamus. In the midbrain is included the tectum and tegmentum. The hindbrain consists of the cerebellum, pons and medulla that together is known as the brainstem. This latter acts as a relay center connecting forebrain and midbrain to the spinal cord, which is the most caudal part of the Central Nervous System (CNS).

The most known structure of the brain is the cerebrum, also called cortex. The human cortex is the largest part of the brain and it is where all cognitive functions, sensory perceptions and consciousness are processed. The cortex can be divided into four different parts accordingly to the functions carried out by them. The frontal lobe is associated with task setting, behavioral/emotional regulation, short-term memory and metacognition. Disorders in the frontal lobe lead to difficulty in carrying out complex behaviors that are appropriate to the circumstances (Purves et al., 2004). The parietal lobe is responsible for controlling different brain functions such as specification of spatial targets for the motor system, the analysis of visual movements

and awareness and, initial perception of somatic sensations. Any disturbance in this part of the brain (Purves et al., 2004) is followed by right-left confusion together with difficulties in writing (agraphia), reading or language related skills (alexia), mathematical problems (dyscalculia) and impaired perception of objects (agnosia). The temporal lobe locates posteriorly to the frontal lobe and inferior to the parietal lobe. It is the place of primary auditory cortex and where the auditory sounds are processed. This region plays key roles in formation of long-term memories, visual recognition, speech comprehension and interpretation of smells and sounds (Abhang et al., 2016). Damages in the temporal lobe are associated, for instance, with impaired auditory and visual perception and long-term memory as well as altered emotional and sexual behavior (Kolb & Wishaw, 1990). Finally, the occipital lobe. This lobe is the major visual processing center in the brain and can be split into primary (V1) and secondary (V2) visual cortex (Ungerleider & Mishkin, 1982). Like neocortex, primary visual cortex is divided into six functionally distinct layers and it is believed that a deep comprehension of this structure could lead to a better understanding of neocortex organization and functions. The V1 receives visual input from the thalamus and processes this information in a spatiotemporal manner controlling orientation, movement, direction and speed. The V2, although less studied than V1, combines V1 actions related to depth, distance, spatial frequency and color but also, responds to more complex tasks (Bull D, 2014).

CORTICAL DEVELOPMENT

The neural tube development concludes with formation of three primary vesicles distributed rostrally: forebrain, midbrain and the hindbrain. The forebrain and hindbrain are splitted into secondary vesicles, respectively, telencephalon/diencephalon and myelencephalon/ metencephalon that eventually generate specific brain structures. The dorsal part of the telencephalon is the main precursor of the cerebral cortex (Agirman et al., 2017). This region encloses a large range of cell types, complexed local and long-distance cortical circuits and is responsible for the remarkable functional capacities (Rakic, 2009) making the study and understanding of the cortex a fundamental and fascinating subject. Furthermore, an abnormal cortical development or any dysfunctions in the cortical network is frequently associated to neurodevelopmental and neuropsychiatric diseases, mostly being still largely misunderstood (lodato & Arlotta, 2015).

EMBRYONIC DEVELOPMENT

In the first stage of development, the cortical primordium is simply formed by a monolayer of neural stem neuroepithelial cells (NECs) (Bayer and Altman, 1991). During cell cycle progression, NECs move their nucleus between the apical and the basal parts of the neuroepithelium to create, by tight junctions, a pseudostratification at the level of the apical domain (Sauer, 1935; Bayer & Altman, 1991; Taverna & Huttner, 2010). Initially, these neuroepithelial cells undergo symmetric self-amplificative divisions, with each division giving origin to two daughter NECs and so, exponentially increasing their number (Miyata et al, 2001). Later, around embryonic day 10 (E10) in the mouse and E33 (gestational week 5 (GW5)) in human cortex, cells start to divide asymmetrically to generate radial glial cells (RGCs) that create the ventricular zone (VZ) of the cortex (Caviness et al., 1996; García-Moreno et al., 2007). RGCs are similar to NECs as both have adherent junctions, an apicobasal polarity that allows them to contact with the ventricular surface and express Nestin, a neural stem cell (NSC) specific marker (Gotz and Huttner, 2005; Fietz and Huttner, 2011; Greig et al., 2013). However, RGCs lose some of their epithelial characteristics to develop specific glial properties such as the loss of tight junctions, the gain of glycogen storage granules and the expression of astroglial genes as brain lipid-binding protein (BLBP) or fatty acid-binding protein 7 (FABP7), astrocyte-specific glutamate transporter (GLAST), and tenascin-C (Campbell and Gotz, 2002). At this stage, one daughter reenters in the cell cycle as an RGC and the other either gets out of the cell cycle or loses contact with the ventricular and basal surfaces to divide again symmetrically as an

intermediate progenitor (IP) cell (Noctor et al., 2004) in a new stratum of dividing cells, the subventricular zone (SVZ) at the basal border of the VZ (Boulder Committee, 1970; Bayer and Altman J, 1991). Actually, the first generated IP cells reside within the VZ dividing symmetrically to produce paired daughter neurons. However, around E13.5 in the mouse, IP cells migrate away from the ventricle and form the SVZ that expands significantly during late corticogenesis (Noctor et al., 2008).

Until recently, RGCs were considered specialized glial cells whose major function was to guide migration of newborn neurons. In 2001, direct evidence obtained by *ex-vivo* experiments showed that RGCs are indeed neuronal precursors with neurogenic capacity and only after embryonic neurogenesis, they shift towards an exclusive generation of astrocytes (Malatesta, Hartfuss and Götz, 2000). Studies performed with RGCs identified the expression of multiple transcription factors, particularly the homeodomain transcription factor Pax6. Pax6 is considered the main marker for radial glia and has demonstrated to be a key regulator for RGC divisions, controlling the switch from symmetric to asymmetric neurogenic divisions (Aaku-Saraste et al., 1996). In this way, RGCs are now seen as the progenitors of most cells in the CNS, with each RGC generating another RGC and an IP cell that will eventually originate neurons, astrocytes or oligodendrocytes. The decision of an apical progenitor to undergo symmetric or asymmetric division correlates in a certain way with the cleavage plane of the apical mitosis. Symmetric divisions are related to division planes perpendicular (vertical cleavage) to the apicobasal axis and asymmetric divisions can have parallel planes (Horizontal cleavage, rarer event) or oblique to the apical-basal axis (Lancaster and Knoblich, 2012). Together with that, the generation of asymmetric fate choices are associated to the inheritance of a larger portion of the apical plasma membrane by one cell, the mother centriole and primary cilia (Wilsch-Brauninger et al., 2012; Das and Storey, 2014). Depending on the partitioning of key cellular components between the two daughter cells, the division can be symmetric or asymmetric.

Progenitor cells in the VZ and SVZ have different morphology, gene expression profiles, microenvironments and neurogenic potentials. The radial glia of the VZ is molecularly characterized by expression of specific transcription factors: Paired box homolog (*Pax6*), Forkhead box protein G1 (*FoxG1*), Lim homeobox 2 (*Lhx2*) and empty spiracles 2 (*Emx2*) (Hanashima et al., 2004; Chou et al., 2013; Suter et al., 2007). The cells in the SVZ, called basal progenitors (BP) instead, are characterized by multipolar shape and lack of radial processes (Smart, 1973). They express distinct transcription factors including neurogenin 2 (*Ngn2*) and its downstream target, t-box 2 (*Tbr2* also known as EOMES), insulinoma-associated protein 1

(*Ism1*), and cut-like homeobox factors 1 and 2 (*Cux1, Cux2*). *Cux1* and *Cux2* are expressed in a subset of dividing cells in the SVZ during the generation of upper-layer neurons and postnatally in some neurons of layers II-IV, suggesting that *Cux* genes might be markers for upper-layer progenitors within the SVZ. Also, *Cux* genes have been fundamental regulators of cell cycle exit of IP cells (Nieto et al., 2004; Englund et al., 2005; Farkas et al., 2008). In the primates, there is an important organization of the SVZ to form a supplementary outer component, the outer subventricular zone (oSVZ), that is not seen in the rodents (Smart et al., 2002). The oSVZ can be defined as an enlargement of the SVZ precursor pool in the primates that could work as an evolutionary mechanism to increase the neuronal output fundamental for building more complexed neocortex and subgranular layers (SGL) (Dehay et al., 1993; Smart et al., 2002). In rodents, the SVZ is only partially self-sustaining and need to receive constant supply of precursors from the VZ (Reznikov et al., 1997; Wu et al., 2005).

CORTICAL LAYERING

The mammalian cerebral cortex develops via a complex sequence of cell proliferation, differentiation, and migration events. In the mouse, cortical progenitors start to produce excitatory projection neurons around E11.5 until birth (P0). The first new-born neurons migrate far from progenitor cells from the ventricular surface, passing through the subventricular zone to get to the intermediate zone (IZ) and start to form the preplate. Neurons born later migrate through the preplate (PP), creating two intermediate layers: the marginal zone (MZ), below the pial surface and subplate (SP), adjacent to the IZ and important to mediate axon targeting during development (Kanold and Shatz, 2006). In the between of these two intermediate layers, the cortical plate (CP) is established. The neurons giving rise to six neocortical layers organize themselves in an *inside-out* manner with early-born neurons populating the deeper neocortical stratum (VI and then, V) and the late-born neurons migrating through the deeper layers to consequentially form the more superficial layers (IV, then II/III) (Loo et al. 2019).

From the moment that post-mitotic neurons have developed their laminar- and neuronal-specific properties, they undergo specific programs to acquire their projection subtype identity. Neuronal specification follows a certain order starting with superficial pyramidal (SP) neurons (*Cajal-Retzius* cells, in the marginal zone, later called layer I of the adult cortex), between E10.5 to E12.5, that are characterized by the horizontal orientation and are thought to be fundamental for the establishment of neuronal patterning in the CP (Angevine, J. B. Jr & Sidman, R. L., 1961).

Besides, they express Reelin (*Reln*), transcription factor T-box brain 1 (*Tbr1*) and neuronal migration protein Doublecortin (*Dcx*) (Boyle MP et al., 2011). As development progresses, corticofugal neurons (CFuPN) appear around E11.5 to E14.5 and can be subdivided in corticothalamic (CT) (layer VI, adjacent to the VZ) and subcerebral projection neurons (SCPN) (layer V) depending where they project subcortically. The Chicken ovalbumin upstream promoter transcription factor-interacting protein 2 (*Ctip2* also known as *Bcl11b*) and the zinc finger transcription factor 2 (*Fezf2*) are the key determinants of subcerebral projection specification in layer V (Leone et al., 2008). Corticogenesis is concluded with layer II-IV. Upper layers are characterized by callosal projection neurons (CPN) that extend their axons only within the cortex (Molyneaux et al., 2007). The pyramidal neurons that are present in these layers are functionally identified by the specific expression of *Cux1, Lhx2* and special AT-rich sequence binding protein 2 (*Satb2*) that regulate the formation of *Corpus callosum* by controlling spine morphology and maturation as well as synapse formation (Yang H et al., 2019). Indeed, Alcamo and colleagues (Alcamo et al. 2008) identified *Satb2* as the gene required for the formation of callosal projection neurons and showed that in its absence layer III-II, projection neurons extend their axons toward subcortical targets. Furthermore, studies have been demonstrating that *Satb2* mutation causes severe cognitive impairments in human and leads to a syndrome called *Satb2*-mutation associated syndrome (SAS) (Lee et al., 2016). More recently, Zhang et al., has shown strong behavior effects of *Satb2* ablation in mice (Zhang et al., 2019). Other key transcription factors such as *Sox5*, *Fezf2* and *Cux1* have been associated with developmental and language delays, intellectual disability, schizophrenia and autism spectrum disorders (Rosenfeld et al., 2009 and 2010; Potkin et al, 2009; Lamb et al., 2012; Parmeggiani et al., 2018; Platzer et al, 2018).

It is worth noting that this class of genes, known as cell identity transcription factors (CITFs), are not only fundamental for specifying the fate of neurons in a precise cortical layer. They are also able to regulate the expression of other transcription factors that in turn control cortical layering formation. For instance, *Tbr1* (similarly to *Sox5*) specifies a corticothalamic neuronal fate for layer VI (Hevner RF et al., 2001; Han et al., 2011) while repressing the expression of *Fezf2*, that in its turn is specific for subcerebral layer V identity (Chen B et al., 2005; Molyneaux BJ et al., 2005). It is important to notice that this repression is mutual as Fezf2 is able to inhibit *Tbr1* as well. Interestingly, the loss of *Fezf2* in mice cortices is followed by the loss of *Bcl11b* expression (Chen et al., 2005; Molyneaux et al., 2005); nonetheless the opposite has not been seen. *Fezf2* acts upstream of *Bcl11b* and so, it is the main regulator of subcerebral

projections. *Fezf2* acts also on the upper layer specification by repressing *Satb2* expression and blockade of CPN formation. Finally, in layer II-IV callosal neurons, *Satb2* prevents the expression of *Bcl11b* that, in turn, represses *Tbr1* expression in layer V, concluding the negative feedback loop (Dennis, DJ et al., 2017).

As described before, these transcription factors are related to neuronal migration and positioning. Therefore, any problems in the formation and organization of a normal and functional cortical circuitry might lead to defects and not only, change the neuronal identity of cortical neurons but most importantly, become key players in the spectrum of cognitive and motor neurodevelopmental disorders.

UPPER LAYER NEURONS

The mammalian neocortex is a fascinating, well-organized structure in which different neuronal phenotypes are separated into different layers. Neurons located at the same layer are generated at similar period during development but among layers, the time of generation may vary within days to a point that, in higher mammals, the moment of the final mitotic division of a neuron can determine its eventual laminar position. Besides, each one of the six cortical layers present different characteristics in what concerns morphology, physiological properties and arrangements of long-distance axonal projections. All these factors can lead to the thought that the fate identity of a young cortical neuron could have been stated earlier on its development, even before its migration out of the ventricular zone into the cortical plate (McConnell SK, 1990; Frantz G and McConnell SK, 1996; Tosches and Laurent, 2019).

The initial idea was that mitotic cells of the neocortical VZ were the single source of all cortical neurons while the SVZ was the source of glial cells only (Levison and Goldman, 1993).

Studies in the beginning of this century, using time-lapse confocal microscopy were able to identify GFP-labelled mitotic progenitors in the VZ and SVZ and track these progenitors to check the final destination of their daughter cells. In the early stages of corticogenesis, as I discussed previously, the cells within the VZ divide mostly symmetrically to increase the progenitor pool. However, as neurogenesis starts, most cell divisions in the VZ are asymmetric. At mid to late stages of neurogenesis, even though the cell divisions are still asymmetric, the daughter cell that exits the VZ moves to the SVZ and becomes a transit amplifying cell, performing symmetric neurogenic divisions and these divisions are, probably, the main

responsible for producing the neurons that eventually migrate into the upper layers (Sidman LR & Rakic Pasko 1973; Smart et al., 2002; Noctor et al., 2004; Noctor et al., 2008).

Even though the study of cortex development has been growing in the last decades and a lot more is known about how the cortex and its layers are formed, studies have been focusing on the mechanisms that produce different subtypes of subcortical projection neurons in the deep-layers (DL). The knowledge about how the subtypes of neurons that settle on the upper-layers (UL) are formed is still very limited.

The cortical UL, which are unique to Class Mammalia, are mainly involved in cortico-cortical connectivity and include homotopic and heterotopic callosal projections to the contralateral hemisphere, probably underlying the greater cognitive abilities of mammals (Marín-Padilla, 1992; Hill and Walsh, 2005), while DL neurons target various subcortical structures (Luzzati 2015; Shepherd 2011, Greig et al., 2013). The enlargement of cortical surface in primates arises in parallel with the expansion of the supragranular layers (II-III) and, impairments in these specific layers II and III lead to epilepsy, due to failure in neural migration (Ferland et al., 2009) and cognitive disorders such as schizophrenia (Rajkowska et al., 1998).

The regulation of upper layer neurons is mostly controlled by the expression of *Satb2*, *POU* domain and *Cut* domain transcription factors. Some of the genes that are part of the *Cut* domain, such as *Cux1* and *Cux2* seem to be present in all UL neurons, while *Satb2* is expressed only in a subgroup of UL cells.

POU-homeobox-domain-containing octamer-binding transcription factors *Pou3f3* and *Pou3f2* (also known as *Brain-1* and *Brain-2*, respectively) are members of the class III POU (Pit1-Oct1/Oct2-UNC86) domain transcription factors and are preferentially expressed in layer II-III and V of the mature neocortex (Hagino-Yamagishi K et al.,1997). *Brain-1* and *Brain-2* are deeply associated to cortical neural migration, upper-layer production and neurogenesis. One of the first studies of these genes established that their absence in the cortex by knockout leads to cortex laminar inversion (McEvilly et al., 2002). A more recent study has shown that *Brn1/2* are essential for producing cortical neurons of the upper layers. In this study, by *in utero* electroporation, researchers were able to knockout *Brn1/2* in a subset of cells in a temporally controllable manner (*Brn2-EnR*, Brn DNA-binding domain fused with the repressor domain of Drosophila engrailed). It was demonstrated that when *Brn1/2* transcription is suppressed, neural differentiation and migration is hazarded around E12.5 and neurogenesis is lost after E13.5, period when upper-layer neurons start to appear. Instead, *Satb2* is fundamental for radial

migration (Britanova et al., 2008) and it is able, almost completely, to rescue the phenotype associated with *Brn2-EnR*. Thus, it has been hypothesized that *Pou3f/Satb2* pathway could be the main regulator of upper-layer specification (Dominguez et al., 2013).

The homeodomain genes *Cux1* and *Cux2*, also known as Cut/Cux/CDP family members, have four DNA-binding domains, including the cut homeodomain (Nepveu, 2001). Both genes are homologues of the *Drosophila Cut* gene and have similar protein structures and transcriptional suppressor activity. *Cux1* expression is more extensive as it is expressed not only in the brain but in all major internal organs except liver, while *Cux2* is mainly expressed in the nervous system (Quaggin SE et al., 1996). *Cux1* acts as a key regulator of the cell cycle; however, the functions of *Cux2* are not yet totally clear. Only recently, it has been demonstrated that *Lhx2* selectively reacts with *Cux2* and activates its expression in upper layer cortical post-mitotic neurons *in vitro* (Yang H et al., 2019), thus suggesting a role in the formation of synapses and dendrites of cortical neurons. Furthermore, *Cux1* and *Cux2* may have complementary functions as *Cux1* gene is associated with proliferation while *Cux2* is related to specification and differentiation, as it is expressed by mature UL neurons (Zimmer C et al., 2004).

SATB2

Gene expression control is profoundly influenced by chromatin structural conformation and, specific genomic DNA segments that present high affinity to the nuclear matrix play a key role in spatial chromatin organization. These regions are known as scaffold or matrix attachment regions (SARs or MARs) and have been hypothesized to arrange the base of chromosomal loops, thus establishing the typical chromatin loop structure in both interphase nuclei and metaphase chromosomes (Gasser and Laemmli, 1987). This chromatin loop-domain structure is not only fundamental to compact genomic DNA, but it might be important from a biological point of view, in particular in establishing and maintaining tissue-specific patterns of gene expression (Scheuermann RH and Garrard WT 1999; FitzPatrick DR et al. 2003).

AT-rich DNA sequences are very closely related with the nuclear matrix or scaffold and are the main regions of SAR/MAR DNA. Therefore, these sequences are of crucial importance as they give origin to the proteins that are key mechanisms for gene regulation by being implicated in transcription, replication, repair and recombination. The specific proteins that interact with and bind to MAR sequences, MAR-binding proteins (MARBP), in neural cells include Cux/CDP, SAF-A, Bright, SATB1 and SATB2 (Dickinson, L. A, 1992)

The special AT-rich binding protein (SATB) family proteins have been identified as crucial regulators of gene expression because, unlike classical transcription factors that bind to one target gene to regulate transcription, SATB family binds to several sites where chromatin is tethering to form loop domains. Therefore, this family of genes are able to control the transcription potential of many genes simultaneously (Alvarez et al., 2000). Studies have demonstrated that *Satb1* gene is crucial for a large range of biological events such as immune system diseases, X Chromosome inactivation (Agrelo R et al. 2009), T cell development and differentiation (Gottimukkala KP et al., 2016), hematopoiesis (Satoh Y et al., 2013), WNT signaling (Notani D et al., 2010) and neural development (Balamotis MA, 2012). The closest homologue of *Satb1, Satb2,* has been identified as part of the chromatin organized family and is involved, as *Satb1,* in transcriptional control and chromatin remodeling (De Belle et al., 1998)

SATB2 was first isolated from a human fetal brain library as part of the Human Unidentified Gene-Encoded (HUGE) project and initially identified as KIAA1034. It is an 82.5KDa protein with 733 amino acids and it is located in a gene-poor region (low GC-content region) across the long arm of chromosome 2 (2q32-2q33). The *Satb2* transcription unit lengths 195.6 kb of genomic DNA (chr2:200,134,223-200,329,831 hg19) with a curiously high conservation in primary sequence along vertebrate evolution (Sheehan-Rooney K et al., 2010) and an open reading frame starting in exon 2 with its first stop codon in exon 11 (FitzPatrick DR et at., 2003, Dobreva et al., 2003). The two proteins of SATB protein family are structurally very similar to each other as both present two CUT domains upstream of the homeodomain that help to increase DNA binding affinity and a Pfam-B_10016 domain, necessary for functional dimers formation, which is ~81% conserved between the two proteins (Harada R et al., 1994; Bürglin TR et al., 2002; Bürglin TR 2011).

In the skeleton formation process, *Satb2* is expressed by neural crest-derived cell progenitors and appears fundamental for the craniofacial patterning and bone formation (Dobreva et al., 2006). The expression of Satb2 in neural crests appears the most evolutionary conserved, as it is common to vertebrates (Nomura et al., 2018; Sheehan-Rooney et al., 2010). In what concerns the central nervous system, while *Satb1* is expressed in different regions of the brain, *Satb2* expression is restricted to subgroups of post mitotic cortical neurons projecting across the *Corpus callosum* to the contralateral hemisphere (Molyneaux et al., 2007). *Satb2* is also important for subcortical projection neurons formation (McKenna et al., 2015) and more recently, it has been stated its role in the differentiation of a subclass of spinal interneurons (Hilde et al, 2016). Finally, Satb2 is expressed also in other pallial (dorsal telencephalon) regions:

Hippocampal layers (Cipriani et al., 2017; Huang et al., 2013) and entorhinal cortex layers (Y. Liu et al., 2021).

As it was described previously, two of the most important markers for subcerebral neurons of layer V are B-cell leukaemia/lymphoma 11B (*Bcl11b*, also called *Ctip2*) (Arlotta et al. 2005; Molyneaux et al. 2005) and *Fezf2*, which is expressed in the VZ before and during the development but in post-mitotic neurons have its expression restricted to layer V and VI. The layers of the cortex, as I have been discussing, have a time-based organization which leads to the *inside-out* arrangement of projection neurons, where the first neurons to be formed are located close to the ventricular zone in the deep layers and the youngest neurons are close to the superficial layers, away from the ventricular zone. This means that there are mechanism controlling the production of neurons of a specific layer at a specific time and at the same time, inhibiting the expression of neurons from another layers.

SATB2 interacts with proto-oncogene *Ski* and the nucleosome remodeling deacetylase (NuRD) complex that includes histone deacetylases HDAC1 and MTA2 (Baranek et al. 2012). This multi-protein complex allows *Satb2* to bind to the MAR sequences (Dobreva et al., 2003) in the *locus* of the deeper layer transcription factor *Bcl11b*, deacetylating it, modifying the chromatin and repressing its expression directly (Alcamo et al., 2008). While inhibiting corticospinal motor neurons fate, *Satb2* supports the specification of corticocortical neuronal identity in the developing neocortex (Britanova et al., 2005; Alcamo et al. 2008; Britanova et al. 2008). Interestingly, at early postnatal stages, the number of $BCL11B^{+}/SATB2^{+}$ double positive cells (C/S+) increase in the cortical area related to touch sense information, the somatosensory cortex (layer IV). This event occurs due to another protein called Lmo4, a transcriptional adapter, that competes with *Satb2* for the binding to NuRD complex through Hdac1 histone. In this situation, *Satb2* is not able to repress *Bcl11b* expression and at layer IV, they are co-expressed, creating two subtypes of neurons that extend projections to different areas of the brain: brainstem in deeper layer IV and contralateral cortex at upper layer IV (Harb et al., 2016).

Satb2 gene is well conserved in the vertebrates where exerts a fundamental role in the facial and secondary palate formation (Sheehan-Rooney K et al., 2010). As I have been discussing before, it is also a key regulator for the formation of the neocortex. More specifically, *Satb2* is expressed in the dorsal telencephalon, also known as *pallium*, not only in humans but also in other amniotes (reptiles and birds), with each species having their own regulatory mechanisms through the same signaling molecules (e.g., *Pax6, Tle4, Bcl11b* and *Satb2*) and

subdivided in homologous embryonic regions (Cárdenas and Borrell 2019; Tosches and Laurent, 2019). It is probable that, these different regulatory interactions among those transcriptional factors help the homologous embryonic structures to acquire different morphologies and connections in the amniotes adult brain; while reptiles and birds develop the dorsal ventricular ridge (DVR), mammals acquire a six-layered neocortex (Striedter and Beydler 1997; Tosches et al. 2018). Even though mammalians, reptiles and birds express *Satb2*, another massive difference between mammals and other vertebrates is the *Corpus callosum*. The *Corpus callosum* is an eutherian-specific brain structure crucial for the higher-order neurological functions characteristic of the higher mammals (Kamnasaran D, 2009).

The conditional knockout for *Satb2* reduces the expression of specific markers for layer IV, such as RORβ (Takeuchi et al., 2007) and serotonin transporter (5-HTT), at P0 and leads to a complete absence at P15. Besides, the lack of *Satb2* leads to the destruction of the boundaries at layer IV established by thalamocortical projection axons associated to sensory information. In this condition, thalamocortical projection axons are spread all over layer IV (Ding et al., 2003) compromising the communication between cortex and thalamus structures. In this model, *Bcl11b* not only showed increased expression in layer V but also, its expression was extended into upper layers II-III. The same increased expression was observed with *Tle4*, a marker for deep layer VI (Chen B et al., 2005; Alcamo et al., 2008; Arlotta et al., 2005; Zhang Q et al., 2019). Finally, *Sox5* is highly expressed in layer VI and at lower levels in layer V. Studies have showed that *Sox5* knockout decreased the expression of *Bcl11b* and subcerebral neurons. Interestingly, the conditional knockout for *Satb2* decreases *Sox5* levels. Therefore, in some complex way, *Satb2* regulates *Sox5* and *Bcl11b*, controlling the development of subcerebral neurons (McKenna et al., 2015). Targeted inactivation of *Satb2* leads to deregulation of 30% of genes related to layer specificity (deep and upper layers) and axon guidance receptors (Alcamo et al., 2008).

Although much is known about *Satb2*-mediated control over corticogenesis, the studies to understand how *Satb2* expression itself is controlled are very limited. In what concerns corticogenesis, there is a mutual regulation between *Fezf2* and *Satb2* (Chen B et al., 2008; McKenna et al., 2015). Satb2 is responsible for the activation of *Fezf2* through the binding of *Satb2* to *Fezf2* highly conserved enhancer "434" at the 3' end of this gene (Eckler et al., 2014), that in turn activates *Bcl11b* and forms the layer V neurons. At the same time, the activation of *Fezf2* represses the high levels of expression of *Satb2* in layer V so that *Bcl11b* is generated in these cells. Actually, the first *Bcl11b*$^+$ deep-layer neurons, generated around E13.5, express *Satb2* mRNA (Britanova et al., 2008) but at E15.5 two different populations of post-mitotic cells, one

BCL11B-positive and the other SATB2-positive, are present in the mantle zone. Nonetheless, the mechanisms controlling SATB2 translation in one of the two populations are still under scrutiny.

MICRORNA (miRNA)

In Metazoans, there are several types of small endogenous RNA molecules: ribosomal RNA (rRNA), small nuclear RNA (snoRNA), small transfer RNA (tRNA), small interfering RNA (siRNA) and micro RNA (miRNA). siRNAs and miRNAs are almost identical in what regard function and biochemical properties distinguishable only in their origin. SiRNAs are specific of plants and are derived from long double-stranded RNA (dsRNA) while microRNAs are present in animals and are generated by double-stranded regions of ~65 nucleotides RNA hairpin precursors (Ambros V et al., 2003; Kim V et al, 2005).

MicroRNAs (miRNAs) are a huge family of small (around 21 nucleotide-long) single-stranded non-coding RNAs, often evolutionary conserved among distant species, that have been classified as important post-transcriptional regulators of gene expression, binding to the 3' untranslated region (UTR) of a target mRNA and repressing their translation (H. Guo et al., 2010).

It is predicted that miRNAs represent 1-5% of the human genome and regulate at least 30% of protein-coding genes (MacFarlane & R. Murphy, 2010). To this date has been estimated the discovery of ~ 2300 human mature microRNAs with 1115 being annotated in miRBASE V22 (Julia Alles et al., 2019). These small sequences have crucial function in several developmental and cellular processes. In eukaryotic species, such as vertebrate neural development (Krol et al., 2010; Chekulaeva et al., 2009;) they play a key role in controlling genes implicating in neocortical development (Cremisi F, 2013) as well as adult neural functions pathways.

The first microRNA to be discovered was *lin-4* (1993) that initially had been characterized as regulator of temporal development in *C. elegans* larvae. Ambros and Ruvkun groups observed that a mutation in *lin-4* would give an opposite effect on another gene, *lin-14.* Later, they revealed that *lin-4*, actually, is a small non-coding RNA and that its sequence is able to bind to *lin-14* gene through its 3'UTR, thus, controlling and regulating *lin-14* at post-transcriptional level (Horvitz HR et al., 1980; Chalfie M et al., 1981; Ambros V et al., 1987; Lee R et al., 2004). Notably, *lin-4* mutation causes a heterochronic development phenotype, suggesting since the beginning of their discovery that miRNAs are involved in regulating the timing of developmental process.

MicroRNA biogenesis begins with pri-miRNAs generation from DNA sequences by RNA polymerase II that transcribes these immature nuclear precursors. Nearly half of the human

microRNAs that have been identified are found in intergenic regions of the genome, and in those cases, miRNAs are transcribed as unique primary transcripts known as clusters, comprising multiple stem-loop structures under the control of independent promoter elements but that will generate very similar microRNAs. Otherwise, microRNAs are located in annotated intronic regions of protein coding genes, although few numbers are found within exons. In this case, they are transcribed autonomously as a specific gene and regulated by their own promoters. MiR-17-92 cluster contain one of the most known group of miRNAs expressed in developing neocortex and it is a type of miRNA-containing gene transcribed from an intragenic region. (Rodriguez A et al., 2004; Kim YK et al., 2007; Hinske LCG et al., 2010; 2013; de Rie D et al., 2017).

After the initial step of transcription, a nuclear complex of proteins called microprocessor complex processes the newly-transcribed pri-miRNA. In this complex, there is a RNA binding protein encoded by Di George Syndrome Critical Region gene 8 (DGCR8), that identifies an N6-methyladenylated GGAC together with other motifs within the pri-miRNA and a ribonuclease III enzyme, called Drosha that cleaves the pri-miRNA to give origin to a stem-loop structure of 60-100 base pair long, known as pre-miRNA (Lee et al., 2003; Denli AM et al., 2004; Han J et al., 2004). Following that, the exportin 5-Ran GTPase (XPO5/RanGTP) system helps pre-miRNAs to move to the cytoplasm where the mature miRNAs are synthetized by RNAse III-like ribonuclease protein called Dicer that removes the terminal loop, leading to the duplex mature miRNA. At this point, only one strand, generally, of the mature miRNA, binds to RNA-induced silencing complex (RISC) in an ATP-dependent manner. Depending on the directionality of the miRNA strand that has been chosen, miRNAs have different names: 3p strand if the 3' end of the pre-miRNA hairpin is chosen and 5p strand if this end is the chosen one instead. The other strand, the passenger strand, is usually released and degraded.

The RIS-Complex is formed by RNA binding proteins of the Argonaute family (AGO1-4) and when it binds to a miRNA, becomes miRNA-induced silencing complex (miRISC). This complex consists of the guide strand and AGO proteins ready to interact with target mRNAs (Denli AM et al., 2004; Okada C et al., 2009) exerting their post-transcriptional effect by destabilization of target mRNA (mRNA deadenylation and decapping) or its translational repression. Structurally, the contact between miRNA and mRNA happens by the seed region of the miRNA that consists in 6 to 8 nucleotides at its 5' end and any region of the target mRNA, that may be at its 3' or 5' UTR or its coding region. Instead, miRNA interaction with promoter region seems to induce transcription (Y. Zhang et al., 2014).

MIRNAS AND NEURAL DEVELOPMENT

The capacity to isolate the mRNA/miRNA/RISC complex, miRISC, by immunoprecipitation of AGO protein allowed to globally evaluate families of mRNAs and miRNAs involved in specific biological processes. For instance, the concerted de-repression of a number of chromatin remodelers from a family of pluripotency-specific miRNAs was shown to control the passage from ground-state pluripotency to epiblast pre-differentiation state of the early mouse embryo (Pandolfini et al., 2016). More recently, miRISC analysis allowed the characterization of many candidate miRNA-mRNA networks regulating cortical expansion and layering (Nowakowski et al., 2018).

As it was described previously, Dicer1 enzyme synthetizes mature microRNAs. Thus, the majority of studies on miRNA function in vertebrate development have been initially performed by targeting its crucial function in miRNA biogenesis. The impossibility to produce homozygous *Dicer1*-null ES cells shows that loss of Dicer could affect stem cell pools at early stages of embryogenesis (Bernstein et al., 2003; Murchison et al., 2005). This was, in part, explained by *Oct4* expression, which, in normal mammalian embryos maintains the proliferation of cells in the inner cell mass of the blastocyst and epiblast. Instead, its loss in blastocysts leads to premature differentiation of stem cells and lethality (Avilion et al., 2003). The same lethality that is observed around embryonic day 7.5 in *Dicer* mutant mice while, mice embryos hypomorphic for *Dicer* present a delayed phenotype surviving until embryonic day 13 (W. J. Yang et al., 2005). Also, it has been proved that ES cells from Dicer-deficient mouse cultivated *in vitro* are defective in differentiation (Kanellopoulou et al., 2005).

In *Xenopus laevis*, *Dicer* inactivation affects cell cycle progression, survival and timing of retinal cells generation consequently, stressing the importance of miRNAs maturation by *Dicer* for normal neural and retinal development (Decembrini S et al., 2008).

In order to better understand Dicer effects during corticogenesis *in vivo*, researchers use conditional knockout (CKO) mice model. This model is produced by breeding Dicer:lox/lox mice with several forebrain Cre-driver mouse strains, such as Emx1:Cre, FoxG1:Cre or Nestin:Cre (see Cremisi F, 2013, for a review). Studies performed with FoxG1:Cre mice embryos CKO, show that *Nestin*, *Sox9* and *ErbB2*, markers for proliferating neural progenitor cells, present abnormally low expression levels. Instead, Reelin, Doublecortin and Rnd2 were increased. In these conditions, progenitor cells are not confined to the VZ and SVZ and could be found spread all over the cortex, leading to an irregular arrangement of dorsal telencephalon (Nowakowski et

al., 2011). Interestingly, Tonelli et al demonstrated that Dicer ablation using Emx1:Cre CKO mice did not affect neuroepithelial cells that were still able to keep proliferating normally. However, committed progenitors together with mature neurons were the most affected by miRNA depletion probably because the gene profiling is different and these cells are more dependent on miRNA-mediated regulation in respect to uncommitted cells (De Pietri Tonelli et al., 2008). Beverly Davidson group, stated altered kinetics in the cell cycle at E15.5 using Nestin:Cre CKO mice and confirmed the low expression of progenitor cells, demonstrated by Nowakowski et al, 2011, in absence of Dicer by showing the increasing of activated Caspase3 at the same developmental time (McLoughlin et al., 2012).

As a result of these data, one could think that cortex layer formation is orchestrated by miRNAs. They could act on the 3'UTR of transcriptional factors regulators of corticogenesis (De Pietri Tonelli et al., 2008; Volvert ML et al., 2012) and organize the *inside-out* fashion characteristic of cortex and that is associated to higher cognitive functions unique to primates.

Embryonic neurogenesis is a period when many miRNAs are enriched (Barca-Mayo and De Pietri Tonelli, 2014; Lv et al., 2014; Miska et al., 2004; Nielsen et al., 2009; Yao et al., 2012) and because the main goal of this thesis is to understand the mechanisms that control *Satb2* during corticogenesis, I am going to focus on this time window. The miRNAs mostly present during corticogenesis can be classified in four different categories:

1) miRNAs that are unceasingly expressed during development such as miRNAs part of the let-7 family;
2) miRNAs that are expressed during a specific short time window during development;
3) miRNAs that are mostly expressed in early stages of development with the expression decreasing throughout time or around perinatal stage as miR-17-92 cluster members;
4) miRNAs that start to be expressed at late stages of development and keep their expression high post-natal.

Studies have been demonstrating the key role of miRNAs during neural development since individual miRNAs or families of miRNAs were shown to regulate gene expression in specific steps of neurogenesis, specific neuronal cell types or even particular regions of a cell. (Stappert et al., 2015; Coolen and Bally-Cuif, 2009; Fineberg et al., 2009; Bian and Sun, 2011). Moreover, miRNAs may work as a protective or a disease promoter agent, accordingly to the

context they are in, being, therefore, possible therapeutic targets for neurodevelopmental disorders.

The first example of a miRNA regulating neural development is miR-430, which was found to orchestrate neural induction in zebrafish by repressing a set of maternal transcripts (Giraldez et al., 2006). Since this original discovery, many miRNAs have been found to target specific mRNAs involved in neurogenetic processes.

In order to start neurogenesis, stem cells must lose their pluripotent characteristics. Numerous evidences indicate a key role for SMAD signaling during neural induction and, because Activin/TGFβ and BMP signaling present SMAD proteins as their main signal-transduction molecules, these pathways have to be silenced (Chambers et al., 2009). This blockade is achieved by miR-125a/b and miR-135b that promote neural induction by targeting receptors and SMAD signal transduction components and consequently, BMP and TGFβ signaling cascades (Boissart et al., 2012; Bhinge et al., 2014). *Oct4*, as mentioned before, is an important gene for pluripotency and, together with *Klf4* and *Sox2*, keep the pluripotency state of undifferentiated hES. These genes interact with miR-145 playing a mutual negative feedback loop where they are upregulated, repressing miR-145.

As differentiation starts, miR-145 is upregulated and blocks their expression (Xu et al., 2009). The same mechanism happens between let7-miRNA and Lin28A and Lin28B. Let-7 miRNA is encoded by the *Lethal-7* gene e plays central roles in proliferation of NSCs/NPCs and in the control of neurogenesis (Zhao et al., 2010), promoting it. Thus, in neural progenitor cells mature let-7 acts downregulating Lin28 and in ES cells Lin28, in turn, is upregulated and represses let-7 expression (Guo et al., 2006; Rehfeld et al., 2015).

Interestingly, there are microRNAs that work on the exact opposite side of the coin, blocking neural induction by targeting inhibitors of pluripotency. MiR-96 is one of those microRNAs, which by targeting the transcription factor PAX6, keeps the pluripotent state of stem cells. The same pattern of action happens with miR-371 and miR-302/607, with these last two not only de-repressing BMP pathway, but also repressing NR2F2, a pro-neural transcriptional factor (Rosa & Brivanlou, 2011).

After the initial step of inducing neural fate, in order to achieve a functionally and morphologically well-structured cortex, it is fundamental that neural stem cell (NSC) expansion and their transition to intermediate progenitors (IPs) are closely regulated. MiRNAs such as miR-

134 and miR-184 are crucial for neural progenitor maintenance and proliferation (Bian et al., 2013) while, miR-124, miR-125b, miR-137, let-7 and miR-9 promote neural differentiation. Among these, miR-124 and miR-9 are two of the most enriched miRNAs in the brain (Coolen & Bally-Cuif, 2009) and, by interacting with gene regulatory complexes, are able to induce neuronal differentiation (Stappert et al., 2015).

Lim et al. demonstrated, with a paper published in Nature in 2005, that overexpression of miR-124 in Hela cells was enough to change their morphology and become similar to neuronal cells (Lim et al., 2005). Later, Yoo et al., that also published in Nature, show that overexpression of miR-124, miR-9 and its passenger strand miR-9* in human fibroblasts induces their conversion into neurons, a process mediated by NEUROD2 (Yoo et al., 2011).

MiR-124 and miR-9/9* crucial importance might be due to their interaction with BAF53 and PTBP complexes. BAF53a and PTBP1 are present in neural progenitors and, by the expression of these two microRNAs, BAF53a and PTBP1 are downregulated to allow the upregulation of their respective counterparts, BAF53b and PTBP2 that promote the activation of neuron differentiation programs (Visvanathan et al., 2007; Yoo et al., 2009). Moreover, both miR-124 and miR-9 target several components of Notch signaling cascade, which is a fundamental pathway for neuronal progenitors' expansion and neuronal development. MiR-124 targets *Jag1*, the Notch ligand, and *Sox9*, Notch downstream effector. Instead, miR-9, controls *Hes* family members, and appears to rely its levels on Notch signaling expression (Coolen & Bally-Cuif, 2009; Stappert et al., 2015)

Vertebrate neural induction was first discovered in amphibians, using *Xenopus Laevis* animal model, with the dorsal region of the ectoderm germ layer giving origin to neuroectoderm (De Robertis & Kuroda, 2004). Eventually, the neuroectoderm, accordingly to anteroposterior (AP) patterning, regionalizes into four domains: forebrain, midbrain, hindbrain and spinal cord (Lupo et al., 2014). In addition, dorsoventrally (DV) patterning separates progenitor domains to form, in the telencephalon, the pallium and the basal ganglia (Wilson & Rubenstein, 2000).

Several classical studies have been elucidating the genetic mechanisms that control the regionalization of the telencephalon. More recent findings have highlighted the importance of miRNAs in controlling and refining the interactions between different growth factor signaling pathways during brain patterning.

MIRNAS IN CENTRAL NERVOUS SYSTEM PATTERNING

To better focus the role of distinct miRNAs in neural patterning, a short summary of the signaling pathways interacting in early neural development is required. According to their position within AP and DV coordinates, early embryonic neural cells are subject to the Wingless integrated-1 (Wnt) signaling, Bone morphogenetic protein (Bmp), Fibroblast growth factor (FGF), Activin/Nodal and Sonic Hedgehog (Shh) signaling pathways (Shimogori et al., 2004). These signaling pathways have been classified as the main drivers for ES cell neurogenesis (Le Dréau and Martí, 2012), giving origin to many distinct neuronal subtypes with diverse neurotransmitter phenotypes, functions and projection targets. Therefore, the uniqueness of neuronal cell types depends on the precise spatio-temporal activation of distinct signaling pathways, exerting the expression of specific transcription factors together with gene expression regulators, such as miRNAs, which in turn control the presence of cell fate determinants in a spatial and temporal manner (Inui et al., 2010; Stappert et al., 2015).

The *activation/transformation* model of Nieuwkoop proposes that neuralizing signals from gastrula mesoderm induce embryonic ectoderm to form neural tissue that, by default, initially has an anterior identity (*activation*). Later, the *transformation* step occurs with this anterior neural tissue being posteriorized possibly due to AP morphogen gradients. This process is called caudalization (Kiecker and Niehrs, 2001).

Wnt and Bmp, important for neuronal progenitor self-renewal, increase their expression gradient in the neural tube throughout the AP axis, thus inhibition of these signaling at early stages of development is essential for the specification of the forebrain (Bertacchi et al., 2013, 2015). Indeed, by inhibiting Wnt, the levels of FoxG1/Pax6 double positive cells that express also Emx1 (marker for the dorsal cortex) increase (Houart et al., 2002; Muzio et al., 2002; Watanabe et al., 2005). On the other hand, in the ventricular walls of the emerging telencephalon, mir-7a presents an expression gradient contrary to Pax6, which constrains the expression of Pax6 protein to the dorsal forebrain and increased dopaminergic neurons in the olfactory bulb (De Chevigny et al., 2012). Besides, human stem cell differentiation into dopaminergic neurons is compromised by the inhibition of miR-181a and miR-125b (Stappert et al., 2015). The inhibition of Bmp is also fundamental for rostral forebrain fate (Bertacchi et al., 2013). However, BMP inhibition by itself is not enough to induce a neural pathway (Bertrand et al., 2003). Another signaling factor, FGF, is crucial for Chordin and Noggin expression in *Xenopus Laevis*, two genes whose deficiency in mice, lead to head nearly absent (Lupo et al., 2002).

Wnts, FGFs and BMPs are crucial for cortical patterning (Rubenstein, 2011) however, the mechanisms by which they exert their roles in the generation of several neuronal fates are not completely clear yet. A possible convergent point for several neurogenic miRNAs is TLX, a known upstream activator of Wnt signaling pathway (Qu et al., 2010). Wnt and FGF activate cyclin D1 gene, which is crucial for cell cycle and its overexpression it is known to lead to tumors although in the brain, seems to facilitate neurogenesis in a cell cycle-independent manner (Lukaszewicz and Anderson et al., 2011). The activation of Wnt and FGF pathways shortens progenitors' cell cycle, promoting proliferation, expansion of apical progenitors and decreased generation of basal progenitors (Salomoni & Calegari, 2010). In the literature, it has been demonstrated that *Let-7b* represses *Tlx* mRNA consequently, inhibiting *cyclin D1* mRNA translation (Zhao et al., 2010). Wnt seems to be modulated by other different microRNAs such as, mir-137 that inhibits histone-specific demethylase I (LSD1), a *Tlx* transcriptional co-repressor (Yokoyama e al., 2008) and miR-15b that inhibits Tet methylcytosine dioxygenase 3 (*Tet3*) mRNA translation which works on the methylation of cyclin D1 promoter and so, inhibits indirectly cyclin D1 expression (Lv et al., 2014).

MIRNAS IN CORTICOGENESIS

Some miRNAs regulating cell identity of cortical neurons were isolated. The differential expression of miRNA in glutamatergic neurons and GABAergic interneurons co-expressing either parvalbumin (PV) or somatostatin (STT) was studied analyzing the active miRNA collection at several specific neuron subtypes. GABAergic neurons had higher expression of miR-133b and miR-187 in respect to glutamatergic neurons, with miR-133b being enriched in PV-expressing and miR-187 in the STT-expressing GABAergic neurons (Stappert et al., 2015).

Even though there are several studies trying to decipher the key components for corticogenesis, further studies are fundamental to the identification of specific miRNAs controlling the neuronal subtype specification. Mir-17-92 cluster, which includes six different microRNAs (miR-17, miR-18a, miR-19a, miR-20a, miR-19b and miR-92a), is fundamental for maintaining radial glial cells and intermediate progenitors by inhibiting translation of *Pten* and *Tbr2* (Shan Bian et al., 2013). Knockout for this miRNA cluster causes embryonic lethality (Ventura et al., 2008) and deletion of this cluster specifically in oligodendrocytes using Cnp-Cre mice lead to impaired oligodendrocyte differentiation (Budde et al., 2010). Notably, cortical cko of miR-17-92 cluster promotes transition of RGCs to IPs, thus suggesting a crucial role in

layering control (Shan Bian et al., 2013). More recently, a paper identified specific miRNAs as fundamental players in the chronological generation of layer-specific neurons, at precise developmental time, by analyzing their temporal gradient of expression over the course of neocortical neurogenesis (Shu et al., 2019). Zhong's research group states that overexpression of miR-128 and miR-9 increases significantly the number of neurons in layer VI and V, respectively at the expenses of neurons in layers IV-II. Instead, overexpression of let-7 shows the opposite effect, with higher number of neurons in layers IV-II at the expenses of those in deep-layer VI. Furthermore, the levels of these miRNAs relative expression throughout corticogenesis, demonstrate that they act in an antagonist specific time manner, generating earlier deeper layer and later upper layer. This was confirmed by co-overexpression miR-128 and let-7 that generates a neutral phenotype.

These studies bring to light fine and strictly controlled regulation of cortical patterning by microRNAs. However, there is much more to be discovered and the knowledge presented until today is just a small window for everything that is to come. In particular, because of their peculiar capability to regulate hundreds of genes via their binding to short mRNA target sequences, miRNAs appear as the best candidates to rapidly evolve and coordinate the expression of many genes involved in the evolution of the mammalian cerebral cortex,

IN VITRO CORTICOGENESIS

The vertebrate development begins with egg fertilization and the formation of the first cell, the zygote. Consequent cell divisions lead to a globular solid mass of blastomeres known as morula. Further cell divisions generate a cavity in the morula, the blastocyst. Early mouse blastocysts are differentiated in the trophectoderm and inner cell mass (ICM) (Evans and Kaufman, 1981; Martin, 1981). From the inner cell mass of the blastocysts, gastrulation happens. At this step, cell mass is called gastrula and its cells can become epiblasts (emerging as part of the mature organism) or they can complete the developing system being differentiated into the placenta, the chorion and the amniotic membranes (Leon E Rosenberg et al., 2012). The embryonic stem cells (ESCs) are the ones that will give origin to the completed embryo. The ESCs are pluripotent cells that have the capacity to renew themselves or to differentiate into any of the three germ layers (ectoderm, mesoderm and endoderm) *in vivo* (Syeda H Afroze et al., 2014) and the majority of cell types *in vitro* when subjected to the appropriate conditions.

The *in vitro* differentiation of mouse embryonic stem cells into neural lineages was first described in 1995 with ES cells growing in suspension in order to allow them to form multicellular aggregates called embryoid bodies (Gerard Bain et al., 1995).

In the last twenty years, pluripotent embryonic stem cells (ESCs, Stavridis & Smith, 2003) have arisen as a promising instrument for neurobiology, as it have been allowing the study of processes involved in organogenesis in a controlled and reproducible manner (Gaspard, Gaillard, et al., 2009). In our case, *in vitro* corticogenesis has been demonstrating great benefits in respect to the usage of primary neuronal cultures. For instance, mESCs have made possible the differentiation of embryonic stem cells into specific neuronal populations of interest by suppling to the culture media precise signaling factors. This method gives a complete view about the intricate regional and temporal patterning, through all its molecular mechanisms, that bring up the cortex complexity. It is noteworthy to mention that ESC-derived cortical neurons behave like endogenous cortical neurons when grafted *in vivo* being also considered as cell therapy for the repair of cortical lesions (Gaspard et al., 2008). Moreover, the *in vitro* corticogenesis has the advantage of allowing the generation of hundreds of millions cells essential to deep and complex studies (Van den Ameele et al., 2014).

Remarkably, when mESCs are cultured at low-density, in serum-free and feeder-free conditions, in chemically defined minimal medium (CDMM) and without exogenous signals, they spontaneously generate Sox1- and Nestin-positive neural progenitors with an anterior neural identity. Interestingly, the *in vitro* identity presents the same timely regulated sequential

neurogenic pattern observed *in vivo* (Eiraku et al., 2008; Tropepe et al., 2001; Smukler et al., 2006; Bertacchi et al., 2013) which, confirms the spatial-temporal conservation of the neural differentiation both *in vitro* and *in vivo* (Gaspard et al., 2009).

In particular, to our interest, several groups have demonstrated that ESCs can be efficiently specified into a collection of neurons that exhibit fundamental characteristics of cortical neurons such as regional and temporal patterns of pyramidal axonal projections. By differentiating ESCs, cells underwent a well-organized neurogenesis with generation of cortical progenitors *in vitro* that followed the same pattern of genuine differentiation that occurs *in vivo*. These studies confirmed that neurons expressing layer-specific markers were generated through a coordinated sequence, as observed *in vivo*, with first Reelin and TBR1 neurons peaking at day 10-11 of corticogenesis, followed by BCL11B neurons (peaking at day 12-13) and, lastly, as expected SATB2 and CUX1 (summiting at day 14-16) (Bertacchi et al., 2013; Eiraku et al., 2008; Gaspard et al., 2008).

RESULTS

Analysis of Layer-Specific Transcription Factors expression shows mRNA-protein incoherence

As described in the Introduction Chapter, cortical layer formation is a well-coordinated process, giving rise to different cell layers. Interestingly, layer cell birth-date (the last cell division) is closely related to the final neuronal identity, which is in turn defined by the timely and cell-specific expression of distinct CITFs. Consequently, CITF mRNA expression is expected to occur in distinct cells starting from their last cell division. In order to understand how mRNAs of CITFs are regulated during corticogenesis, I re-analyzed single-cell RNA sequencing (scRNA-seq) datasets of mouse cortex at E11.5, E13.5, E15.5 and E17.5, generated by Drop-seq from dissociated whole embryonic cortices (average depth more than 50.000 reads/cell; transcriptomes from 2.000 cells at E11.5, E13.5, E17.5; 5.000 cells at E15.5) (Yuzwa et al., 2017). I have selected this scRNA-seq dataset, as it is the only available in the literature providing a deep transcriptional identity through the transition from embryonic RPs at early corticogenesis stage (E11.5) to adult NSCs at late corticogenesis (E17.5). This analysis allowed me to have a complete perspective of cortical layering formation during embryogenesis.

I have focused my attention on a number of crucial markers of RG (E13.5), RG/BP/DPN (E13.5), BP/DPN/SPN (15.5) and DPN/SPN (E17.5) (Figure 1A). The results demonstrate that the onset of mRNA expression for some CITFs analyzed is not always in accordance with the time of detection for the correspondent protein. In particular, *Satb2* showed the largest incoherence between mRNA and protein onset of detection. *Satb2* is the main gene for the specification of callosal neuronal identity. This evolutionary new class of neurons, exclusively of Eutherians, present fibers that extend to the contralateral hemisphere giving origin to the *Corpus callosum* (Alcamo et al., 2008; Leone et al., 2015; Suárez et al., 2018). While *Satb2* is transcribed in the early cortex from E11.5 (Sasaki et al., 2008) and its mRNA is found in scRNA-seq at the same step of corticogenesis (Figure 1B), before E14.5 there is no signal of SATB2 protein in the cortex (Britanova et al., 2005) with its levels being detectable only at E15.5 in the first SPNs (Figure 1C). It is important noticing that at E13.5, the levels of *Satb2* mRNA are similar to the levels of housekeeping genes. This fact indicates that *Satb2* levels should be enough to produce a biological effect at this point of cortex development. Instead, the absent protein indicates a post-transcriptional repression. From the literature, it is known that *Satb2* represses the DPN gene *Bcl11b* and, through this repression, has a fundamental role on the establishment of SPN (Alcamo et al., 2008; Leone et al., 2008; Srinivasan et al., 2012). Moreover, *Satb2*

ablation in mice leads to strong behavioral consequences (Zhang et al., 2019) and *Satb2*-mutation associated syndrome (SAS) causes dramatic cognitive impairments in humans (Lee et al., 2016). All these evidences put together, led us to focus on the mechanisms underlying the control over CITFs and specifically, *Satb2*.

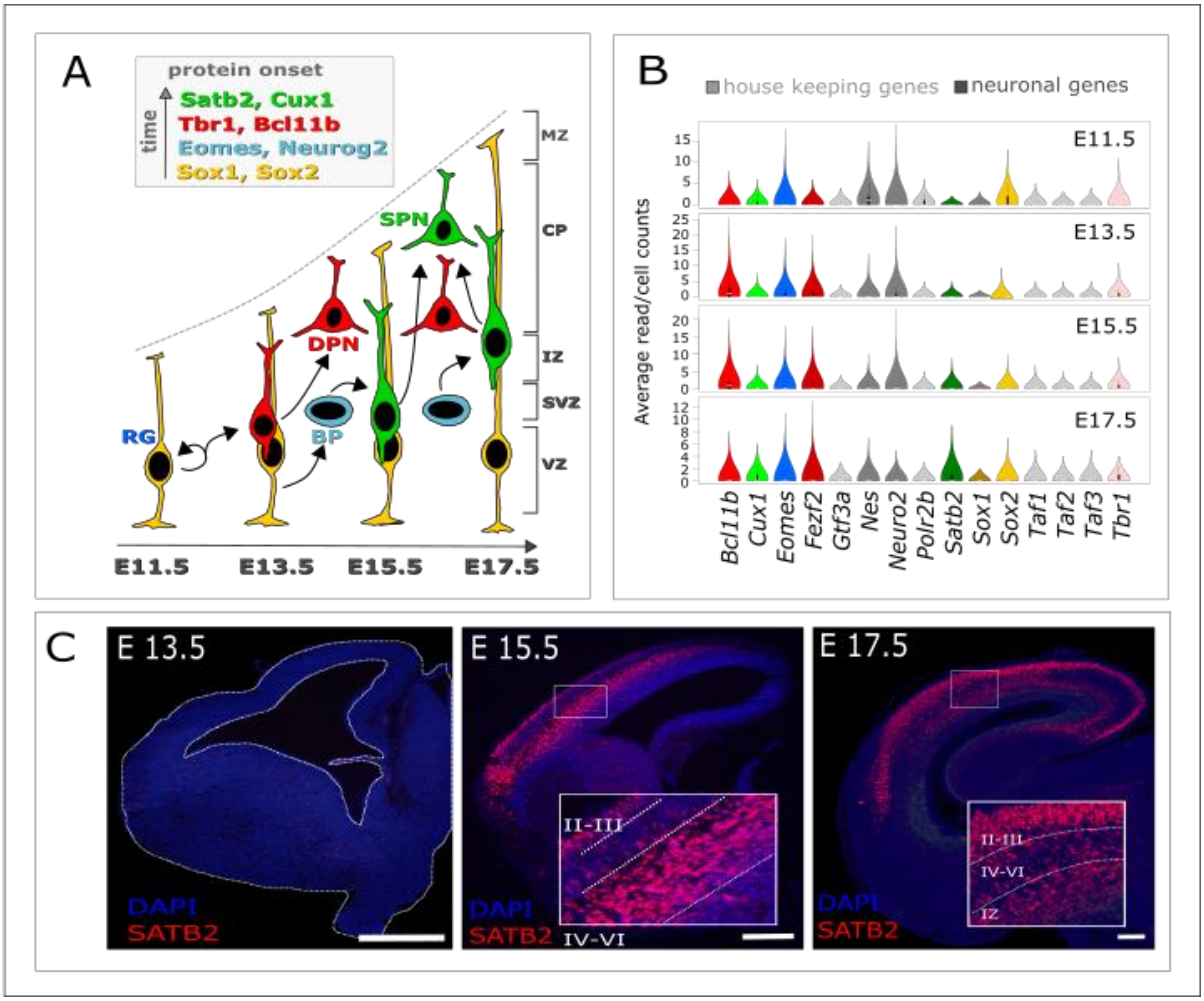

***Figure 1* - mRNA-protein incoherence in CITFs expression along corticogenesis**. (A) Simplified outline of cortical layering. MZ, mantle zone; CP, cortical plate; IZ, intermediate zone; SVZ, subventricular zone; ZV, ventricular zone. E11.5-E17.5, embryonic day 11.5-17.5. (B) Violin plots show normalized, average read count/cell of genes indicated in labels. Constitutive gene names are in grey. (C) SATB2 immunodetection (red fluorescence) on developing cortex coronal sections. Insert show layer magnification. Scale bars, 100 µm

At early stages of corticogenesis, CITFs are not restrained to a cell subset

To get insight on the mechanisms of CITF transcriptional activation in specific cell subsets I have studied CITF co-expression in single cell datasets. However, ScRNA-seq is characterized by low efficiency that prevents the detection of many expressed genes in single cells, especially in droplet-based experiments. An innovative method to analyze datasets of single cell RNA-seq was developed in our lab by Silvia Galfrè, PhD, using Unique Molecular Identifiers (UMI) to count matrices without the need of normalization and independent from the zero-inflation. Contingency Table Analysis (COTAN) gives, for each cell, a robust estimation of the UMI detection efficiency (UDE), measuring the co-expression of gene pairs by associating the number of cells that have zero UMI counts for both genes. This methodology is associated to the idea that technical zeros are always independently distributed, while biological zeros may be correlated to genes associated to cell differentiation (Galfrè & Morandin, 2021).

COTAN thus, assesses the correlated or anti-correlated expression of gene pairs in single cells, providing a correlation index with an approximate p-value. Moreover, through its global differentiation index (GDI), COTAN allows to analyze also the global degree of co-expression of one gene with all the other genes of the dataset. In fact, COTAN GDI discriminates between constitutive and non-constitutive genes by globally integrating COEX (co-expression) values of all the possible gene pairs (Figure 2, left panel). Notably, there is no evident correlation between GDI and relative gene expression at global level (Figure 2, middle upper panel) and global GDI are comparable among the four developmental times (Figure 2 lower middle panel), indicating that GDI is not biased by transcriptional rate and developmental time.

The GDI for constitutive genes such as *Actb* is very low, as expected for constitutive genes expressed in all cell subpopulations (Figure 2, right panel). Instead, CITFs genes should present high GDI for the developmental stages that have been analyzed as their proteins are expressed in only specific types of cells (Figure 1A). At E11.5 *Tbr1* showed a peak in agreement to early localized TBR1 protein expression in layer I neurons. Conversely *Bcl11b*, *Fezf2* and *Cux1*, which are transcribed at relevant levels (Figure 1B), and *Satb2*, show very low GDI. Even though it is possible to see an increase in GDI levels of deeper (*Bcl11b* and *Fezf2*) and upper (*Satb2* and *Cux1*) CITFs at E13.5, *Satb2* GDI level is still very low, indicating that at this developmental step it might not yet be transcribed in well-defined cell subsets. Indeed, at E15.5 all CITFs increase their GDI (Figure 2A, right panel) in line with their specific pattern of protein expression in cell subsets (Figure 1A). Interestingly, at E17.5, when corticogenesis is close to its

end the GDI levels drop. This might be due to increased complexity of the cell types co-expressing different combination of CITF proteins at this time point (Kang et al., 2011; Lodato & Arlotta, 2015), although I do not exclude it can be also due to post-transcriptional regulation. Overall, I can conclude that low GDI levels correlate with initial phases of CITF transcription when protein expression is not yet detected and that, among the CITFs, *Satb2* shows the longer time with low GDI and the largest delay between transcriptional and translational onset.

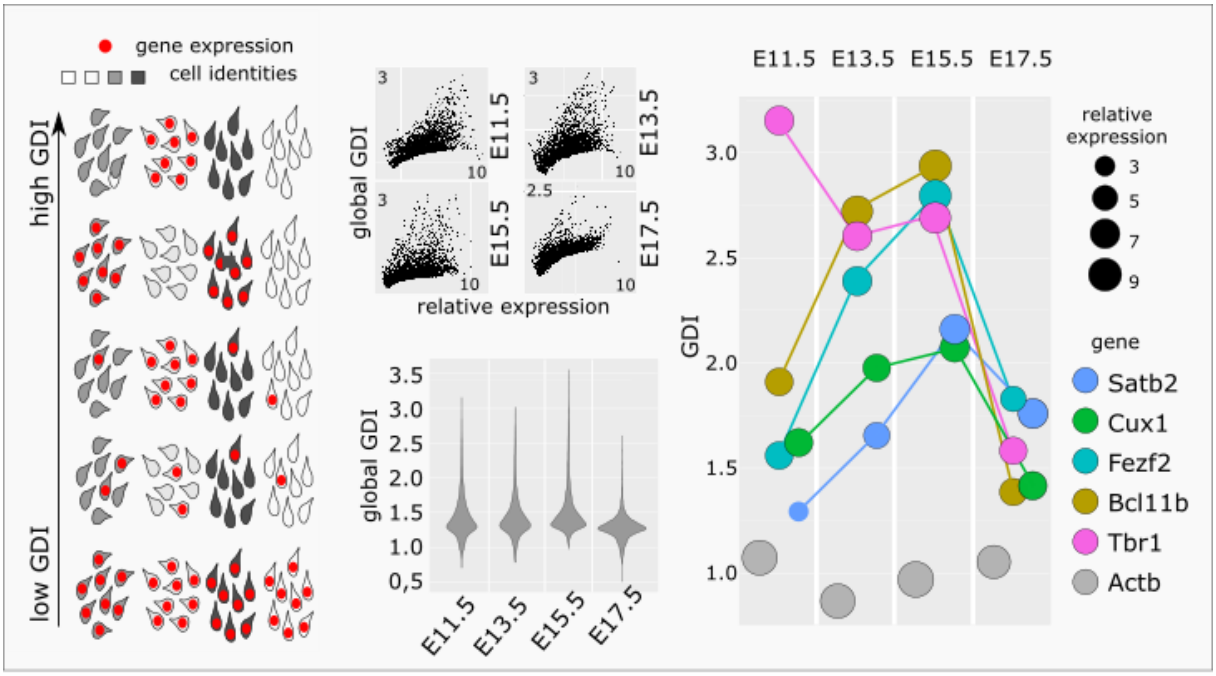

***Figure 2* - CITFs acquire specific identity at late stages of corticogenesis.** GDI (left) globally infers the degree of gene pair co-expression in respect to mRNA expression level (middle upper panel) and developmental time (middle lower panel). Distinct CITFs show different GDI according to their translational onset (right panel).

Satb2 acquires the identity as a callosal marker only at late stages of corticogenesis

GDI analysis suggested that in the early stages of corticogenesis cell identity is not yet well defined. Thus, I was curious to check how genes would interact to each other in the early stages at the single cell level.

The COTAN correlation index (COEX) estimates the probability that two different mRNA species are co-expressed in a single cell of a cell subset, screening out the constitutive genes. If two genes are co-expressed the COEX is positive, while split expression is shown by negative COEX. Moreover, constitutive genes present a COEX near to zero (Figure 3A).

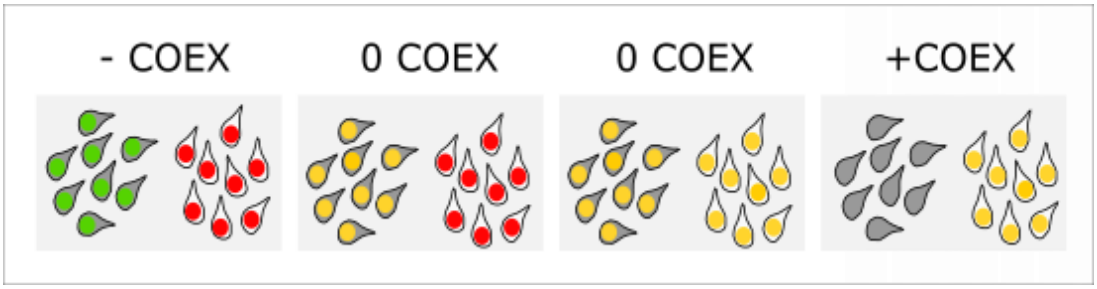

Figure 3 **- Schematic representation of COTAN correlation index (COEX).**

After analyzing the data, low correlation/anti-correlation (COEX close to 0) levels for constitutive mRNA pairs was observed. On the contrary, high correlation (positive COEX) is seen in mRNA pairs of neural progenitor cells (*Nestin, Vimentin, Notch* and *Hes1-5*) or in post-mitotic cells and neurons during process of differentiation (*Dcx, Tubb3, Map2*). Finally, negative COEX, which means high anti-correlation, is detected during all the process of corticogenesis, between neural progenitor cell mRNAs and post-mitotic cell and neuron mRNAs (Figure 4). These preliminary observations indicate that COTAN analysis is a robust method to study gene pair co-expression in single cell. At E13.5 *Satb2* mRNA correlates with *Tbr1* mRNA, an early CITF. Besides, *Satb2* shows correlation with *Bcl11b*, marker of DPN and known for being repressed by SATB2 later in the corticogenesis. Instead, *Satb2* anti-correlates with *Eomesodermin* and *Neugenin2*, fundamental during the differentiation pathway. These data show that at early stages *Satb2* mRNA expression has not acquired yet its restricted pattern in a subset of callosal identity cells (see Figure 1A).

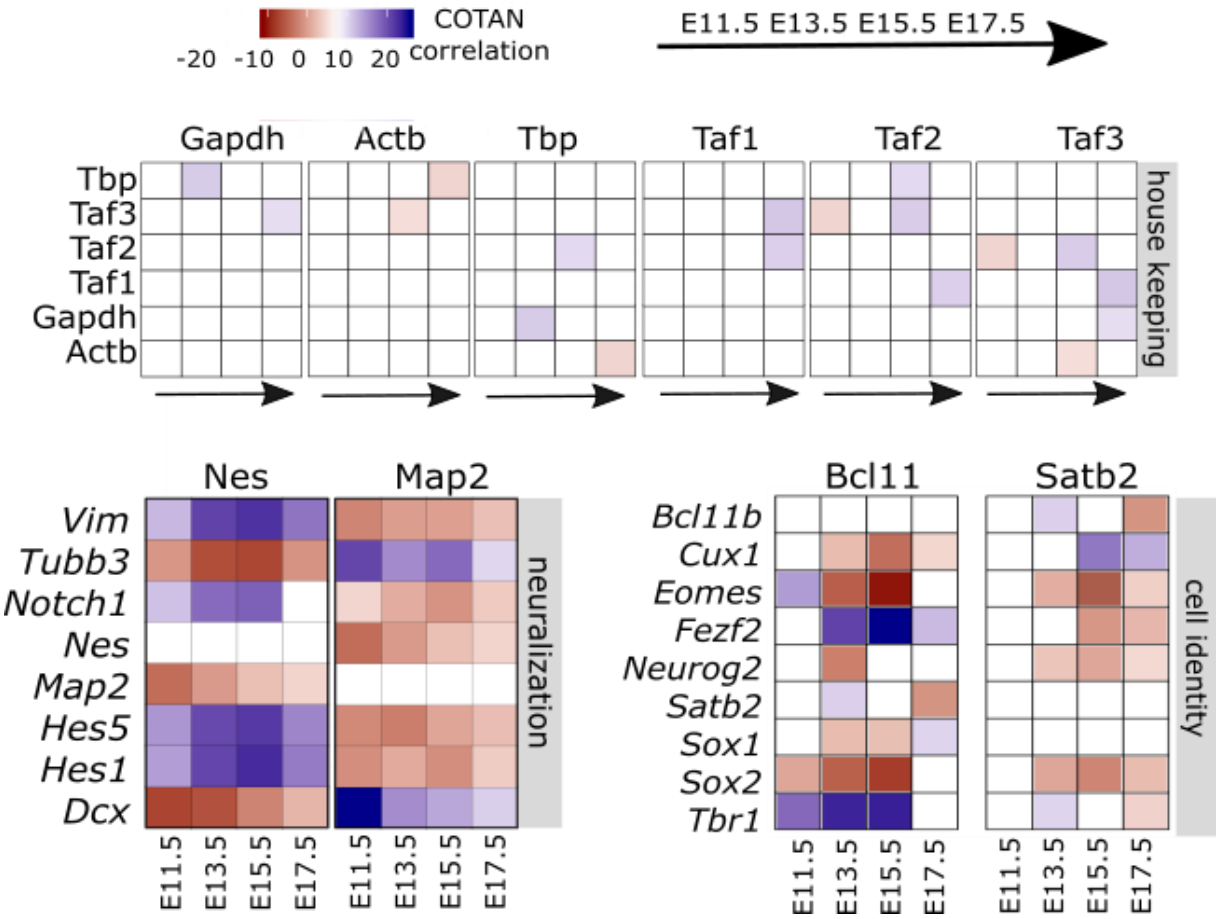

***Figure 4* - COTAN correlation index (COEX) values for CITFs at single cell in a cell subset.** COTAN COEX values of couples of constitutive genes (upper matrix), neural differentiation markers (lower left matrix) or layer identity genes (lower right matrix) at the different developmental times E11.5, E13.5, E15.5 and E17.5.

The callosal identity specification is likely due to post-transcriptional control over *Satb2*

Based on the previous results, the next step was the analysis of early cells clustering for differential mRNA expression through T-distributed Stochastic Neighbor Embedding (t-SNE). t-SNE is capable of visualize high-dimensional data by giving each datapoint a location in a two or three-dimensional map and reveals global structure such as the existence of clusters at numerous scales (Maaten & Hinton, 2008; Kobak & Berens, 2019). The results demonstrated an incoherence between the mRNA differentially expressed for the clustering of early cells (Figure 5) and the spatial-temporal protein expression of SATB2 and BCL11B at E13.5 (Figure 1A), even though at late stages (E17.5) the distribution pattern of *Satb2* mRNA is in accordance to SATB2 protein pattern of expression in restricted cell subsets. These outcomes indicate that, in single progenitor cells from E11.5 to E15.5, the mRNA of *Satb2* and of DPN CITFs are not mutually exclusive. From the literature, it is known that SATB2 and DPN CITFs are responsible for the identity of superficial vs deep layer, respectively and thus, the callosal identity specification seems due to post-transcriptional control over *Satb2*.

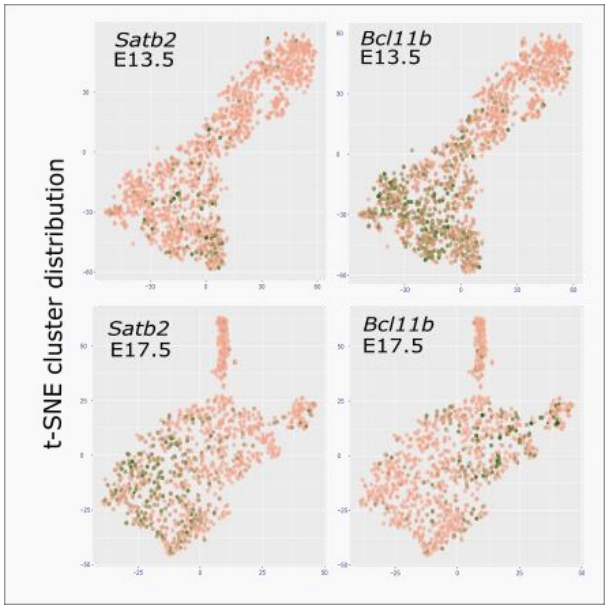

***Figure 5* - *Satb2* and *Bcl11b* differential mRNA expression by t-SNE analysis.**
CITFs t-SNE clustering of early (DIV13.5), or late (DIV17.5) cells.

The onset of SATB2 translation coincides with developmental time in which *Satb2* mRNA becomes stable

On the bases of single cell mRNA count analysis (Figure 1B), it was safe to assume that at E13.5 *Satb2* mRNA expression is already robust. Thus, I checked if the lack of SATB2 protein at this stage of cortical development was due to *Satb2* mRNA instability. To do so, we took advantage of Exon-Intron Split Analysis (EISA) (Figure 6) (Gaidatzis et al., 2015; Manno et al., 2018). We have analyzed an additional available RNA-seq dataset of progenitor cells (Chui et al., 2020) in order to investigate both intronic and exonic reads at the mouse embryonic stages when layer identity commitment is established and before neuron's birth date (McConnell & Kaznowski, 1991; Telley et al., 2019).

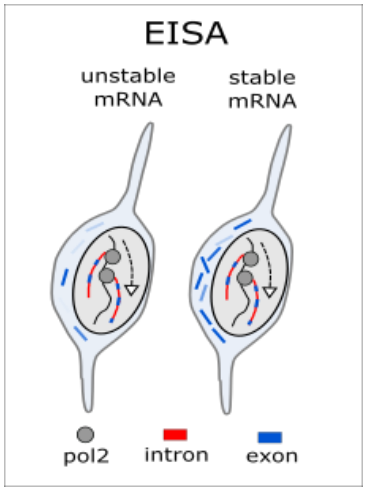

***Figure 6* - Exon-Intron Split Analysis (EISA) methodology.**
Schematic difference between unstable and stable mRNA for EISA analysis

The Exon/Intron (E/I) ratio indicates the mRNA stability levels and it is an indicator of the amount of RNA that can be translated into protein. Silvia Galfrè executed EISA bioinformatics procedures and I performed the analysis of E/I ratio during corticogenesis. As expected, *Bcl11b* increases its stability from E11.5 until E15.5 followed by increased *Fezf2* mRNA stability from E13.5 to E15.5, in accordance to respective protein translation time points of the two genes (Chen et al., 2008) (Figure 7).

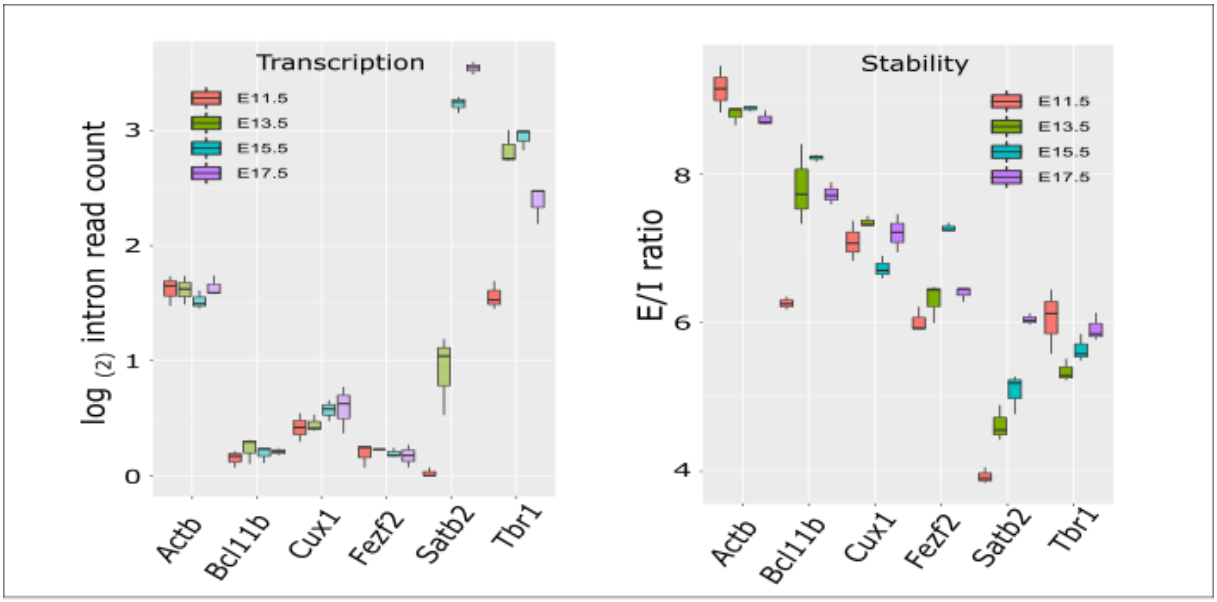

***Figure 7* - Intronic and E/I ratio folded expression using RNA-seq data of main CITFs during corticogenesis at different in vivo embryonic times.** Outline shows different ratio of exonic and intronic sequences in relation to mRNA stability. Box plots show exon/intron and intron reads for distinct CITFs and Actb (constitutive) in cortical progenitors at different in vivo embryonic times.

Interestingly, *Satb2* E/I ratio as well as its transcription rate increase since E11.5 all the way until the end of corticogenesis both in RNA-seq data (Figure 7) and RT-PCR using RNA extracted from tissue (Figure 8).

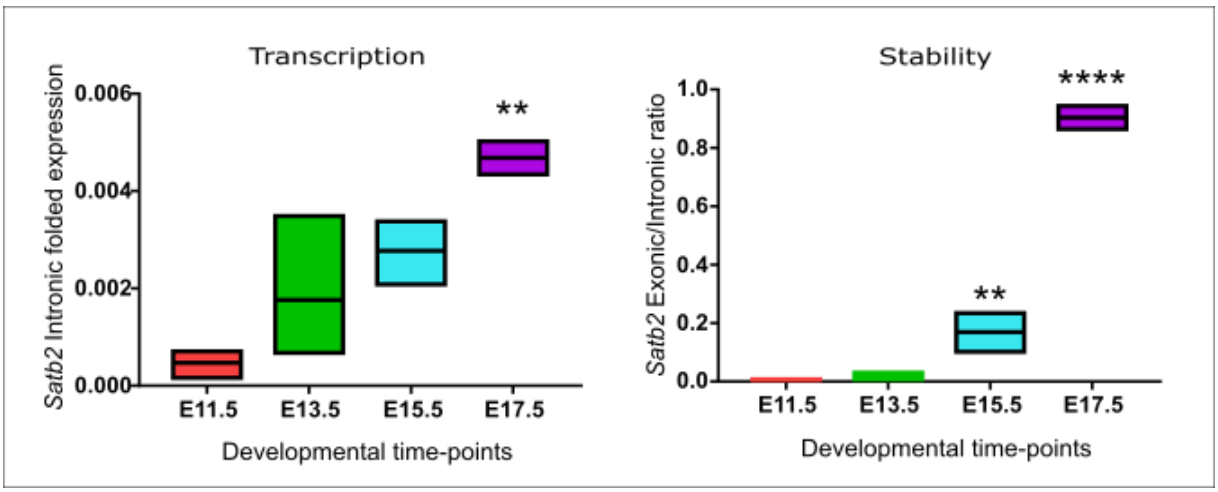

***Figure 8* - Intronic and E/I ratio folded expression analysis by RT-PCR of *Satb2* at different in vivo embryonic times.**

Finally, the *Satb2* E/I fold change between E13.5 and E15.5, the critical period of corticogenesis, settles in the highest quartile of E/I increase (Figure 9).

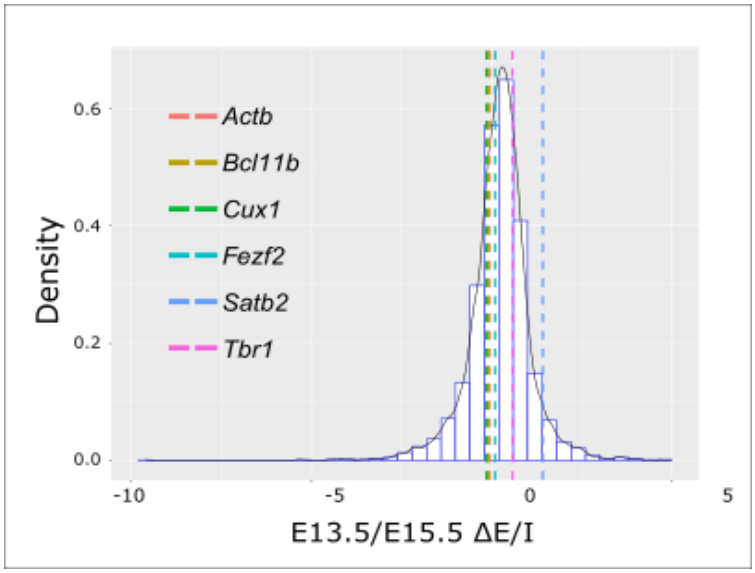

***Figure 9* - Density plot of Exon/Intron (E/I) ratio fold change between E13.5 and E15.5.**

Altogether, these data indicate a high biological relevance of the developmental changes of *Satb2* mRNA stability and an evident association between increase of *Satb2* mRNA stability and onset of SATB2 translation. Therefore, the post-transcriptional regulation of *Satb2* became our main subject of thought.

miRNA-mediated mechanism controls SATB2 translation

I hypothesized that changes in the *Satb2* mRNA stability through corticogenesis could be due to miRNA-dependent mechanisms. In fact, by high-throughput analysis of miRNA-mRNA interactions at single cell level, several miRNAs have been associated to mechanisms controlling different cortical cell identities (Nowakowski et al., 2018). To understand better miRNA expression during early stages of corticogenesis, I employed mESCs, which *in vitro* neural differentiation precisely reproduces the early corticogenesis development, including time-regulated expression of SATB2 protein (Bertacchi et al., 2013; Terrigno et al., 2018a, 2018b). I have enriched cultures in progenitor or post-mitotic cells by sorting Sox1::GFP corticalized mESCs, or by treating them with Ara-C, respectively (Bertacchi et al., 2013; Bertacchi et al., 2015), and then Marco Terrigno performed small RNA-seq to obtain miRNAomes of the different culture conditions. I first aimed to evaluate the general differences between samples. Using Principal Component Analysis (PCA) I compared miRNA global expression in these cells at different time-points of corticalization. It was also included miRNAomes of ESCs at initial stages of differentiation (DIV0-6) and miRNAomes of embryonic (E12) and newborn (P0) cortex as internal references. The overall comparison of ESC-derived cells and cortical miRNAomes highlighted a consistent similarity of miRNAomes of neuronally differentiated cells of both origins (*in vitro* and *in vivo*), which clustered together and were well separated from the miRNAomes of non-neuronal cells (DIV0-6 ESCs) by the first two principal components (Figure 10A left). This first observation is in line with the capability of mESC corticalization protocols to reproduce a bona-fide naive corticogenesis process *in vitro* (Gaspard et al., 2008; Bertacchi et al., 2013, 2015; Terrigno et al, 2018). The second component of miRNAome PCA distributes both Sox1::GFP and Ara-C cells by the developmental time, demonstrating that the development of both progenitor and post-mitotic cells is tightly controlled by miRNAs (Figure 10A right). Moreover, this result also demonstrates that the mechanisms of miRNA-mediated post-transcriptional control can be consistently studied using corticalized mESCs. It is fundamental to notice that both neuron and progenitor miRNAomes are distributed through PC3 by their *in vitro* developmental time and in agreement with *in vivo* E12 and P0 cortex miRNAomes (Figure 10B). This data confirms the tight conservation of the mechanisms related to the timing of layer formation *in vitro* and the identity of neuronal and progenitor's cultures along the differentiation process.

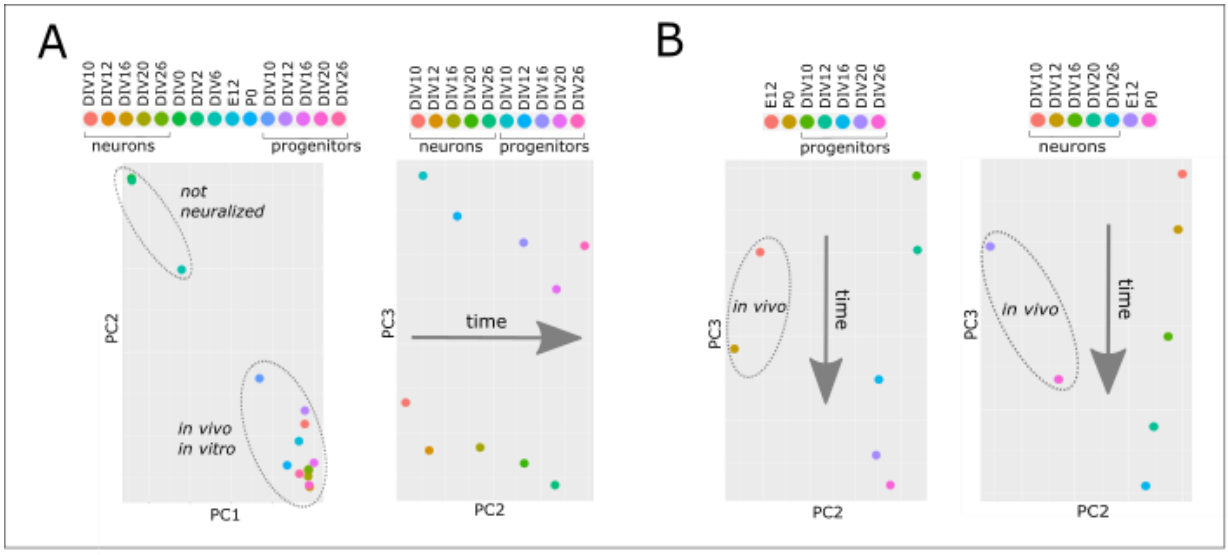

Figure 10 **- PCA of miRNA global profiles of non-neuralized mES cells, neural progenitor cells (Sox1::GFP corticalized mESCs), post-mitotic cells (Ara-C-treated corticalized mESCs) and mouse cortex at different developmental times.** (A) Neuronal cells' miRNAome from both *in vitro* procedures and *in vivo* origin cluster together and are a part from miRNAome of non-neuronal cells (left). Neuronal cells are organized accordingly to their developmental time shows a clear distinction between progenitors and neurons from the miRNAome profile (right). (B) Progenitor and neuronal cells are separated through PC3 accordingly to their *in vitro* developmental time miRNAome profile.

After the miRNAome analysis, I checked if *Satb2* mRNA instability could be associated to interactions between *Satb2* mRNA and RISC. In this way, I have quantified the enrichment of *Satb2* mRNA after AGO2 immunoprecipitation (Pandolfini et al., 2016). Using qRT-PCR, it was noticed a significant enrichment of AGO2-bound *Satb2* mRNA in cells that are cultured for 12 days *in vitro* (DIV) in respect to control (GFP-bound *Satb2*). This data proved the miRNA silencing effect at early stage of *in vitro* corticogenesis (Figure 11). Interestingly, at DIV18, a time when SATB2-positive cells are significantly increased (Bertacchi et al., 2015), there is no enrichment of AGO2-bound *Satb2* mRNA.

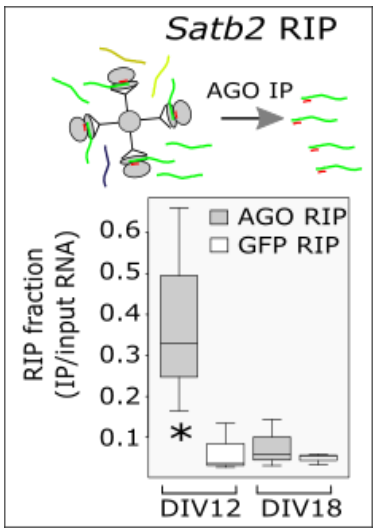

***Figure 11* - RNA immunoprecipitation of Argonaute-interacting (AGO) *Satb2* mRNA.** Values on Y axis report the ratio of RT-PCR-detected, immunoprecipitated Satb2 mRNA with respect to the input (AGO RIP). GFP RIP, control immunoprecipitation with anti-GFP Ab. N= 3 biological replicates. *p = 0.049 (Student's t test).

There is general agreement on the primary role of the 3'UTR in acting as the main target of miRNA inhibitory activity of protein translation (Didiano & Hobert, 2008; Fang & Rajewsky, 2011). In order to verify whether *Satb2* mRNA 3'UTR contain cis-acting signal of translational inhibition, I proceeded with the transfection of a GFP reporter carrying *Satb2* 3'UTR at DIV12 and DIV11 (Figure 12). At DIV12, GFP intensity is significantly weaker for cells transfected with GFP-*Satb2* 3'UTR in respect to control (only GFP). On the other hand, as expected, at DIV18 the reporter activity is not considerably affected. Notably, the binding of AGO2 to *Satb2* mRNA, seen only in early stages of corticogenesis (Figure 11), is in accordance to the capacity of the 3'UTR of *Satb2* to inhibit SATB2 translation only in early cortical cells. These observations confirmed previous results obtained in our lab suggesting translational delay of SATB2 during mESC corticalization (Bertacchi et al., 2015).

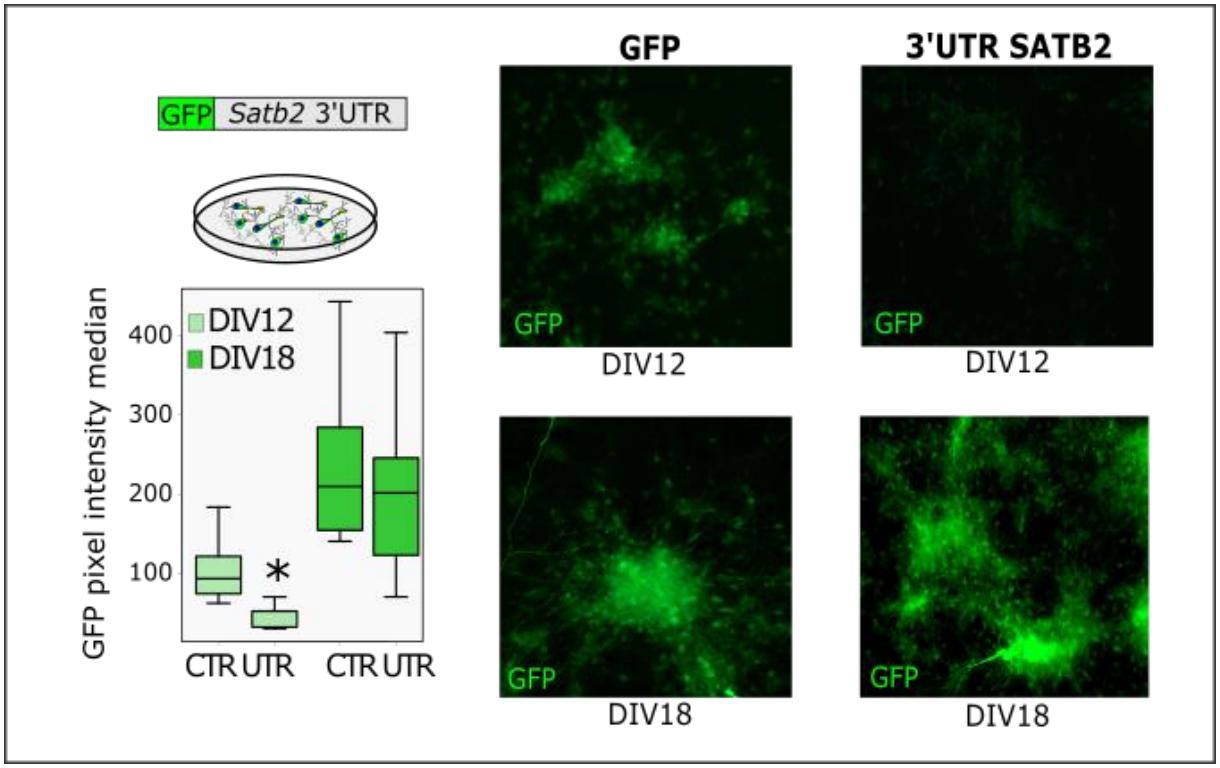

***Figure 12* - Expression of *Satb2* 3' UTR-bearing GFP reporter after lipofection in corticalized mESCs.** N= 3 biological replicates. * p = 0.000061 (Wilcoxon signed rank test).

Satb2 3'UTR represses translation in early cortical neurons

After concluding that the 3'UTR of *Satb2* is able to inhibit the translation of GFP at early stages *in vitro*, I wondered if it would be possible to see the same *Satb2* 3'UTR control over translation *in vivo*. To do so, in collaboration with Professor Paola Malatesta from Università Degli Studi di Genova, they have electroporated a GFP reporter carrying *Satb2* 3'UTR or GFP alone as control (Figure 13). Animals were electroporated at E13 and the analysis was done 7 days later (P0). I analyzed seven animals electroporated with GFP-3'UTR and eight animals electroporated only with GFP. For each electroporated brain, I analyzed 10 images and experiment was repeated twice. At E13 electroporated mice, the number of SATB2-GFP double-positive cells in comparison to GFP-positive cells is significantly higher and more concentrated in the upper layers, in a cortex electroporated with the 3'UTR bearing sensor in respect to a control-electroporated cortex. This observation indicates that *Satb2* 3'UTR by itself is able *in vivo* to inhibit the translation in early cortical neurons that are not SATB2 positive.

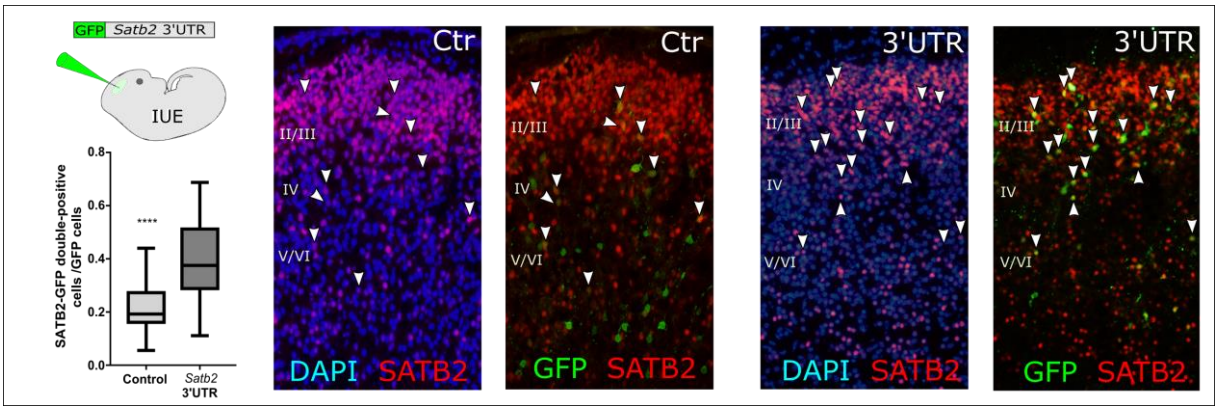

***Figure 13* - Effect of Satb2 3'UTR over translation *in vivo*.** *In vivo* electroporation of mouse embryonic cortex at E13 with GFP reporter carrying the *Satb2* 3'UTR or GFP alone. Arrowheads point to GFP-SATB2 double positive cells. Roman numerals indicate layers. Scale bar, 50 µm. N = 8 control animals and 7 experimental animals. Images were obtained with fluorescence microscope and the analysis was done by ImageJ software. Unpaired parametric t-test two-tailed pValue <0.05 (pValue <0.0001).

As it was mentioned before and has been already described in the literature, SATB2 and BCL11B proteins are mutually exclusive in the majority of neocortical cells at the time they begin to establish connections with other neurons (Britanova et al., 2008). Thus, I wondered if the same *Satb2* 3'UTR could also block the translation of BCL11B in the deeper layers *in vivo*. I performed immunohistochemistry (IHC) using an antibody against BCL11B in the slices

electroporated with GFP reporter carrying *Satb2* 3'UTR or GFP alone at E13 of cortex development.

The analysis was performed at the same developmental time as before (P0), using the same parameters (number of animals per condition, number of images per animal, type of analysis and statistical method significance). It was observed that, the number of BCL11B^{+}/*Satb2* 3'UTR-GFP^{+} double-positive cells is significantly lower in comparison to BCL11B^{+}/GFP^{+} double-positive cells (Figure 14). This observation supports the hypothesis that the 3'UTR of *Satb2* by itself might be able to block BCL11B translation in deeper layers *in vivo*.

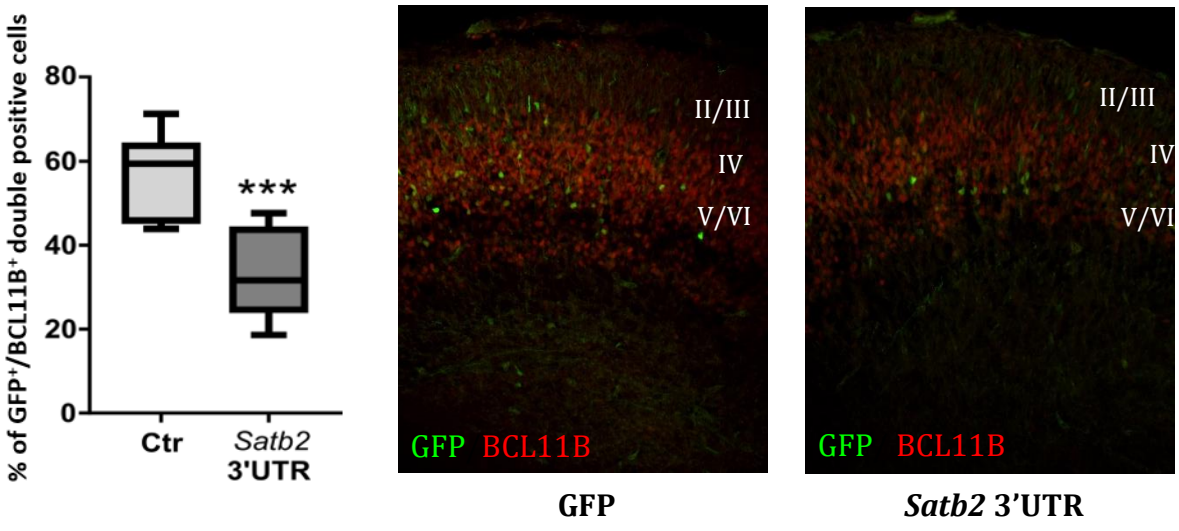

***Figure 14* - Blockade of BCL11B translation by *Satb2* 3'UTR *in vivo*.** *In vivo* electroporation of mouse embryonic cortex at E13 with GFP reporter carrying the 3'UTR Satb2 or GFP alone. GFP/BCL11B double positive cells were counted with ImageJ software. Roman numerals indicate layers. Scale bar, 50 µm. N= 3 biological replicates.

Isolation of miRNAs interacting with *Satb2* 3'UTR

At this point, it became fundamental to isolate and identify the miRNAs that directly bind to *Satb2* 3'UTR. Performing the protocol of mESCs corticalization until DIV12 and DIV18, I have identified specifically the miRNAs that bind to the 3'UTR of *Satb2* at these two stages of corticogenesis through the novel miR-CATCH technique (Marranci et al., 2019). I focused on these two time-points in order to have a precise analysis on the miRNAome when *Satb2* is greatly repressed (DIV12) and when SATB2 is abundant in the cortex (DIV18).

The miR-CATCH is able to pull down the microRNA species that are bound to an endogenous target mRNA of interest using two sets (ODD and EVEN) of biotinylated DNA antisense probes (Marranci et al., 2019). Each of these sets is incubated with a replica of the biological sample for each time point (DIV12 or DIV18). The splitting of the probes into two independent pools increases the power of the outcome as independent pools of probes can present different binding efficiency and compete with diverse microRNAs for the binding to precise RNA regions. Besides that, it offers an internal control as biological samples incubated with the probes work as a control for each other.

After incubation of biological samples with ODD and EVEN probes, the microRNAs were identified comparing reads with sequences from miRBase repository (miRBase release 21) and the abundances were calculated in reads per million (RPM). The enrichment was measured by the quantity of a miRNA in respect to the total miRNAs (input) using small RNA-sequencing (Figure 15A), which was performed by Milena Rizzo e Alberto Mercantani. To establish a threshold of significance for the data obtained, we based on NOISeqBIO R-package. This method implements a non-parametric statistical system based on empirical distribution and is capable of count data, filter low-counts, normalize the results and provide the differential gene expression analysis with high efficiency in controlling the false discovery rate (FDR) in the experiments replicates (Tarazona et al., 2015).

Looking at the overall expression, miR-381 and miR-99 were very abundant at DIV12 but after NOISeqBio analysis, they did not present convincing affinity to *Satb2* 3'UTR as demonstrated by the differential expression values. Instead, at this developmental time, twelve miRNAs were significantly enriched for *Satb2* 3'UTR (Figure 15B). I have already demonstrated that *Satb2* mRNA is present since early stages (E11.5) but its protein is not around until E14.5 (Bertacchi et al., 2015) so, I supposed that one of these miRNAs represses SATB2 translation. Therefore, I looked for their level of expression at DIV18, as they should not be enriched

anymore at this stage. Ten out of those twelve miRNAs were still enriched and thus, I tended to exclude them as possible candidates for the control of SATB2 inhibition. However, a more careful analysis was carried out looking at the developmental pattern of expression of the miRNAs captured at DIV12.

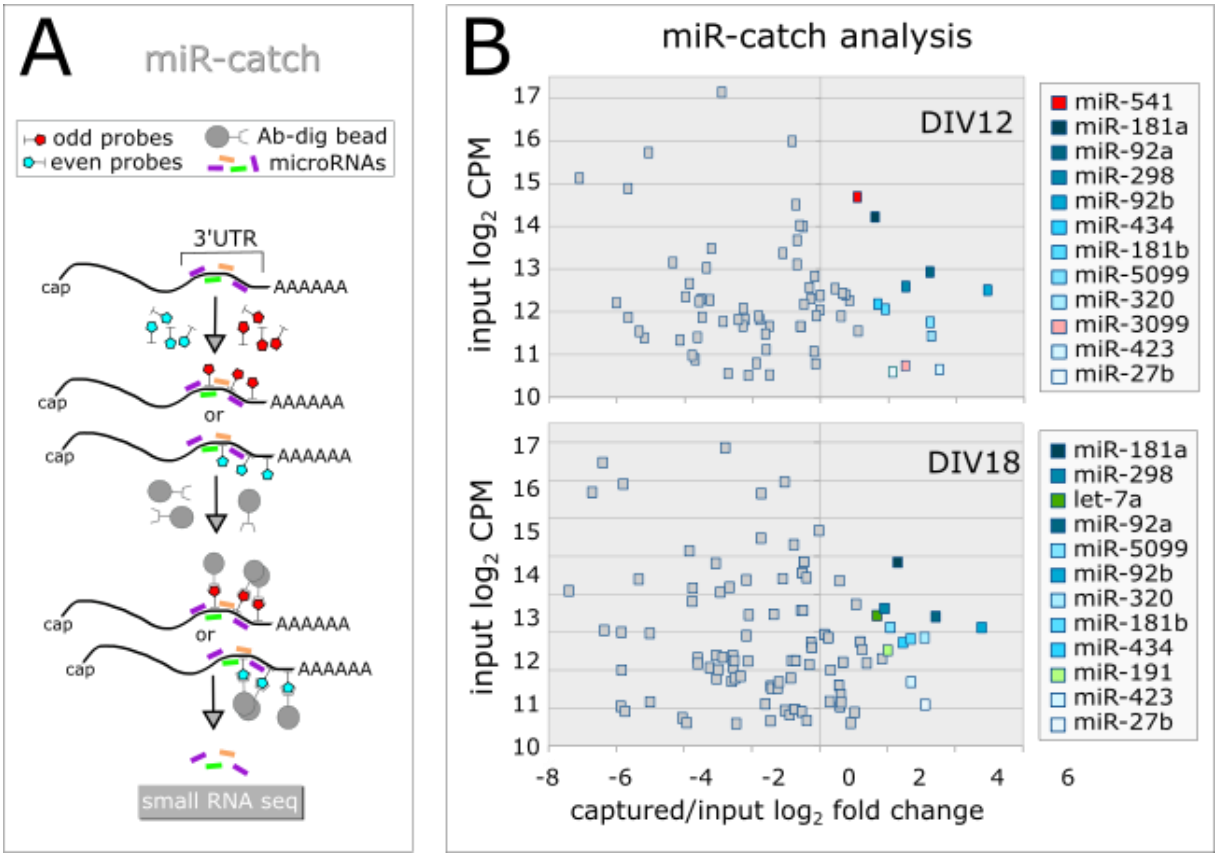

***Figure 15* – Identification of miRNAs interacting to *Satb2* 3'UTR.** (A) outline of miR-catch method. (B) enrichment of captured miRNAs (x-axis) with respect to input (Y axis) at the indicated time. CPM, counts per million. Color labels indicate miRNAs significantly enriched (non-parametric NoiSeqbio test probability > 0.9) (Tarazona et al., 2015).

MiR-541 is the best candidate to control *Satb2* translation

To understand better their dynamics throughout corticogenesis, I analyzed the expression of those twelve miRNAs enriched by miR-CATCH at DIV12 comparing to miRNAome profile of Sox1::GFP cortical progenitors. MiR-541 and miR-3099 are the only two miRNAs enriched at DIV12 and not at DIV18, thus rendering them the best candidates to inhibit SATB2 translation.

MiR-541 expression decreases from DIV12 to DIV16, in accordance to SATB2 protein increase at the same developmental period. On the contrary, miR-3099 did not behave accordingly to our expectations, as its levels increased from DIV16 until DIV20 and thus, it is unlike its involvement in SATB2 early inhibition. Instead, miR-92b showed a robust decrease from DIV12 to DIV16, when SATB2 translation starts (Figure 16A). Thus, even if it is still captured by RISC at DIV18 in our assay, I considered also it for further analysis aiming to identify miRNAs potentially involved in the early *Satb2* control.

After the analysis, I concluded that miR-541 pattern of expression is the one in best temporal accordance to the SATB2 translational inhibition with a very convenient decay of expression between DIV12 and DIV16, followed by downregulation in cortical progenitors from DIV10 to DIV26 of a subset of miRNAs (Figure 16B). However, as explained, I continued to consider mir-92a/b. This choice is explained by miR92a/b very high expression and miR-CATCH capture levels as well as their continuous decrease during corticogenesis. Besides, miR-92 is part of miR-17-92 cluster which regulates neural stem cell expansion and transition to intermediate progenitors during neocortex development (Bian et al., 2013). This cluster plays a key role in the inhibition of EOMESODERMIN (TBR2) and consequently, in the repression of basal progenitors' early generation (Nowakowski et al., 2013; Bian et al., 2013) by inhibiting the transition from RGCs to IPs. However, mir-92 decreases as soon as corticogenesis starts in order to give origin to IP and consequently, neurons.

Using miRanda algorithm (v3.3a; Enright et al., 2003), I could check *in silico* the affinity of these miRNAs to bind to the *Satb2* 3'UTR binding sites. Binding score > 120 and energy lower than -18 Kcal/mol were chosen as thresholds for strong affinity. Taking into consideration these constraints, miR-541 has been identified with the highest predicted affinity for *Satb2* 3'UTR, harboring three *in silico* binding sites for this miRNA. Instead, miR-92 binding affinity to *Satb2* 3'UTR was weaker, with miR-92b slightly stronger than miR-92a (Figure 16C).

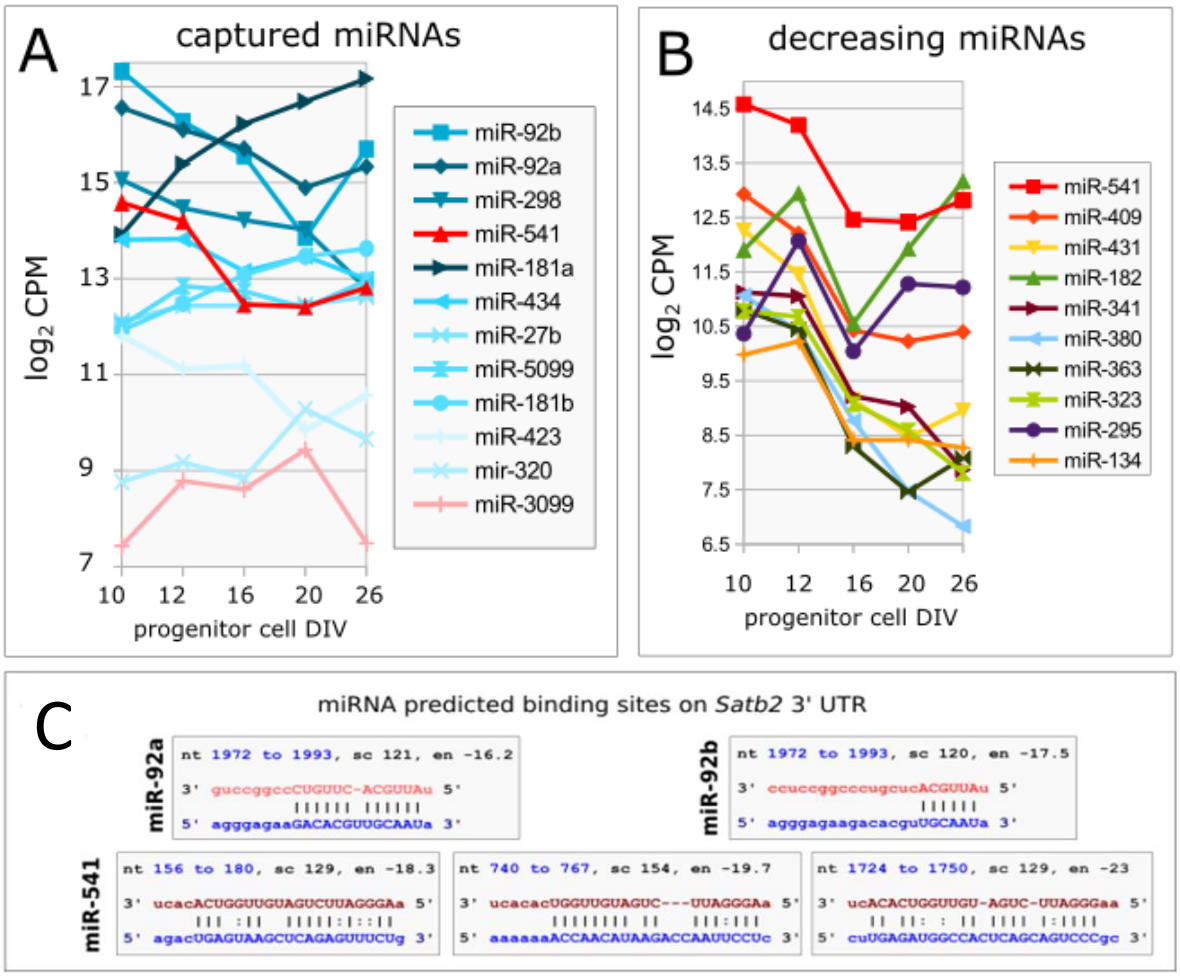

Figure 16 – **MiR-541 is the best candidate to control *Satb2* translation.** (A) Developmental patterns of *Satb2*-captured miRNA expression in Sox1::GFP progenitor cells. (B) Developmental expression of miRNAs with highest monotonic developmental decrease in Sox1::GFP progenitor cells. CPM, counts per million. (C) the best miR-541 and miR-92a-b sites on Satb2 3'UTR (blue sequence, 2.7 kb total length), as predicted by MiRanda (Enright et al., 2003). sc, MiRanda score; en, energy (Kcal/mol).

MiR-541-Satb2 3'UTR interaction

To better define miR-541/*Satb2* 3' UTR interactions, I mutated the three strongest predicted miR-541/*Satb2* 3'UTR binding sites. The predicted binding sequence to the seed of miR-541 at +156, +740 and +1724 of the *Satb2* 3'UTR were replaced with NotI restriction sequence (GCGGCCGC), dramatically reducing the predicted binding affinity (For more details go to material and methods section) (Figure 17).

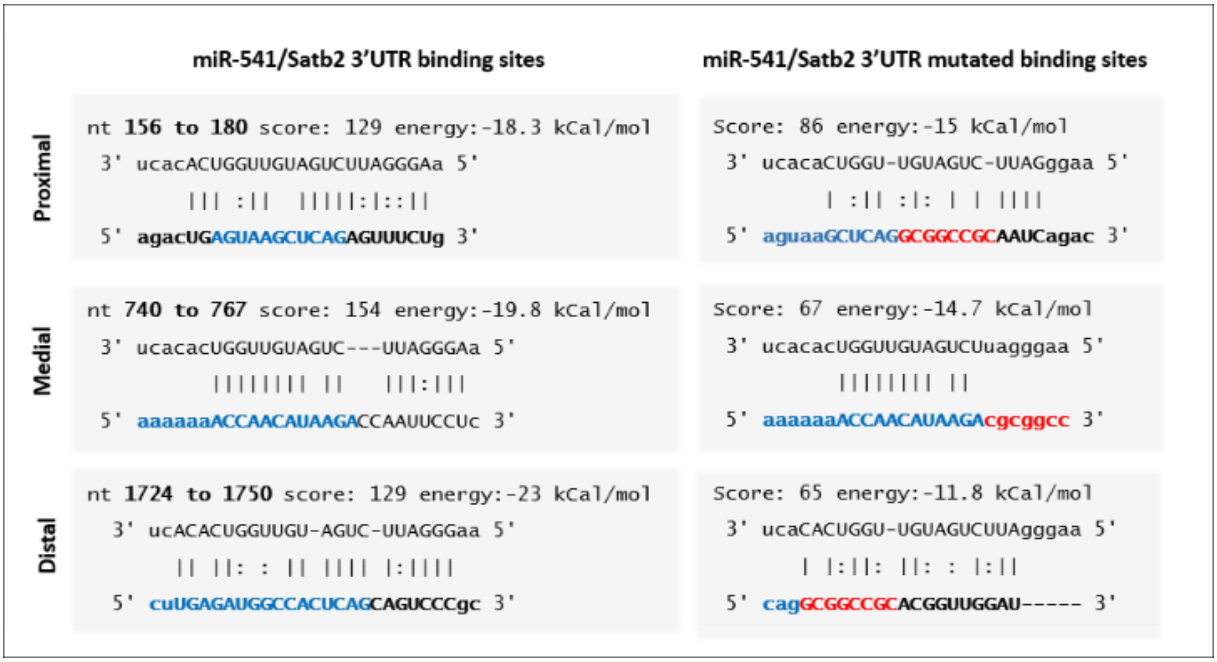

***Figure 17 - In silico* predictions for the binding affinity between mmu-miR-541-5p and Satb2 3'UTR.** Score > 120 estimates strong probability of interaction and energy < -18 kcal/Mol energy indicates strong chemical binding affinity. miRNA sequence (above) against UTR sequence (below), seed in red, upstream bases of interaction in blue. Panels show the wt (left) and corresponding mutated site (right).

I have first assayed the miRNA/mRNA binding affinity with an indirect method based on the transfection of a GFP reporter in a cell line deployed of mature miRNAs due to Dicer inactivation, the HTC-116 Dicer -/- colorectal cell line (Marranci et al., 2019). Cells were co-transfected the miR-541 mimic RNA or control mimic RNA sequence together with GFP reporter constructs bearing wt or mutated Satb2 3'UTR for each of these mutations (+156, proximal site; +740, medial site; +1724, distal site), in order to check the strength of these binding sites in inhibiting the translation of GFP reporter. The cells were incubated for 4 to 6 hours, the immunocytochemistry was performed two days after the transfection and the median of GFP pixel intensity was analyzed using ImageJ software (Figure 18A).

The mutation in the distal binding site (position +1724), which from the initial screening was revealed with the strongest predicted affinity (energy -23 Kcal/mol), affects reporter translation (Figure 18B).

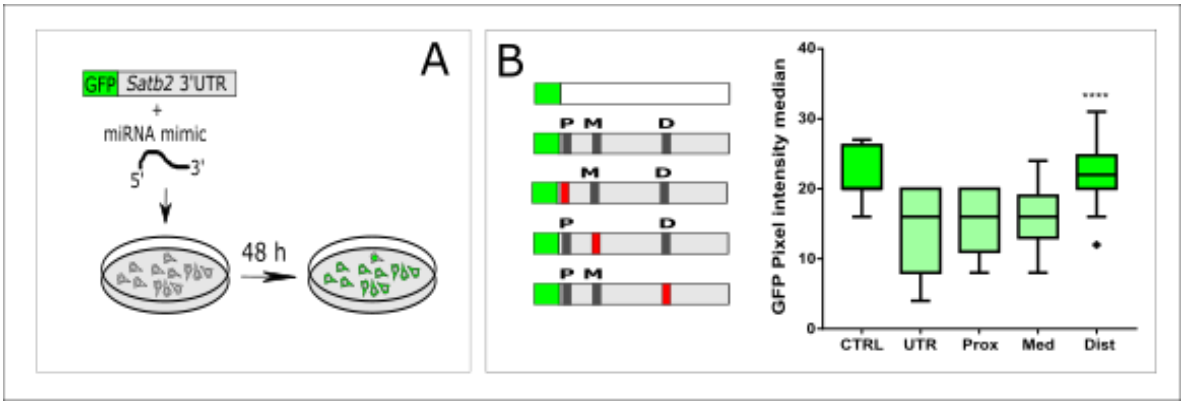

***Figure 18* – Analysis of miRNA/Satb2 3'UTR binding affinity with an indirect method.** (A) Schematic methodology representation of *in vitro* co-transfection assay of mature miR-541/control mimic together with GFP reporter constructs carrying *Satb2* 3'UTR mutated binding sites in HTC-116 colorectal cell line. (B) Median of pixel intensity for GFP (ICD) in HCT-116 cells (3 replicates per condition), measured by ImageJ software, one-way ANOVA significance test pValue < 0.05 (3 replicas per condition). P (proximal), M (medial) and D (Distal). Mutated seeds are shown in red. Dot represents outlier.

Next, I wondered if miRNA antagonism affected SATB2 translation directly or indirectly. Taking advantage of our *in vitro* corticalized mESCs cultures, progenitor cells at DIV12 were transfected with GFP reporter carrying *Satb2* 3'UTR sequences that had *NotI* included in the predicted binding sites for miR-541 and immunocytochemistry for GFP was performed after two days (DIV14) (Figure 19A). This allowed evaluating the translational inhibitory effect of endogenous miR-541 on the different mutated reporters. I compared the translation of GFP under WT *Satb2* 3'UTR reporter to the expression levels of mutated reports. As expected, the more distal site exerts the highest inhibition in agreement to the *in silico* predictions and the mutation in the medial site is also able to rescue SATB2 translation significantly, achieving levels similar to the control (GFP alone) (Figure 19B). These results are in accordance to the previous experiment of mature miR-541 transfection (Figure 18B) and confirm a direct interaction between miR-541 and the high affinity binding sites on the *Satb2* 3'UTR.

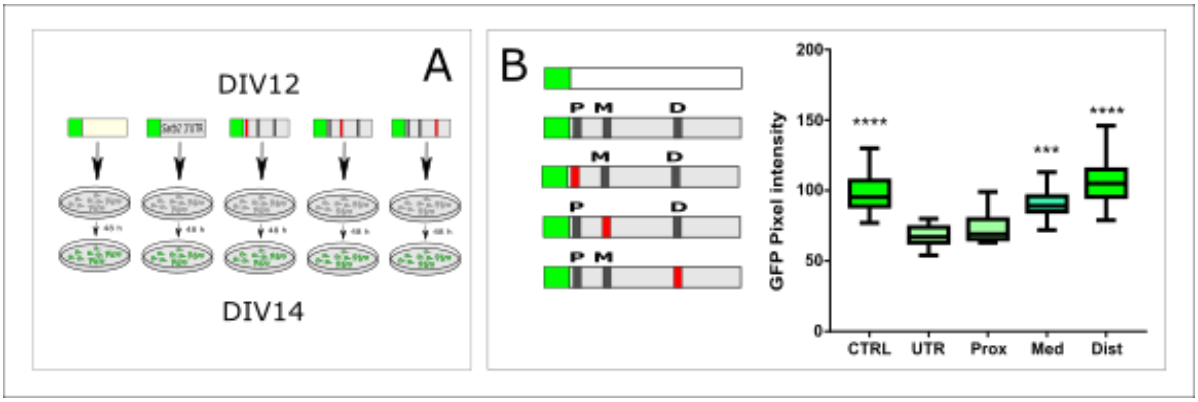

***Figure 19* - Direct interaction between miR-541 and the high affinity binding sites on the *Satb2* 3'UTR.** (A) *In vitro* transfection assay of GFP reporter carrying *Satb2* 3'UTR mutated binding sites in corticalized mESCs at DIV12. Mutated seeds are shown in red. (B) Pixel intensity for GFP (ICD), measured by ImageJ software, one-way ANOVA significance test pValue < 0.05 (3 biological replicas). P (proximal), M (medial) and D (Distal).

MiR-541 represses SATB2 translation *in vitro*

Next, I aimed to directly show if the inhibition of miR-541 and mir-92a/b could anticipate SATB2 translation in early cortical progenitor cells. To this aim I used the same protocol of mESC corticalization *in vitro* and transfected the cells with locked-RNAs complementary to the three miRNAs (antagomiRs) in order to functionally inhibit them (Figure 20A). AntagomiRs are small synthetic RNAs with a sequence perfectly complementary to the specific miRNA target and as such are used to silence endogenous microRNA (Krützfeldt et al., 2005). AntagomiRs against miR-541 and miR-92a/b were obtained from Qiagen and used according to the manufacturer's protocol (see Methods, Cell Trasfection). AntagomiRs were transfected at DIV10, when *Satb2* transcriptional level is very low, or at DIV12, when *Satb2* transcription is already robust but SATB2 translation is not detected, and SATB2 protein expression was analyzed 48 hours after transfection. The number of SATB2-positive cells is significantly increased in respect to cells transfected with a scrambled LNA, which sequence was not complementary to the *Satb2* 3'UTR (Figure 20B). Even though no significant differences have been found by transfection of antagomiR-541 and antagomiR-92a/b, antagomiR-541 seems to slightly increase SATB2 translation in comparison to the effect of miR-92 antagonist. The miR-541 repression anticipates the onset of protein detection (as seen by the effect of transfection at DIV10) also increasing the efficiency of translation at later time-points (indicated by the outcome of transfection at DIV12). Notably, the experiments of GFP reporters' transfection in corticalized mESCs reported above indicate that the effect of miR-541 on SATB2 translation is mediated by the high affinity binding sites in the 3'UTR.

Eventually, Keagan Dunville and I executed similar experiments with corticalized human induced pluripotent stem cells (hiPSCs) which I analyzed posteriorly (Figure 20A). HiPSCs were corticalized *in vitro* according to Chambers et al (Chambers et al., 2009). We transfected antagomiRs at DIV36, a time of *in vitro* cortical differentiation that roughly corresponds to mouse DIV12, respectively, in terms of corticalization progress (Gunhanlar et al., 2018; Portmann et al., 2012). miRNA depletion exerted similar effects to the ones with mouse cells (Figure 20B). These results support a general evolutionary conservation of the miRNAs and 3'UTR target sequences involved in SATB2 translational delay. In fact, binding sits for miR-541 and mir-92a/b are predicted in the human *Satb2* 3'UTR.

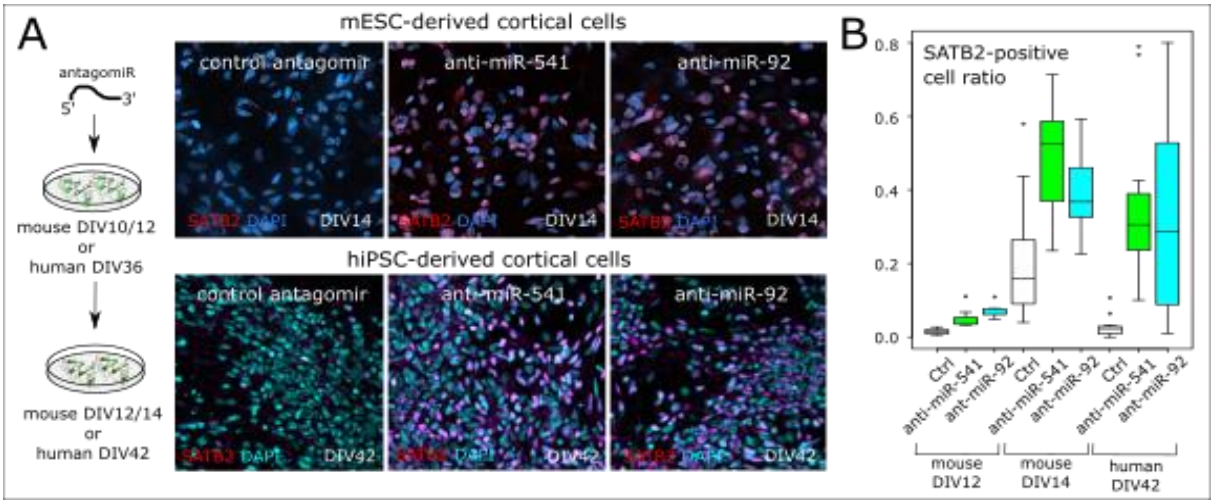

Figure 20 – **miR-541 repression on SATB2 translation in mESCs and hIPSCs.** (A) Effect of inhibition by LNA-antisense oligonucleotide transfection in corticalized mESCs. ICD show SATB2-positive nuclei 2 days after mESC transfection and 6 days after hiPSC lipofection, respectively. (B) Box plots report SATB2-positive nuclei proportion. Ctr, scrambled sequence LNA lipofection. Anti- miR-92 LNA oligonucleotide was used to inhibit both miR-92a and miR-92b, which share seed sequence. (n= 2 biological replicates) or hiPSCs (n= 3 biological replicates). Dots indicate outliers.

MiR-541 role in upper layer formation

As miR-541 revealed to be the best candidate for the regulation of SATB2 translation, which in turn is a crucial factor of superficial layer neuronal identity, I tried to better clarify the role of miR-541 in upper layer formation. First, I compared the level of miR-541 expression to the level of SATB2 protein in embryonic cortical sections, combining miR-541 *in situ* hybridization with SATB2 immunocytodetection. At early developmental stage (E13.5), miR-541 is spread all over the ventricular, subventricular and marginal zone (VZ, SVZ and MZ, respectively) while SATB2 is almost completely absent (Figure 21A). Later, when I compared the miR-541 and SATB2 expression at E15.5, I observed that SATB2 is present in SVZ, in the intermediate zone (IZ) and in migrating cells, but miR-541 showed an unexpected pattern being still strongly present in the cortical plate even though did not clearly co-localize with SATB2 (Figure 21B). I thus, speculated that miR-541 expression in cortical plate at E15.5 could be related to the inhibition of other CITFs than SATB2.

Previous studies have demonstrated that upper layers of the cortex are formed not only by SATB2 positive neurons but also Unc5D/Svet1 positive neurons, with this second class appearing only later (P2) (Hevner et al., 2001; Tarabykin et., 2001; Britanova et al., 2008). Thus, I was curious to understand if these two classes are both under the control of miR-541 and this could account for miR-541 presence in the cortex at E15.5.

Unc5 receptors are a family of Netrin1 receptors that include Unc5A, Unc5B, Unc5C and Unc5D. From the literature, it is known that Netrin1 receptor Unc5C is under the control of *Satb2* (Srivatsa et al., 2014) and I wondered if Unc5D could also be related to *Satb2*. Thus, I investigated the Unc5A-D expression throughout corticogenesis. As expected, Unc5C levels were aligned with *Satb2* increase (Srivatsa et al., 2014). However, also Unc5D shows increased level of expression throughout corticogenesis in accordance to *Satb2* pattern. By COTAN, high COEX index was observed between *Unc5D* and *Satb2* at E13.5, meaning that early cells co-express both mRNAS, but this co-localization is lost at E15.5 (Figure 21C). After this observation, I reasoned that both SATB2- and UNC5D-positive cells could be generated by means of post-transcriptional control processes. To assay if also Unc5D could be under miR-541 control, we checked for *in silico* miR-541 binding sites in its 3'UTR (Enright et al., 2003) and found three binding sites, two of them with high score and low energy values (Figure 21D). I speculate that Unc5D may be under both SATB2 and miR-541 control and, that miR-541 persistence in some cells of the cortical plate at E15.5 might delay UNC5D translation and

UNC5D-positive neurons generation that conclude their maturation at P2. However, it is not clear how *Satb2* could escape mir-541-mediated translational inhibition in some cells at DIV 15.5. In this view, one possible explanation of the differential inhibition of *Satb2* and *Unc5d* by miR-541 might be a differential affinity of the miRNA to the two 3'UTRs. While miR-541 binding affinity to *Satb2* 3'UTR is -23kcal/mol, miR-541 binding affinity to *Unc5d* is -18kcal/mol. Further experiments in the differentiation mechanism of Unc5D cells and mir-541 characterization over corticogenesis are needed to better discuss miR-541 involvement in UNC5D-positive neurons.

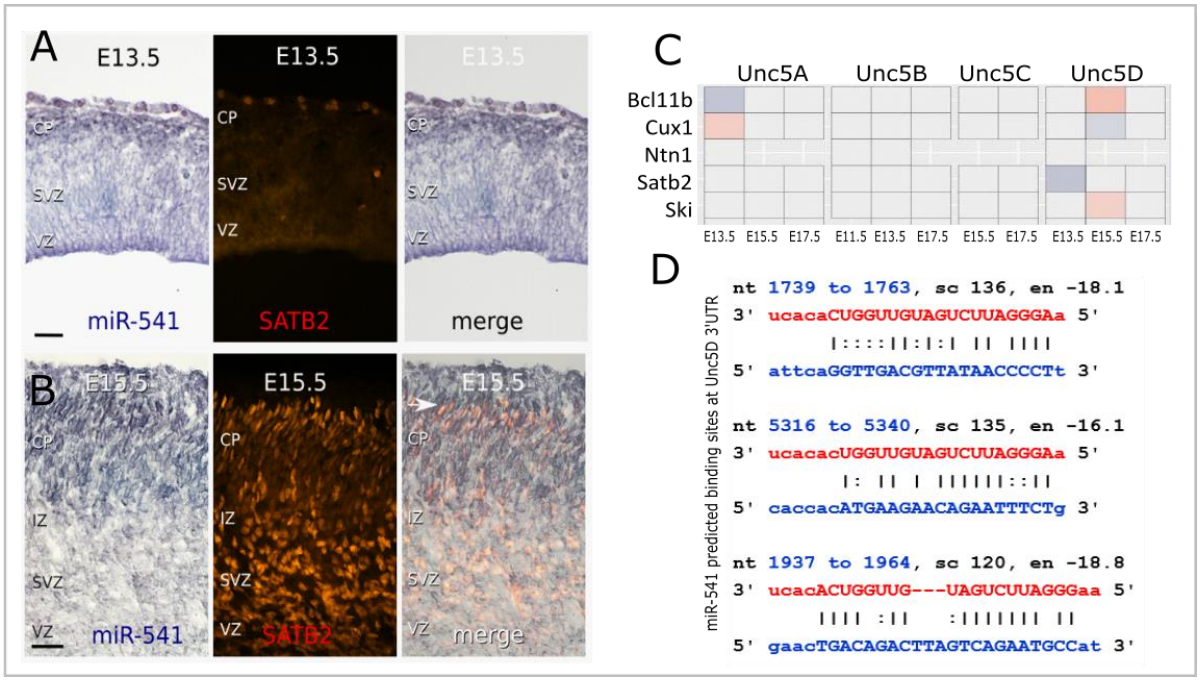

***Figure 21* – miR-541 and its intricate role in upper layer formation.** (A) (E13.5) and (B) (E15.5) In situ hybridization (ISH) miR-541 detection (BM-purple staining) compared to SATB2 immunodetection (red fluorescence). CP, cortical plate; IZ, intermediate zone; SVZ, subventricular zone; VZ, ventricular zone. Arrow indicates newly migrated SATB2-positive cells. Scale bar, 50 µm. (C) COTAN COEX values of Netrin 1 receptors (Unc5A-D) at the different developmental times E11.5, E13.5, E15.5 and E17.5 in respect to main CITFs for corticogenesis. The absence of time-points is due to absent detection of gene at respective time-point. (D) Best miR-541 sites on Unc5D 3'UTR (blue sequence, 6.17 kb total length), as predicted by MiRanda (Enright et al., 2003). sc, MiRanda score; en, energy (Kcal/mol).

MiR-541 and let-7b have opposite expression patterns, controlling inversely the SPN identity formation

As it was described in the Introduction chapter, miR-9, miR-128 and let-7 are the main regulators of cortical layering as they work with temporally opposite gradients of expression in order to change the competence of the stem cells during corticogenesis and create all the six layers accordingly to a time-manner regulation (Shu et al., 2019). When I checked their pattern of expression along corticogenesis using Sox1::GFP progenitors, I noticed that it is not similar to the one observed by miR-541 (Figure 22). While miR-541 decreases between DIV10 and DIV16, miR-128 and miRNA-9 keep their levels relatively high throughout corticogenesis. Moreover, let-7b shows an opposite pattern of expression in respect to miR-541, increasing at late stages of cortical development. Indeed, this information confirms the inverse capability to repress and promote SPN identity, respectively.

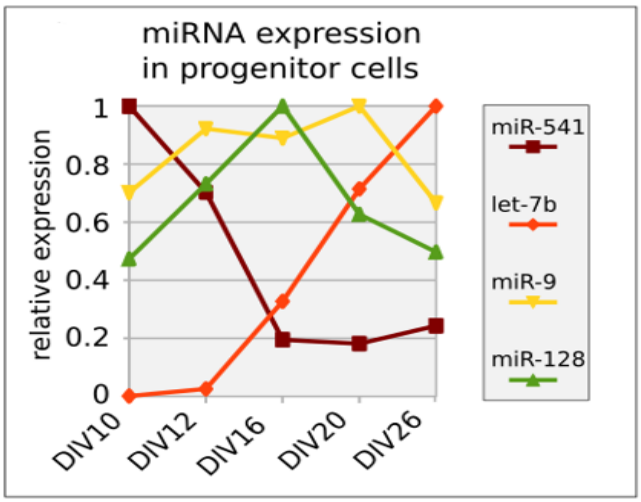

Figure 22 **- Developmental expression patterns of different miRNAs involved in layer identity.**

miR-541 and miR-92a/b cortical targets

To analyze the biological relevance of miR-92a/b and miR-541 in corticogenesis, I started by comparing miRNAs *in silico* predicted binding sites to *Satb2* 3'UTR with the predicted binding sites of the whole mouse miRNAome. To perform such analysis, I have used the same *in silico* prediction approach (Enright et al., 2003) through miRanda software, that revealed itself successful in identifying the high affinity binding site of miR-541 to *Satb2* 3'UTR. I used the same thresholds as before (score > 120 and energy < -18 Kcal/mol) for all miRNAs in the mouse database, checked for their affinity to the *Satb2* 3'UTR and plotted the sum of the scores normalized for each binding site that matched our criteria.

From the analysis, the majority of mouse miRNAs shows no predicted binding site to *Satb2* and, among those with affinity over the threshold, miR-92a/b are very expressed in cortical progenitors (high average of counts), but belong to the group with the lowest affinity. On the other hand, miR-541 shows lower level of expression but much higher *in silico* affinity to *Satb2* 3'UTR than mir-92a/b (Figure 23A). This is in accordance to the similar effect exerted by miR-541 and miR-92a/b inactivation on SATB2 levels, because miRNA-mediated translational inhibition is expected to depend both on their affinity to mRNA target and on miRNA expression level, due to the stoichiometric mechanism of miRNA action (Chekulaeva et al., 2009; Guo et al., 2010).

The time-based generation of layer-specific neurons is controlled by precise miRNAs that present temporal gradient of expression during the process of neocortical neurogenesis. The overexpression of miR-128 and miR-9 boosts significantly the generation of layer VI and V, respectively with consequent decrease of neurons in layers IV-II. Instead, let-7 overexpression leads to the opposite effect, increasing the number of neurons in the upper layers at the expenses of those in deep-layer VI. Interestingly, co-overexpression of miR-128 and let-7, that present opposite patterns of expression, lead to a neutral phenotype (Shu et al., 2019). Previous result demonstrated that miR-541 presents a different pattern of expression from these miRNAs. Thus, the next step was to compare miR-541 and miR-92a/b targets with the targets of these three miRNAs of corticogenesis.

We took advantage of the system established by Galfrè & Morandin, 2020 that selected the most known markers of cortical layer identity (10 genes in total) and divided into five clusters accordingly to their layer identity (*Vim* and *Hes1* as genes for progenitor cells; *Reln* and *Lhx5* as genes related to layer I; *Cux1* and *Satb2* as genes for layer II/III; *Sox5* and *Rorb* as genes for layer

IV; *Bcl11b* and *Fezf2* as genes for layer V/VI identity). Then, they identified the top genes most associated to each one of these markers (25 genes for each of the primary genes), to a total of 215 secondary markers as 35 genes were shared by two primary markers. The normalized co-expression index of these genes was used as input data for the screening the whole dataset. This technique allows the identification of novel markers for corticogenesis kept unknown so far. We then, correlate the six miRNAs (miR-541, miR-92a/b, let-7, miR-9 and miR-128) with a signature of 404 layer identity genes previously obtained by the above described approach (Galfrè & Morandin, 2020). Among the six miRNAs, *let*-7 and miR-541 presented *in silico* affinity with more than half of the genes with embryonic cortical marker signature (Figure 23B).

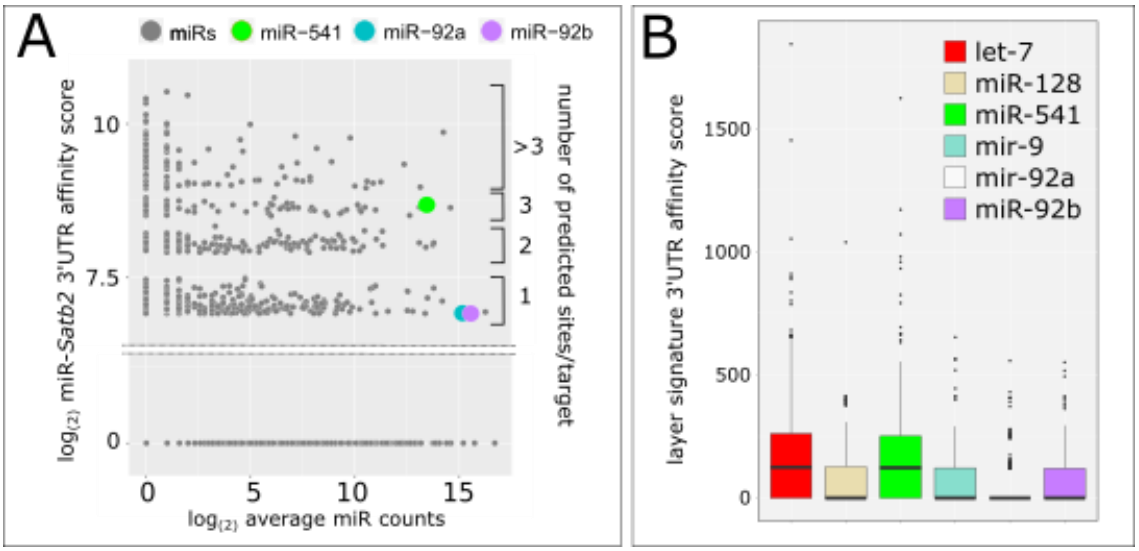

***Figure 23 - In silico* analysis of miRNA/mRNA interactions.** (A) *In silico* comparison of the affinity of mouse miRNAome (grey dots), miR-92a/b and miR-541 (colored dots) to *Satb2* 3'UTR (Ensembl Mus musculus Satb2-201 cDNA 3' UTR), in relation to the average miRNA expression levels during corticogenesis. (B) *In silico* affinity of cortical miRNAs to the 3' UTR of an embryonic layer gene signature (385 genes) (Galfrè et al., 2020).

Next, I investigated which functional pathways the genes with highest *in silico* affinity to the six miRNAs were involved. Gene ontology has been used to associate genes accordingly to GO terms. These terms separate genes in respect to their biological processes, cellular components and molecular functions. To perform this search, I used *G*ene *O*ntology en*RI*chment ana*L*ysis and visua*L*iz*A*tion tool (*GORILLA*). GORILLA software applies a flexible threshold statistical method in order to identify enriched GO terms in ranked lists of genes. The outcome is organized in a hierarchical charter with all the associations among genes, where each one of

these might be annotated to one or more terms (Eden et al., 2009). I have selected the two unranked list of genes as running mode to confront the target set of genes (enriched for specific miRNA) against all the genes from Galfrè & Morandin 2020 (P-value threshold of 10^{-3}). Remarkably, among the mRNAs with the highest *in silico* affinity (total score higher than 400) for the 6 miRNAs, only the putative targets of miR-541 showed significant enrichment in GO terms (Figure 24A). Interestingly, all the enriched genes were associated to biological processes related to structural morphogenesis and out of the 13 possible target genes, 8 presented highest enrichment in biological processes associated to axonal projection functions (cortical neuronal layering and migration, axon guidance, corpus callosum disturbances) (Figure 24A). In the panel of mir-541 gene targets enriched GO, were found genes associated with neural progenitor proliferation (*Rbfox2* and *Zeb2*), neuronal migration (*Dcx*, *Plxna4* and *Tcf4*), neuronal polarization (*Cntn2*), neurite outgrowth (*Gas7*) and upper layer formation (*Cdk5*) (Figure 24B) (Caubit et al., 2016; Chen et al., 2016; Hatanaka et al., 2019; Li et al., 2019; Namba et al., 2014; Okamoto et al., 2013; Pramparo et al., 2010; Shinmyo et al., 2017; Ton and Kathryn Iovine, 2012; Zhang et al., 2016).

Finally, I compared the change of E/I read counts by EISA of 7 out of the 8 genes (not enough *Cdk5r* read counts were available for a significant analysis) to that of the genes of the embryonic cortical marker signature (Figure 24C). The results indicate that all these 7 genes increase their E/I read count ratio between E13.5 and E17.5 and that there is a general correlation between E/I read count increase and mir-541/mRNA affinity score, supporting a relevant role of miR-541 in their post-transcriptional control during early corticogenesis.

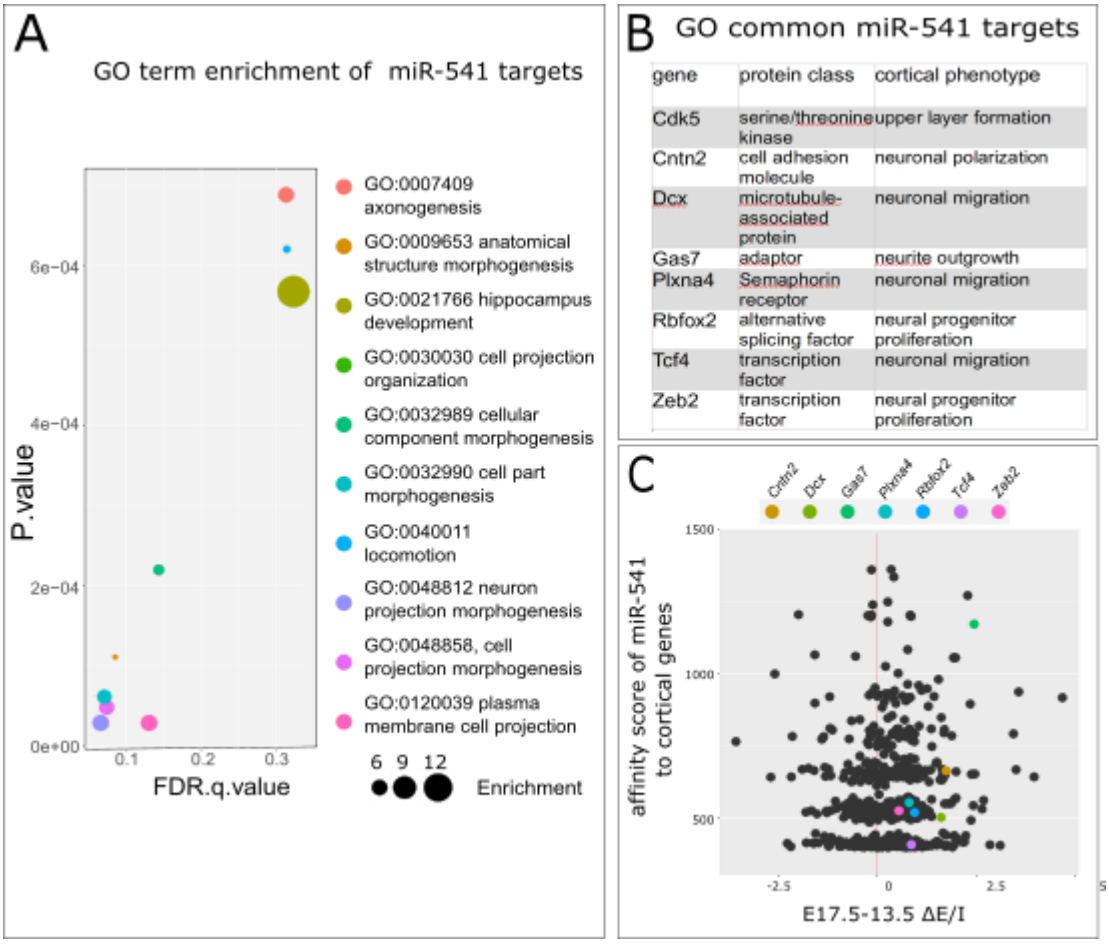

Figure 24 – ***In silico*** **miR-541 GO analysis.** (A) GO enrichment of the mir-541 gene targets with high *in silico* affinity to *Satb2* 3'UTR (cumulative score higher than 400, n=48) (Enright et al., 2003) with respect to the layer gene signature employed in B. (B) list of the 8 genes common to all the GO terms shown in A. (C) plot showing E/I read counts developmental increase (X-axis) with respect to miR-541/mRNA affinity score (Y-axis) to genes of the embryonic cortical marker signature (Galfrè et al., 2020). Colored dots indicate genes listed in D. Names in labels indicate the 5 genes with the highest E/I read count ratio increase and mir-541/mRNA affinity score.

miR-541 evolutionary conservation

Unlike let-7b, miR-128 and miR-9, which are evolutionarily conserved in all animals, mir-541 appeared recently during mammalian evolution. In the murine, miR-541 is encoded by Mirg (miRNA-containing gene), inside the Dlk1-Dio3 locus (Teixeira et al., 2008). I speculated that Satb2 3'UTR acquired high affinity binding sites for miR-541 after appearance of Mirg in Eutherians. Using miRANDA prediction, I investigated *in silico* the affinity of *Satb2* 3'UTR for miR-541 binding in different Eutherian and non-Eutherian species. In fact, the binding affinity of miR-541 to *Satb2* 3'UTR seems stronger and evolutionary conserved in eutherian species (Figure 25), according to a model of co-evolution of the miRNA and its mRNA target (see Discussion).

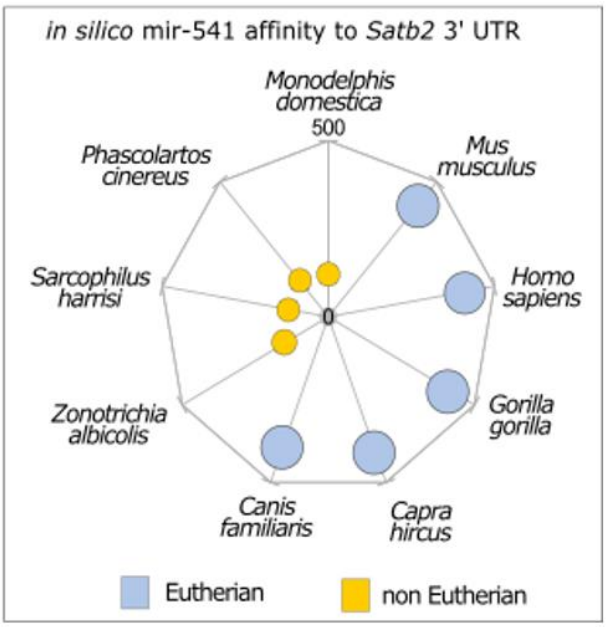

***Figure 25 - in silico* affinity of *Satb2* 3'UTR for miR-541 binding in different Eutherian and non-Eutherian species.**

DISCUSSION

Satb2 is under post-transcriptional control

It was investigated the pattern of CITF expression through single-cell RNA-seq. This analysis allowed to point out already known interactions of CITFs and to highlight an unexpected pattern of Satb2 mRNA expression at the single cell level.

First of all, *Satb2* is present and expressed at the same level of housekeeping genes since E11.5. Housekeeping genes are genes constitutively expressed in all cells in the organism and are fundamental for the conservation of basal cellular functions (Eisenberg & Levanon, 2013). Therefore, I would expect *Satb2* gene expression to be biologically active since the beginning of cortex development. Instead, SATB2 is not present until late stages in the cortex. Besides, at the same developmental time, E11.5, *Bcl11b* shows already strong correlation with *Eomes* (*Tbr2)* and *Tbr1*, markers for radial glia cells (RGCs) to intermediate neural progenitors (IPs) transition and early post-mitotic cells, respectively; however, *Satb2* does not correlate at all with any markers.

At E13.5, *Bcl11b* anti-correlates with *Neurogenin2* (*Neurog2*) and *Tbr2* transcription factors. It is known that *Neurog2* transcription factor, through activation of *Tbr2* transcription, sponsors the transition from RGCs to IPs and specify dorsal glutamatergic projection neurons before they initiate migration (Kovach et al., 2013). This anti-correlation is probably due to the fact that *Bcl11b* cells are starting to migrate to form layer V, thus at least some of the cells in these subsets do not express these markers anymore. To support this hypothesis, it is possible to see that at the same developmental time, E13.5, *Satb2* shows, as expected, the same pattern of expression of *Ctip2* but with faint intensity. This happens since deeper layers are being generated and SATB2 only appears later in corticogenesis (Bertacchi et al., 2015; Alcamo et al., 2008; Britanova et al., 2008; Gaspard et al., 2008; Leone et al., 2008; Salazar et al., 2017; Leone et al., 2015).

Another interesting fact is that *Bcl11b* shows high correlation with *Tbr1* (Hevner et al., 2001). This is explained by the fact that *Tbr1* is a marker for early-born neurons of the preplate and layer VI. At E13.5, the main marker for subcerebral projection neurons, *Bcl11b*, is very likely to produce cells that, through migration from the preplate, form the deeper layers of the cortex. Instead and supporting this theory, *Satb2* shows a very slight correlation with *Tbr1*, probably because around E13.5, when deeper layers are originated, this gene is still very much repressed.

Surprisingly, at this same stage (E13.5), *Satb2* does not show anti-correlation with *Bcl11b*. Previous studies demonstrated that *Satb2* represses the DPN gene *Bcl11b* and, through

this repression, becomes fundamental for the establishment of SPN (Alcamo et al., 2008; Leone et al., 2008; Srinivasan et al., 2012). Thus, the data observed can be due to two different reasons. First, the deeper layers are still being formed so *Bcl11b* mRNA is very much expressed and needed at that stage. Secondly, the amount of stable *Satb2* is still not sufficient to block *Bcl11b* mRNA and consequently, to block DPNs formation and to start SPNs generation. Thus, one can conclude that even though *Satb2* mRNA is expressed since E11.5, its translation is probably repressed by some post-transcriptional mechanism at least until E13.5. In fact, this interpretation is well in line with the original observation that SATB2 protein is not detectable before E14.5 in mouse developing cortex (Britanova O et al., 2005).

Taking advantage of COTAN analysis, I could check the global degree of co-expression of any single gene in respect to all the other genes of the dataset by the Gene Differentiation Index (GDI) integrating COEX values (Galfrè and Morandin, 2020). This method allows us to infer the propensity of CTIFs to be expressed in restricted cell subsets during corticogenesis.

Interestingly, *Tbr1* mRNA presents a high GDI expression in the beginning of corticogenesis and it decreases dramatically in the end of the process. This fact could be due to its functions related to guidance of cortical axons and thus, must be present in order to insure correct laminar organization and proper projection formation of several neuronal subtypes. Besides, it has been demonstrated to have high degree of connectivity with other transcription factors such as *Fezf2* and *Satb2*, working together in the M8 hub of genes (Kang et al., 2011). *Fezf2* and its downstream effector *Bcl11b* increase their GDI levels between E13.5 and E15.5 in accordance to the time of subcerebral projection neurons generation (Chen et al., 2008).

Instead, *Satb2* increases its relative expression from E11.5 to E15.5 together with *Cux1*, elevating also their GDI along corticogenesis, according to their pattern of protein expression in cells subsets. It is worthy noticing that even though *Satb2* increases its GDI, its levels are never too high. Previous studies have demonstrated that SATB2 is expressed in not only upper layers, where it is crucial for callosal projections generation, but it is also present in layer IV and V of the cortex thus, its GDI levels do not come as a surprise (Fame et al., 2011; Harb et al., 2016).

Finally, the lack of a cell-type restricted distribution of *Satb2* mRNA especially at early stages is also suggested by its partial overlap with *Bcl11b* mRNA in E13.5 cell clusters, as compared to E17.5 clusters by the t-SNE analysis. It is interesting to point out the fact that the small amount of co-localization between *Bcl11b* and *Satb2* at E17.5 is due to the formation of layer IV related to somatosensory cortex. In this layer, LMO4 protein competes with *Satb2* for the binding to *Bcl11b* and its consequent repression and thus, *Satb2* is not able to block *Bcl11b* completely, allowing the co-localization of two neuronal subtypes that project to brainstem in

deeper layer IV and contralateral cortex at upper layer IV (Harb et al., 2016). Besides that, recently De Léon Reyes et al. have identified numerous exuberant CPN in layer IV in new-born mice that gradually decreases during postnatal development (De León Reyes et al., 2019). Thus, it is possible that this co-localization is due to layer IV cortical neurons that present transient callosal axons but that are eventually eliminated with brain maturation.

Together with that, callosal projection neurons have been found also in the deep layer V with around 40% of these CPN projecting to the prefrontal motor cortex (Fame et al., 2011). Thus, the fact that at E17.5 there is co-localization of *Bcl11b and Satb2* transcripts could just mean that *Satb2* has other functions besides CPN in the upper layers and these other functions in the other cortical layers are probably controlled by different mechanisms.

Taking all this data together, I can conclude that, in the early stages of corticogenesis not all CITF transcripts have yet committed to a particular neuronal identity. In particular, *Satb2* shows the lowest specificity and this observation prompted us to investigate the mechanisms at the bases of such fascinating incoherence between its RNA and protein levels.

RNA-induced silencing complex controls *Satb2* 3'UTR

Initially, gene expression studies in eukaryotes were based on the analysis of steady-state mRNA levels. However, it is now known that mRNA transcription rates, the stability of mRNAs and the different levels of translational initiation are dynamically expressed along the neocortical prenatal neurogenesis (Keene, 2007). Guo H et al. in 2010 have demonstrated that miRNAs can change mRNA levels and gene expression causing mRNA destabilization that leads to reduced protein output. Consequently, in the last decade, several studies have been focusing on the post-transcriptional control during corticogenesis (Rosa & Brivanlou, 2011; De Chevigny et al., 2012; McLoughlin et al., 2012; Bian et al., 2013; Nowakowski et al., 2018;; Terrigno et al., 2018). More specifically, for our interest, *Satb2* has already been associated with strong post-transcriptional regulation in carcinogenesis but the post-transcriptional control over *Satb2* during corticogenesis is still under scrutiny (Yang et al., 2013; Jiang et al., 2015; Luo et al., 2016; Chen et al., 2018; Chen et al., 2019).

Exon-Intron Split analysis (EISA) demonstrated that the time *Satb2* transcription starts is not in accordance to *Satb2* mRNA stability and consequent SATB2 translation. This lack of mRNA-protein correlation serves as another proof of post-transcriptional regulation over *Satb2*, which I proceeded to investigate further on this thesis.

I based myself on the previous results and wondered which kind of post-transcriptional control could be involved in the formation of upper layer callosal projection neurons. I speculated that a tight inhibitory regulation of translation could be achieved through microRNA (miRNA) and the RNA-induced silencing complex (RISC). Thus, I performed Chromatin immunoprecipitation (CHIP) for Ago2 in order to evaluate RISC-mediated inhibition of *Satb2* expression (Pandolfini et al., 2016). The results confirmed my theory of miRNA-mediated control over *Satb2* translation. The experiments with GFP-3'UTR *Satb2* transfections *in vitro* demonstrated that the GFP protein was faint in the early stages (DIV12) when *Satb2* 3'UTR is repressed.

At this point, I look at the effect of *Satb2* 3'UTR *in vivo*. I observed that SATB2-GFP double positive cells in the control (cortex electroporated with GFP alone) are present in all layers of the cortex. However, it is obvious to notice that SATB2-GFP double positive cells in the cortex electroporated with GFP reporter carrying *Satb2* 3'UTR are more concentrated in the layers II/III of the cortex. This fact proves that *Satb2* 3'UTR by itself is able *in vivo* to inhibit translation in early generated neurons that do not express SATB2 protein.

As it was mentioned before and has been already described in the literature, SATB2 and BCL11B proteins are mutually exclusive in the majority of neocortical cells at the time they begin to establish connections with other neurons (Britanova et al., 2008). Thus, I wondered if the same *Satb2* 3'UTR could also block the translation of BCL11B in the deeper layers *in vivo*. I performed immunohistochemistry (IHC) using an antibody against BCL11B in the slices electroporated with GFP reporter carrying *Satb2* 3'UTR or GFP alone. At the same developmental time as before (E13.5), the number of BCL11B/GFP double positive cells is significantly lower in the cortex electroporated with *Satb2* 3'UTR-GFP in comparison to the cortex electroporated with GFP alone. This result is in good agreement with the hypothesis that the 3'UTR of *Satb2* by itself is able to block BCL11B translation in deeper layers *in vivo*. Our results are also in accordance to Tarabykin's group that in 2014 has identified a Netrin1 receptor, Unc5C, that is fundamental for commissural axon guidance, to be under the control of *Satb2*. By the combination of *in situ* hybridization (ISH) using a probe against Unc5C and IHC using antibodies against SATB2 and BCL11B their group demonstrated that Unc5C was present in both upper and deeper layers. However, they have seen that Unc5C and SATB2 were usually co-expressed while, the Unc5C and BCL11B were almost never expressed in the same cells, even in layer V where they found Unc5C and SATB2 co-expression but none of those cells were BCL11B positive (Srivatsa et al., 2014).

MiR-541 controls SATB2 and mediates the SPN formation

The results from miR-catch analysis point out two possible miRNAs as responsible for SATB2 inhibition in early stages of cortical development, miR-92a/b and miR-541. Looking into the literature, miR-92 is part of miR-17-92 cluster which regulates neural stem cell expansion and transition to intermediate progenitors during neocortex development (Bian et al., 2013). This cluster plays a key role in the inhibition of EOMESODERMIN (TBR2) and consequently, in the repression of basal progenitor early generation (Nowakowski et al., 2013; Bian et al., 2013) by inhibiting the transition from RGCs to IPs. Indeed, as the production of early neurons by RGs starts, miR-92 levels decrease in order to give origin to IP and consequently, neurons.

Another interesting fact is that miR-92b is also associated to commissural axon guidance and correct callosal projection neurons' organization. The development of nervous system depends on complex interaction networks intermediated by diverse attractive and repulsive guidance cues sent to navigating axons and the way these axons respond to those signals (Cárdenas et al., 2018; Dominici et al., 2017). Indeed, *Netrin1* and its receptor Deleted in Colorectal Cancer (DCC) are crucial for axonal crossing through the midline by commissural projection neurons. However, this mechanism is tricky as neocortical callosal axons are neither directly attracted to the midline by *Netrin1* (Fothergill et al., 2014) nor *Netrin1* by itself is necessary for the commissural axonal guidance (Dominici et al., 2017). Instead, callosal axons use DCC to inhibit *Robo1* and attenuate *Slit2* repulsiveness, the real fundamental gene for commissural axon projections and midline crossing. If *Slit2* repulsiveness is prevented in the pre-crossing axons, they are able to approach and cross the midline, forming *Corpus callosum* (Fothergill et al., 2014). Even though studies in callosal axons projections through the midline are still under scrutiny, it has been demonstrated that, in early stages of corticogenesis miR-92b binds to the 3'UTR of *Robo1*, repressing it and consequently, preventing *Slit2* repulsiveness from the midline in the spinal cord (Yang et al., 2018). Thus, miR-92b could have the same function in callosal axons projections and be helping them to approach the midline. Instead, at late stages, when *Slit2* repulsiveness is crucial, miR-92b decreases its levels of expression. Together with that, Fothergill et al. showed that DCC expression significantly decreases over time from E16 to P0, in accordance to the miR-92b pattern of expression observed in our experiments. This decreasing of DCC expression leads to the increase of *Robo1* levels and consequently, *Slit2* repulsiveness, allowing the axons after crossing the midline to be repelled away from it and form the *Corpus callosum*.

Several studies have been reporting miR-541 involvement in numerous tumors with possible potential to work as tumor suppressor in lung cancer (Leivonen et al., 2014; L. Xu et al., 2018). Although its role in corticogenesis has not yet been much studied, it has been also considered a crucial miRNA for axonal maintenance and neuronal differentiation (Jun Zhang et al., 2011). In our results it demonstrated a strong expression that is also in temporal accordance to the SATB2 translational inhibition with a very convenient decay of expression of this miRNA between DIV12 and DIV16 (Figure 16A), followed by downregulation in cortical progenitors from DIV10 to DIV26 of a subset of miRNAs (Figure 16B). By the *in silico* analysis, it showed very convincing binding sites to *Satb2* 3'UTR and stronger affinity in respect to miR-92a/b. One possible explanation for this effect could be the fact that miR-92 mechanism of action is not over SATB2 directly and specifically but over callosal projection neurons in general, including in cells that do not express *Satb2* while miR-541 would act more specifically over *Satb2* 3'UTR.

Taking advantage of our *in vitro* protocols of mESC and iPSC corticalization, I transfected mouse and human progenitor cells with antagomiR for miR-541 and miR-92a/b and both cell lines increased SATB2 translation upon treatment with both repressors.

It is worth noting that SATB2 translation after miR-92a/b repression could be associated with an indirect activation of *Tbr2*. *Eosomesodermin* (*Tbr2*) is specifically expressed in the intermediate basal progenitor cells of the developing cerebral cortex (Sessa et al., 2008). The miR-92a/b present binding sites for *Tbr2* and the inhibition of this miRNA could be associated with increased levels of Tbr2-positive cells. However, miR-541 does not present predicted binding sites on *Eomesodermin* 3'UTR. Thus, the increasing in the expression of SATB2 is not related with increased levels of Tbr2, that would lead to increase in IPCs, surface expansion and thickness and higher number of neurons in the cortical layers. The effect observed, probably, is due to a direct interplay between miR-541 and *Satb2* 3'UTR. Moreover, the exceeding SATB2 positive neurons observed at early stage of *in vitro* development might be born by direct neurogenesis from RGs. An important evidence is the evolutionary functional conservation of miR-541, as mouse and human miR-541-depleted cells show the same expected phenotype of anticipated SATB2 translation.

By combining *in situ* hybridization with immunohistochemistry, I used a probe against mature miR-541 and antibody against SATB2 to check how they would interact *in vivo* at E13.5. It was observed an interesting and not expected pattern of expression. It is important to notice that, at this time-point, miR-541 is still present in the cortical plate even though there is no co-localization between miR-541 and SATB2 cells. This fact is probably because there are two different subpopulations of upper layer neurons. The first type are SATB2-positive cells that start

to migrate as they exit cell cycle and are the first ones to arrive at the cortical plate around E14.5. Thus, mir-541 decreases to allow the translation of the first SATB2-positive neurons in the upper layers. However, the second type are Unc5D/Svet1 cells that undergo a longer waiting period in the SVZ (3 to 4 days) and only start to migrate after E17.5 (Britanova et al., 2008; Tarabykin et al., 2001).

Previous in this discussion, I mentioned the fact that Netrin1's Unc5C receptor is under the control of *Satb2* (Srivatsa et al., 2014). By single cell data sets, I saw co-localization of *Unc5D* and *Satb2* at E13.5 that, eventually, at E15.5 is lost and instead, *Unc5D* anti-correlates with *Satb2* inductor factor, *Ski*. This can be interpreted as a true indicator of two subtypes of callosal projections: the ones that are only S*atb2* since the beginning and migrate suddenly at E13.5 and the others, that lose their *Satb2* expression at E15.5 becoming only *Unc5D* progenitor cells. Therefore, it is likely that at E13.5, all cells that are committed to become callosal neurons present *Satb2* mRNA. I hypothesized that, at least for a while, these cells would be under the control of miR-541, which would not only block *Satb2* but also repress *Unc5D*. Using miRanda analysis, I found three binding sites for miR-541 in the *Unc5D* 3'UTR, two of them with high score and low energy values. Thus, a further evidence of a possible miR-541 repression over all callosal cells during corticogenesis. This fact would also explain why miR-541 is still expressed in the upper layers at E15.5. This mir-541 remains in the upper layers to prevent the expression of the second type of upper layer neurons that should start translation only after E17.5. Indeed, when this second class of cells start to migrate, their *Unc5D* expression is downregulated (Yamagishi et al., 2011). I speculate that this downregulation might occur in part to allow those later cells to cross FLRT2-positive layers and in part, probably, because of the miR-541-mediated repression over these cells. Actually, cells only reacquire UNC5D expression again and conclude their maturation after P2 when mir-541 is not present anymore. Even though this could be considered a theory, it is reasonable to take it into account and future studies on *Unc5D* and miR-541 interaction should be performed to clarify the point.

The *in vitro* GFP reporter activity of *Satb2* 3'UTR mutants and the overexpression of mature miR-541 in cell cultures transfected with *Satb2* mutants confirmed the affinity of miR-541 for 3'UTR and the potency of its repression over SATB2 translation.

It is crucial to point out that the effect seen by miR-541 could be due to a blockade of BCL11B at late stages instead of the repression of SATB2 at early stages. However, this is very unlikely event. Primarily, by *in silico* analysis, I checked that miR-541 does not present binding sites to the 3'UTR of *Bcl11b*. Besides that, the pattern of miR-541 expression by *in situ*

hybridization contradicts this hypothesis as miR-541 should be present in the deeper layers at late stages (to repress *Bcl11b*) but instead, it is present in the upper ones.

Evolutionary appearance of eutherian animals is in accordance with time of miR-541 appearance

Distinctly from *let*-7b, miR-128 and miR-9, which are common to invertebrates, vertebrates and mammals (Ha et al., 2009), there are miRNAs that show specific phylogenetic expression. This is the case for miR-541 that appeared recently during vertebrate evolution and it is present only in Eutherian mammals. The miR-541 was identified as a member of miR379-410 family (Fiore et al., 2009), a large cluster of brain-specific miRNAs encoded by *Mirg* (miRNA-containing gene), inside the Dlk1-Dio3 locus and it was classified as key regulator for axon maintenance and function during neuronal differentiation (Zhang et al., 2011). Curiously, *in silico* affinity of miR-541 to *Satb2* 3'UTR is evolutionary conserved in Eutherians but is lower in Methatherians, which indicates that, the target sequence for miR-541 in the *Satb2* 3'UTR might have appeared only after *Mirg* appearance.

Retroposons, such as **s**hort **in**terspersed **e**lements (SINEs), are able to propagate into the host genome through RNA intermediates. A study performed on a specific SINE family, AmnSINE1, identified 124 loci in mammals with one-fourth been positioned close to genes related to brain development. Specifically, locus AS021 located 390 kbp upstream from *Satb2* gene was shown to be specifically activated in early-born $Satb2^{+}$ cells and to display specific enhancer activity in developing neocortex by transgenic mice experiments (Sasaki et al., 2008; Tashiro et al., 2011). Another huge difference from reptiles and birds is that in these species, SATB2 and BCL11B are co-expressed, and even though SATB2 tries to silence *Bcl11b* by binding to its cis-regulatory promoter sequence, this binding has very low efficiency. Instead, in mammals SATB2 is able to repress *Bcl11b* expression (Nomura et al., 2018).

Together with that, *Satb2* and other CITFs are expressed in the dorsal telencephalon (pallium) of birds and reptiles as well. However, the pattern of co-expression of these CITFs at single cell level are different from the patterns observed in the mammalian neocortex (Tosches et al., 2018). This fact suggests that the same CITFs are responsible for various mechanisms of cell identity regulation in homologous telencephalic structures in different vertebrates (Cárdenas and Borrell, 2019; Tosches and Laurent, 2019).

For instance, subtle changes in the time SATB2 is expressed can dramatically affect the axonal direction. Súarez's group at Queensland Brain Institute has recently demonstrated that by heterochronic anticipation of SATB2 protein translation in mouse (in comparison to dunnart marsupial model), the commissural axons from layer II/III were rerouted toward the anterior

commissure, which is the evolutionary older inter-hemispheric connectivity route, instead forming the *Corpus callosum* (Paolino et al., 2020). Súarez and colleagues also demonstrate that the supragranular cells of layer III-II are produced earlier in dunnart compared to mouse, at a time when the midline might be not permissive to the formation of a *Corpus callosum*. This and other experimental evidences found by Súarez's group indicate that just the delayed time of SATB2 translation allowed the evolution of a new route for the inter-hemispheric connections, the *Corpus callosum*, in higher mammals. This notion is now supported at a mechanistic level by our findings. The new, eutherian-specific miR-541 can bind to *Satb2* 3'UTR, inhibit its translation both *in vitro* and *in vivo* and consequently, delay SATB2 protein production in the mouse cortex. Indeed, the appearance of miR-541 in the higher mammal genome might have posed a milestone in the evolution of the cerebral cortex: a new molecular mechanism which allowed the appearance of the *Corpus callosum* in eutherians. In perspective, *in vivo* functional experiments of both miR-541 gain and loss of function in mouse cortical development through IUE are crucial to validate or deny our working hypothesis that miR-541 just controls the corpus callosum formation. In particular, an interesting hypothesis is whether miR-541 expression heterochrony can affect the formation of callosal fibers in mouse embryo. We successfully inhibited miR-541 using a specific antagomiR, causing premature Satb2 translation *in vitro*. Using the same tool in future experiments of IUE might allow to induce premature Satb2 expression *in vivo* and to assay if this would alter the number of callosal neurons being generated.

During rodent corticogenesis, the progenitor expansion phase precedes the beginning of neurons generation and only a small fraction of RGCs increase progenitor numbers during neurogenesis (Noctor et al., 2004; Gao et al., 2014). Instead, Livesey's group in 2015 discovered that the duration and range of the progenitor expansion period in primates were not only significantly longer than rodents but also, diverged among different primates. For instance, humans, that clearly present larger cerebral cortices and consequently, more neurons in respect to rodents but also to other primates like macaque, have a much longer proliferative phase in which they must balance progenitor cell expansion with neurogenesis. It is important to point out the fact that this mechanism is cell-autonomous as it resisted to environmental signals and thus, it is likely to be under genetic control (Otani et al., 2016). Previous studies have been proving that this increase in cortical size in humans is due to the relative number of oRGCs generated in advanced stages of cortex developmental process. The oRGCs typically undergo multiple rounds of cell division before generating the largest proportion of late-born, upper layer neurons (Florio & Huttner, 2014; Geschwind & Rakic, 2013). Recently, it has been demonstrated that TMEM14B, a primate-specific gene expressed in oRG cells in human cortex is, in a mice model,

able to increase $Tbr2^+$ cells, induce IPs generation and oRGCs expansion, leading to gyrification. In their work, they observed increases in both deep layer $BLC11B^+$ and upper layer $SATB2^+$ neurons what could propose that proliferation in all progenitor subtypes, specially IPs, is directly associated to the cortical folding observed in the mouse (Liu et al., 2017). Still, they could not conclude whether the augmented IP cells originated from vRGC, oRGCs or through self-division. Instead, another recent study from Huttner's lab took advantage of a ferret model to study an additional human-specific gene, ARHGAP11B, considered a crucial element for the evolutionary expansion of the neocortex. Huttner demonstrated that ARHGAP11B increased proliferative basal radial glia that, elongating the neurogenic period, was able to increase the thickness of layer II-IV and marked increase in SATB2+ upper-layer neurons (Kalebic et al., 2018). The difference between the phenotypes observed in mouse and ferret by those researchers could be an explanation to the way different mammalian orders respond to the increase in cortical neuron number, in accordance to other studies that have established a correlation between evolutionary increase in neocortex size with neuron number between humans and other great apes (Lewitus et al., 2014).

Nonetheless, a major feature describing the evolution of the mammalian cortex is just the continuous expansion of the supragranular layers and the *Corpus callosum* in primates compared to lower mammals (Dehay et al., 2015). Actually, none of the aforementioned studies addressed this aspect from a mechanistic point of view. In fact, the molecular mechanism of oRGC comparison during evolution seems still elusive. The exact nature of the control over the ratio of supra-and infra-granular neurons in different species is not clear and the expression regulation of the genes involved is far from being elucidated in different mammals. MicroRNAs are considered fertile evolutionary humus for the sudden generation of new networks of gene interactions during evolution. The reason is associated to their peculiar mechanism of function, which allows the control of hundreds of genes at one time by one miRNA, and the easy by which different target mRNA sequences can rapidly evolve small seeds of binding sequence. Many evolutionary new miRNAs have been found expressed in the developing mammalian cortex and there is general concordance that some of them might have directed major changes in its ontogeny, including the expansion of the supragranular layers (Kosik & Nowakowski, 2018). MiR-541 is a candidate among them. In fact, I have found that beside *Satb2*, miR-541 has many more possible interesting targets in *silico*. If validated by direct experimental evidence, these targets indicate that miR-541 might play a role in controlling the nature and the proliferation of cortical precursors. Among the possible targets, there are genes playing crucial roles in neural progenitor proliferation (*Rbfox2* and *Zeb2*), neuronal migration (*Dcx*, *Plxna4* and *Tcf4*), neuronal polarization (*Cntn2*), neurite

outgrowth (*Gas7*) and upper layer formation (*Cdk5)* (Caubit et al., 2016; P. F. Chen et al., 2016; Hatanaka et al., 2019; Li et al., 2019; Namba et al., 2014; Okamoto et al., 2013; Pramparo et al., 2010; Shinmyo et al., 2017; Ton & Kathryn Iovine, 2012; Z. Zhang et al., 2016). Future perspectives thus, include also experiments aiming to investigate the relation between miR-541 expression, oRGC identity and the control over the ratio between infra-and supra-granular cells.

Finally, I could imagine a scenario in which the appearance of a novel regulatory mechanism could lead to different transcriptional control for *Satb2* in the mammalian neocortex. This mechanism, miR-541-mediated, would delay *Satb2* mRNA translation, causing the heterochronic shift of SATB2 presence and to the alterations in the projection features of callosal neurons (Paolino et al., 2020). Besides, modifications in the regulatory sequences of *Bcl11b* would have facilitate the bind and consequence repression of BCL11B by *Satb2*. Therefore, synchronized developmental tools such as efficient SATB2 repression over *Bcl11b* promoter (Alcamo et al., 2008; Britanova et al., 2008; Nomura et al., 2018), a new *Satb2* cortical enhancer (Sasaki et al., 2008; Tashiro et al., 2011) and miR-541 (present thesis) might be crucial for the introduction of callosal projection neurons in the evolution of Eutherian corticogenesis. Thus, comprehending the cortical mechanisms that control miR-541 expression throughout cortical development becomes essential (Figure 26).

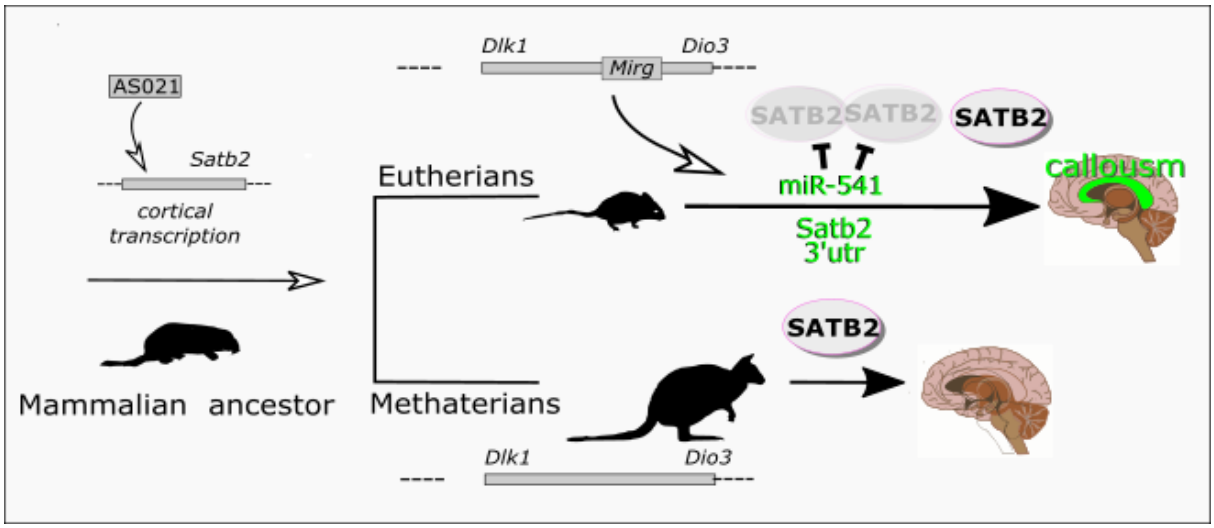

***Figure 26* - Model of evolution of Satb2 cortical expression in mammals.**

METHODS

Mouse ES cell-derived neural cell culture

Murine ES cell lines E14Tg2A (passages 25-38) and 46 C (transgenic Sox1::GFP ESC kindly provided by A. Smith, University of Cambridge, UK, passages 33–39) were cultured and neuralized essentially as described (Bertacchi et al., 2013), with minor modifications. For ES cell expansion, cells were grown on gelatin-coated tissue culture dishes (pre-treated 10' with 0.1% gelatin in PBS) at a density of 40000 cells/cm^2. ES cell medium, which was changed daily, contained GMEM (G5154, Sigma-Aldrich), 10% Fetal Calf Serum (12133C, Sigma-Aldrich), 2mM Glutamine (25030, ThermoFisher Scientific), 1mM sodium Pyruvate (25030, ThermoFisher Scientific), 1mM non-essential amino acids (NEAA, 11140, Sigma Aldrich), 0.05mM β-mercaptoethanol (M3148, Sigma Aldrich), 100 U/ml Penicillin/Streptomycin (15140, ThermoFisher Scientific) and 1000 U/ml recombinant mouse LIF (PMC9484, TermoFisher Scientific). Chemically defined minimal medium (CDMM) for neural induction consisted of DMEM/F12 (21331-046, ThermoFisher Scientific), 2mM Glutamine, 1mM sodium Pyruvate, 0.1Mm NEAA, 0.05mM β-mercaptoethanol, 100 U/ml Penicillin/Streptomycin supplemented with N-2 Supplement 100X (175020, ThermoFisher Scientific), and B-27 Supplement minus Vitamin A 50X (125870, ThermoFisher Scientific). The protocol of ES neuralization consisted of three steps. In Step-I, dissociated ES cells were washed with DMEM/F12, seeded on gelatin-coated culture dishes (65000 cells per cm2) and cultured in CDMM plus 2.5μM 53AH Wnt inhibitor (C5324-10, Cellagen Technology) and 0.25μM LDN193189 BMP inhibitor (SML0559, Sigma Aldrich), for 3 days. In Step-II, ES cell were dissociated and seeded (65000 cells per cm^2) on Poly-ornithine (P3655 Sigma-Aldrich; 20 μg/ml in sterile water, 24 hours coating at 37°C) and natural mouse Laminin (23017015, TermoFischer Scientific; 2.5 μg/ml in PBS, 24 hours coating at 37°C). Cells were cultured for four additional days in CDMM Plus Wnt/BMP inhibitors, changing the medium daily. Serum employed for Trypsin inactivation was carefully removed by several washes in DMEM/F12. In Step-III, cells were dissociated and seeded (125000 cells per cm2) on Poly-ornithine and Laminin coated wells. Subsequently, isocortical culture were kept in CDMM Plus Wnt/BMP inhibitors for four additional days. On the eleventh day of differentiation, DMEM/F12 was replaced with Neurobasal and NEAA were removed from the CDMM to avoid glutamate-induced excitotoxicity. Medium was changed daily until the day of cell fixation.

To identify progenitor cells at different times of corticalization *in vitro*, 46 C Sox1::GFP cells were employed (Bertacchi et al., 2013). For fluorescence activated cell sorting of GFP-positive cells, 10^7 cells were collected at each time of differentiation by trypsinization, washed,

and resuspended in PBS, 2 % FBS, and 2 mM EDTA at a concentration of 10M cells per mL and kept on ice. The Sox1::GFP$^+$ population was sorted on BD FACSJazz (BD Biosciences). Sorted cells (10^5 - $5*10^5$, depending on the culture stage), were immediately pelleted and total RNA extracted using miRNeasy Mini Kit (217004, Qiagen). Three replicates for each time of analysis (DIV10, DIV12, DIV16, DIV20, DIV26) were pooled and small RNAs were extracted for RNAseq. To deplete cultures of post-mitotic cells, Cytarabin (AraC, 5 μM; AC449561000, TermoFisher Scientific) was added to medium for two days before cell collection, as described (Bertacchi et al., 2015). Three replicates were pooled and small RNAs were extracted for RNAseq.

hiPSC-derived neural cell culture

Neural cell cultures were differentiated from a commercial reprogrammed fibroblast line (ATCC-DYS0100 line, American Type Culture Collection). Cell neuralization was carried out essentially as described (Chambers et al., 2009), with minor modifications. Reprogrammed stem cells were seeded at $3x10^4$ cells/cm^2 cultured on 1:100 geltrex and maintained in Essential 8 medium for two days. After two days incubation, cultures were switched to neural differentiation media: DMEM/F12 1:1 (21331-046, ThermoFisher Scientific) containing 2mM Glutamine (25030, ThermoFisher Scientific), 1mM Sodium Pyruvate (11360070, ThermoFisher Scientific), 100 U/mL Penicillin-streptomycin (15140, ThermoFisher Scientific), 1mM Non-essential amino acids (11140, Sigma Aldrich), 0.05mM β-mercaptoethanol (M3148, Sigma Aldrich), 10μM 53AH (C5324-10, Cellagen Technology), 10μM LDN193189 hydrochloride (SML0559, Sigma Aldrich), 1μM RepSox (R0158, Sigma Aldrich), N-2 Supplement 100X (175020, ThermoFisher Scientific), and B-27 Supplement minus Vitamin A 50X (125870, ThermoFisher Scientific). After 10 days in neural differentiation medium, cells were displaced from substrate via incubation at 37ºC for 20 minutes in Accutase solution (A6964, Sigma Aldrich). Cells were harvested, diluted in 5 volumes of 1X PBS, centrifuged for 4 minutes, and replated at 10^5 cells/cm^2 on poly-ornithine (P3655, Sigma Aldrich)/recombinant human Laminin (AMS.892 021, Amsbio) in half volume of neural differentiation media + 5 μM Y-27632 (SM02, Cell Guidance Systems). Cells were maintained for 4 days in fresh neural differentiation media without ROCK inhibitor followed by an expansion of 7 days in neural differentiation media without TGFβ, WNT, and BMP inhibitors. After 11 days, cells were displaced again from substrate via incubation at 37ºC for 20 minutes in Accutase solution. Cells were harvested, diluted in 1X PBS at a volume 5 times that of Accutase, centrifuged for 4 minutes, and replated at $2.5x10^5$ cells/cm^2 on poly-ornithine (P3655, Sigma Aldrich)/purified mouse Laminin (CC095-M, Merck Millipore) in Eppendorf

glass bottom dishes (H 0030 741 021, Eppendorf). Cells were maintained in neural differentiation media without inhibitors for 12 days and then switched to neuronal maintenance media based on Neurobasal (21103049, ThermoFisher Scientific) and containing 2mM Glutamine (25030, ThermoFisher Scientific), 1 mM Sodium Pyruvate (11360070, ThermoFisher Scientific), 100 U/mL Penicillin-streptomycin (15140, ThermoFisher Scientific), 0.05mM β-mercaptoethanol (M3148, Sigma Aldrich), Ascorbate, 0.5mM (A92902, Sigma Aldrich), Recombinant human BDNF, 20 ng/mL (NBP2-52006, Novus Biologicals), and B-27 Supplement minus Vitamin A 50X (125870, ThermoFisher Scientific) until fixation at DIV 42. Cells were fixed with 2% PFA warmed to 37°C for 15 minutes at room temperature.

Cell transfection

Plasmid transfections in mouse cortical cells were performed in 24-multiwell plate using 1µg plasmid DNA diluted in 2.5 µL/well of Lipofectamine 2000 (12566014, TermoFisher Scientific) in a final volume of 0.5 mL/well OPTI-MEM (31985062, TermoFiscer Scientific). Reporter activity plasmids were pEGFP-C1 (Clontech; control) and PEGFP-C1 bearing normal or mutated 3' UTR of *Satb2* between HindIII and XbaI sites.

LNA anti-miRNA (antagomiR) transfection in mouse cortical cells was performed using Lipofectamine 2000 according to the manufacturer's instructions. AntagomiRs used are miRCURY LNA™ microRNA Inhibitors to miR-541-5p and miR92-3p provided by QIAGEN. MiRCURY LNA miRNA Inhibitors are antisense oligonucleotides that sequester the target miRNA in highly stable heteroduplexes, preventing the miRNA from hybridizing with its target mRNA.

miRCURY LNA™ microRNA Inhibitors to miR-541-5p, miR92-3p and ctrl antagomiR (MIMAT0003170, YI00199006 and MIMAT0000539, respectively) were resuspended in TE buffer (10 mM Tris pH 7.5, 1 mM EDTA) to a final concentration of 50 µM. Cells were transfected in 24-well plate using 25pmol of LNA diluted in 2.5 µL/well of Lipofectamine 2000 in a final volume of 0.5 mL/well OPTI-MEM.

For mature (mimic) miRNA transfection, colorectal cancer cell line HCT-116 cells were cultured in McCoy's 5A Medium (M4892, Sigma Aldrich) supplemented with Fetal Bovine Serum (FBS; 2055.00, ThermoFisher Scientific), were co-transfected in 24-multiwell plate with 25 pmol of miR-541 mimic RNA (5'AAGGGAUUCUGAUGUUGGUCACACU3'), or control mimic RNA (5'CUCCGAACGUGUCACGUU3'), and 100ng of reporter plasmid PEGFP-C1 (Clontech) bearing normal or mutated 3' UTR of *Satb2* between HindIII and XbaI sites.

After transfection, cells were incubated at 37°C and 5% CO2 for 4-6 hours and then the medium was replaced to complete Neurobasal medium (mouse cortical cells) or complete McCoy medium (HCT-116 cells).

Satb2 3'UTR cloning

The entire *Satb2*-3'UTR sequence (2802 bp) was obtained from Genome Reference Consortium Mouse Build 38 patch release 6 (GRCm38.p6) and amplified by PCR with Q5 High-Fidelity DNA Polymerase (M0491, NEB) with a forward and reverse primer carrying, correspondingly, a HindIII and XbaI restriction site at their 5'end (forward, CACAAAGCTTGTGAACTCCGCAGGCAGAGC; reverse, CACATCTAGAGCGTTTTATTTAACAACCAAAAAATTCTAACAGCC). The plasmid carrying the *Satb2*-3'UTR was constructed using mammalian expression vector pEGFP-C1 (Clontech) cut at HindIII position and XbaI positions inside the multiple cloning site and ligated with HindIII/XbaI restricted amplification product by T4 DNA ligase (M0202, NEB).

In order to identify potential target sites for our miRNA of interest (mmu-miR-541-5p) in the *Satb2* sequence, miRanda algorithm (v3.3a; Enright et al., 2003) was used. Miranda selected miR-541/*Satb2* binding sites with score >120 and energy < -18kd. Mutations in the three predicted sites were performed. The seed sequence of miR-541 at +156, +740 and +1724 were replaced with NotI restriction sequence (GCGGCCGC). To this aim, upstream and downstream halves of mutated 3'UTR were generated by PCR through external forward or reverse primer NotI together with a mutated internal reverse of forward primer, respectively. The mutated internal primers for miR-541 mutation at position +156 were miR-541_mutA_fw CACAGCGGCCGCAATCAGACGTCACCTTGGCAAAG and miR-541_mutA_rev CACAGCGGCCGCCTGAGCTTACTCAGTCTATAGGCTATCCTGTG. The mutated internal primers for miR-541 mutation at position +740 were mir-541_mutb_fw CACAGCGGCCGCCAGAGGACATAATGCACACCTTAAGAC and miR-541_mutB_rev CACAGCGGCCGCGGTCTTATGTTGGTTTTTTTGACATGCCC. The mutated internal primers for miR-541 mutation at position +1724 were miR-541_mutC_fw CACAGCGGCCGCGAGTTGTATCCTCATGCAACCTTGTC and miR-541_mutC_rev CACAGCGGCCGCCTGAGTGGCCATCTCAAGCC. After PCRs, both upstream and downstream mutated halves were digested with NotI enzyme, ligated and used as a template for PCR together with external forward and reverse primers (forward, CGCAGGCAGAGCAATAGATGG; reverse, GGCGGGAAATTGTGCTTTGTCAAGA). PCR

products were cut with HindIII/XbaI restriction enzymes, purified and re-inserted in the pEGFP-C1 vector.

Immunocytodetection (ICD) and imaging

Cells prepared for immunocytodetection experiments were cultured on Poly-ornithine/Laminin coated round glass coverslips. Cells were fixed using 2% paraformaldehyde for 12 minutes, washed twice with PBS, permeabilized using 0.1% Triton X100 in PBS and blocked using 0.5% BSA in PBS for 1hr at RT. Embryonic cortical sections were thawed and let to dry at room temperature 1hr, then they were briefly washed three times (5' each) in PBS before antibody staining.

Cells/slices were pre-treated 1hr at room temperature with blocking solution: 1% BSA, 10% goat serum, 0.1% Triton X100 in PBS. Primary antibodies used for microscopy were SATB2 ab (1:1000; ab34735, Abcam), GFP ab (1:1000, ab13970, Abcam). Primary antibodies were incubated over/night at 4°C in PBS containing 1% BSA and 10% goat serum in PBS; cells/slices were then washed three times with PBS (10' each). Alexa Fluor 488 and Alexa Fluor 546 anti-mouse, anti-rabbit or anti-chicken IgG conjugates (1:500; A32723, A-11034, A-11039, A-11003, A-11010, A11040, Molecular Probes) were incubated 1 hour at RT in PBS containing 1% BSA and 10% goat serum, followed by three PBS washes (10' each). Nuclear staining was obtained with DAPI (D1306, TermoFisher Scientific). Cells/slices were cover slipped with Aqua Poly-mount (18606-100, Polysciences).

Mouse neural cells were imaged using a Nikon Eclipse E600 epifluorescence microscope with a 20 X objective and a Photometrics Coolsnap CF camera. Five to ten optic fields from two or more biological replicates were acquired. In the experiments of EGFP pixel intensity quantification, all the pictures were acquired with the same parameters and the median of pixel intensity of the entire acquired field was analyzed. For cell counting, double blind analysis was performed.

Human neural cells were imaged using a Leica SP2 confocal microscope with a 40X oil objective. Z-stacks were attained between 9-12 µm thick optical sections. Three biological replicates were attained per treatment group and subdivided into 5 technological replicate z-stacks resulting in 15 total acquisitions. Stacks were flattened in ImageJ (RRID:SCR_002285) using the Z-stack projection function, set as a representation of standard deviation, and backgrounds were subtracted as a function of disabled smoothing and rolling ball radius of 20

px2. The resultant Hoechst$^+$ and SATB2$^+$ images were then subjected to an automated cell counter in ImageJ macros which analyzed separate channels at a 16-bit threshold set between 30-65355 and individual cells were counted using the "Analyze Particle" function set at circularity 35-150 px2 and circularity 0.33-0.99 to only include positive nuclei and minimize false positives.

Sc-RNAseq datasets

Sc-RNAseq datasets available in literature (Yuzwa et al., 2017) were used to analyze cortical gene expression at E11.5, E13.5, E15.5 and E17.5. Raw counts were obtained from GEO GSE107122 and used to plot red/cell values by vioplot R package.

COTAN

CO-expression **T**ables **AN**alysis (COTAN) aims to estimate the UMI detection efficiency (UDE) of each cell, finds an approximation of the probability of zero read counts for a gene in a cell, and test the null hypothesis of independent expression for gene pairs, by counting zero/non-zero UMI counts in single cells (co-submitted paper). Briefly, mitochondrial genes and genes expressed in less than 0.3% of cells were eliminated. UDE for each cell and average expression for each gene were estimated as described (Galfrè et al. 2020) (*linear* method was used). PCA and hierarchical clustering (two clusters) were then carried out on UMI counts normalized dividing them by UDE. After removal of cell outliers resulting from PCA and hierarchical clustering, UDE and average expression were estimated again. Cells with very low UDE values were also removed. Together the two cleaning steps removed in all the datasets less than 3% of the cells (E11.5 dropped from 1,418 cells to 1,379 cells, E13.5 dropped from 1,137 to 1,119, E15.5 dropped from 2,955 to 2,921, E17.5 dropped from 880 to 863 cells).

Expected values for contingency table analysis were obtained as described (Galfrè et al. 2020) using cells UDE and genes average expression estimated with linear method, and genes dispersion estimated by fitting the observed number of cells with zero UMI count. COTAN then provided both an approximate p-value for the test of independence and a signed co-expression index (COEX), which measures the direction and intensity of the deviation from the independence hypothesis. The heatmaps in Figure 1D are colored by COEX value (blue for co-expression and red for disjoint expression).

For each gene, GDI was computed by normalizing P, the 0.001 quantile of the p-values of COTAN test for co-expression with all other genes. Our chosen normalization is ln(-ln(pval)). Genes with GDI > 2.2, which corresponds to ln(-ln(10^{-4})), were generally non constitutive genes (Galfrè et al., 2020). Plots were generated with ggplot2 in R environment. The following R

packages were employed: matrixStats, ggfortify, dplyr, rray, propagate, data.table, ggsci, gmodels, parallel, tibble, ggrepel.

Sc-RNAseq bidimensional analysis

UMI counts were divided by COTAN UDE for normalization. PCA was performed with normalized counts in R environment. Eigenvalues were plotted for selection by "elbow" point analysis (the number of components used were: 10 for E11.5, 10 for E13.5, 15 for E15.5 and 10 for E17.5). Selected components were employed as input for t-SNE function in sklearn.manifold python package (Loo et al., 2019), using the following parameters: perplexity 30, number of iterations 7000 and learning rate 700. Plots were obtained by ggplot2 R package.

Cell cluster analysis by Seurat

The datasets from GSE107122 series were used and, in detail, the "Combined_Only_Cortical_Cells" matrixes were analysed for each time point of development. For the single cell RNAseq data clustering the standard workflow of the R package Seurat 4.0 was followed. No cleaning was needed and the detection of nearest neighbours was performed using respectively 10, 15, 15 and 20 principal components for the E11.5, E13.5, E15.5 and E17.5 datasets. For all samples, the original Louvain algorithm was used for the clustering with a resolution of 1. The same number of principal components were used to perform the Uniform Manifold Approximation and Projection (UMAP) dimensional reduction.

Exon-Intron split analysis (EISA)

EISA on mouse cortex transcriptomes of cortical progenitor cells at E11.5, E13.5, E15.5 and E17.5 (Chui et al., 2020) was performed as previously described in (Gaidatzis et al., 2015; La Manno et al., 2018), with modifications. Mapping of datasets to mouse genome annotation GRCm38.98 was carried out as described in https://www.kallistobus.tools/velocity_index_tutorial.html (La Manno et al., 2018). Briefly, by using USCS table browser we obtained intron BED file, cDNA file and genome fasta files. A mouse GTF file was obtained from the Ensembl.t2g utility and used to map transcripts to gene map (https://github.com/sbooeshaghi/tools/releases/tag/t2g_v0.24.0). Intron BED file was converted to fasta format by bedtools (v2.25; https://github.com/arq5x/bedtools2/releases).

Association of intron and exon identifiers was performed modifying the fasta file headers as described in (https://www.kallistobus.tools/velocity_index_tutorial.html). An index was eventually produced by Salmon (version 1.1.0) (Patro et al., 2017) using the modified fasta files. Read pseudo-counts obtained by Salmon were normalized as reads per million (RPM). Log_2 (CPM) expression levels (exonic and intronic) were calculated and the exons/introns ratio was defined as the difference between log_2 exonic pseudo-counts and log_2 intronic pseudo-counts for each experimental condition.

In Utero Electroporation (IUE)

All animal procedures were approved by the internal Ethical Committee for Animal Experimentation (OPBA) of the Ospedale Policlinico San Martino and by the Italian Ministry of Health according to the Italian Law D. lgs 26/2014 and the European Directive 2010/63/EU of the European Parliament. In all the experiments the C57BL/6J strain from Jackson Laboratory was used.

In utero intraventricular electroporation was performed on E13 mouse embryos following laparotomy of deeply anesthetized pregnant females. Embryos were injected within the telencephalic ventricles with approximately 2µl (2µg) of PEGFP-C1 (Clontech; control) or PEGFP-C1 bearing normal *Satb2* 3' UTR, which were immediately after electroporated at 35V with 4 pulses lasting 50 ms and spaced by 950 ms with a NEPA21 (NepaGene, Chiba, Japan) electroporator. Brains were dissected 7 days after electroporation and fixed overnight at 4°C in 4% paraformaldehyde in PBS. Brains were then cry protected overnight in 20% sucrose, embedded in Tissue Teck O.C.T. compound (4583, Sakura) and sectioned with a Leica CM3050 S cryostat at 12 µm thickness.

RNA Immunoprecipitation

Cross-linking Immunoprecipitation (CLIP) was carried out to enrich AGO-interacting RNA. Cells were differentiated into cortical neurons until DIV12 or DIV18. Adherent cells were rinsed twice in PBS, cross-linked 150mJ/cm2 at 254nm wave length, scraped, spun down 10 seconds at top speed and lysed on ice for 10 minutes in 1 mL of fresh lysis buffer (Tris-HCl pH 8.0 25mM, NaCl 150 mM, MgCl2 2 mM, 0.5% NP-40, DTT 5 mM) with protease inhibitors (1 tablet/10 mL lysis buffer of EDTA-free Complete Protease Inhibitor Cocktail Tablets, 11697498001, Sigma Aldrich) and RNasin (250 U/mL final, N2115, Promega). Cell lysate was

centrifuged at 10000 rpm at 4ºC for 10 minutes and the supernatant was kept at 4ºC for later procedure.

In the meantime, protein A Dynabeads (10001D, ThermoFisher Scientific) were rinsed 3 times with PBS/0.5% NP40 and incubated with 5 µg rabbit monoclonal Anti-argonaute-2 antibody EPR10411 (ab186733, Abcam), or anti-GFP antibody A-6455 (A-6455, TermoFisher Scientific) in PBD/0.5% NP40 for 1 hour. After the initial binding, antibody-protein A beads were blocked with 0.5 mg/mL yeast RNA (10 µg/µL, 10109223001, Sigma Aldrich) and 1 mg/mL BSA (20 mg/mL, A3294-100G, Sigma Aldrich) for an additional 30 minutes and beads were then, washed. Twice in PBS/0.5% NP40 to remove the unbound IgGs and then, twice in lysis buffer. The beads were resuspended in 100 µL of lysis buffer. The lysate was subjected to preclearance by incubation with pre-blocked Protein A beads at 4ºC for 60 minutes (100 µL of total lysate after preclearance, but before co-IP, was separated for total RNA – input – analysis). The remaining lysates proceeded to co-IP with anti-Ago-Protein A beads at 4ºC for 90 minutes. After the incubation the beads were washed three times with lysis buffer, twice with lysis buffer high-salt content (Tris-HCl pH 8.0 25 mM, NaCl 0.9 M, MgCl2 1mM, NP-40 1%, DTT 5Mm) and again, once, with lysis buffer. After washes, beads were incubated with 100 µL of SDS 0.1% and Proteinase K (0.5 mg/mL, P8107S, NEB) for 15 minutes at 55ºC. RNAs that co-immunoprecipitated with anti-AGO or anti-GFP antibodies were extracted adding 700 µL Qiazol (79306, Qiagen) and 140 µL chlorophorm according to manual and then purified using Nucleospin RNA XS purification system (740902.50, Macherey-Nagel) and following manufacturer's instructions.

Semiquantitative Real-Time PCR

RNA quantity and quality was measured using NanodropTM Lite UV Visible Spectrophotometer (ThermoFisher Scientific) followed by reverse transcriptase protocol. For each sample, 100 ng of total RNA were reverse transcribed. Reverse Transcriptase Core kit (RT-RTCK-03, Eurogentec) was employed for cDNA synthesis. primers for amplification were 5'CATGAGCCCTGGTCTTCTCT3' (*Satb2* forward) and 5'AACTGCTCTGGGAATGGGTG3' (*Satb2* reverse). Amplified cDNA was quantified using Sensi Fast SYBR Green (BIO-98050, Bioline) on Rotor-Gene 6000 (Corbett). Amplification take-off values were evaluated using the built-in Rotor-Gene 6000 "relative quantification analysis" function and relative expression was calculated with the 2-ΔCt method.

Small RNA-Seq

Total RNA was extracted with miRNeasy Mini Kit (217004, QIAGEN). Small-RNA libraries were prepared using TruSeq Small RNA Sample Preparation Kit (RS-200-0012/24/36, Illumina) following the manufacturer's instructions starting from 1µg of total RNA per sample. Libraries were multiplexed, loaded into a V3 flow cell and sequenced in a single-reads mode (50 bp) on a MiSeq sequencer (Illumina), obtaining ~4 million reads per samples. Raw sequences were demultiplexed to FASTQ format using CASAVA v.1.8 (Illumina). Quality control checks were performed with the FastQC algorithm. Adapters were trimmed from the primary reads using Cutadapt v1.2.1 (Martin, 2011). Remaining reads, with a length of between 17bp and 35bp, were clustered by unique hits and mapped to pre-miRNA sequences (miRBase release 21; (Kozomara and Griffiths-Jones, 2014)) with the miRExpress tool v 2.1.3 5 (Wang et al., 2009). Read counts were CPM normalized for comparative analyses. PCA was carried out by PCA.GENES R package.

miRCATCH

miRCATCH analysis (version 2.0, Marranci et al. 2019) was carried essentially as described, with minor modifications. Three biological replicas for each time of *in vitro* differentiation were included in the study. Mouse cells (>10^7/sample) were harvested at DIV12 and DIV18 of the cortical differentiation protocol by trypsinization, washed with PBS and fixed with 1% formaldehyde for 10 minutes at room temperature. The reaction was quenched with 1.25M glycine for 5 minutes at room temperature and cells were centrifuged at 200g for 5 minutes at 4°C. The pellet was resuspended in ice cold PBS (50 mL) and centrifuged at the same conditions as previously twice. Cells were then resuspended in 1ml Lysis Buffer: 50mM Tris-HCl pH 7.0, 5mM EDTA, 1% SDS plus supplements: 1mM Phenylmethanesulfonyl fluoride (PMSF, P7626, Sigma Aldrich), 1X Protease Inhibitor Cocktail (P8340, Sigma Aldrich) and 80U/ml RNAsin (N2115, Promega); all the components were added freshly before use. Cells were sonicated in ice-cold Lysis Buffer with a Soniprep 150 ultrasonic disintegrator (MSS150.CX3.1, MSE) for 12 rounds at 70% amplitude for 30 seconds pulses with 45 second cool down pauses in between. Sonicated lysates were pooled in order to have a minimum of 1ml for pool of probes (odd/even).

DIG-label probes to *Satb2* 3'UTR were designed:

PROBE #	PROBE (5'-> 3')	PROBE POSITION *	PERCENT GC
1	aaagtccttggacccatcta	24	45.0%
2	tctgagcttactcagtctat	154	40.0%
3	cttccataagttggcaggaa	273	45.0%
4	attgtaaagttctctgtccc	408	40.0%
5	agtgactcactgtgaagtgg	492	50.0%
6	attacccattaaaagctgcc	627	40.0%
7	ctctggaggaattggtctta	753	45.0%
8	ctcgatacagtgctggcatg	835	55.0%
9	ggtccaacgtcaaaacgtca	928	50.0%
10	gaaggaaagggtaacaccct	1048	50.0%
11	tctaaccgggcagaaacttc	1231	50.0%
12	tctggctaaagtgaagggga	1336	50.0%
13	tcacttactttattgcctgg	1441	40.0%
14	tggcattagttctgctttac	1537	40.0%
15	ctggaaggtaatgctactgt	1635	45.0%
16	tgctgagtggccatctcaag	1724	55.0%
17	tgtattgcaacgtgtcttct	1976	40.0%
18	gctcatgtcaagggtaactg	2078	50.0%
19	ggagatcaggaagcagcaac	2196	55.0%
20	agagtgacttcagcaacagc	2245	50.0%
21	gatgccatcgatcgatgaac	2310	50.0%
22	aaatgcccacagattcactt	2436	40.0%
23	ctttgtcaagaggcactaca	2557	45.0%
24	acagcctaacaatgcacata	2739	40.0%

Dynabeads MyOne Streptavidin C1 (65001, TermoFisher Scientific) were washed (30 µl for each experiment) three times with 1ml unsupplemented Lysis Buffer and resuspended in 30 µl complete Lysis Buffer. The beads were added to 1ml lysate in a 1.5ml tube and kept on rotation in a 37°C hybridization oven for 30 minutes. Then, the lysates were cleared from beads twice using a magnetic stand and transferred to a 5ml round-bottom tube where 2ml of supplemented Hybridization Buffer (750mM NaCl, 1% SDS, 50mM Tris-HCl pH 7.0, 1mM EDTA and 15% formamide plus supplements: 1mM PMSF, 1X protease inhibitor cocktail and 80U/ml RNAsin that were added fresh before use) was added. At this point, a total amount of 100pmol probes (capture odd/even or scrambled control probes, 1 µl from a 100 µl pool previously mixed) were added to each lysate and put again in the 37°C hybridization oven for 4 hours in rotation. While the probes were incubating with the lysate, 200 µl of beads were washed three times with unsupplemented Lysis Buffer and resuspended in 200 µl supplemented Lysis Buffer. 100 µl of beads were added to the lysate plus probes sample and rotated in the hybridization oven for an additional 30 minutes at 37°C. Passed these 30 minutes, the beads were pelleted using the magnetic support and resuspended in 1 ml of Wash Buffer (2X SSC Buffer, 0.5% SDS and 1mM PMSF added fresh) pre-warmed at 37oC. Five washes of 5 minutes each using hybridization oven in rotation at 37oC were performed with the Wash Buffer. At the last wash, the beads were spin down, the entire wash buffer was removed. Beads were then resuspended in 185 µl Proteinase K buffer (100mM NaCl, 10mM Tris-HCl pH 7.0, 1mM EDTA, 0.5% SDS) and add 15 µl 20 mg/ml Proteinase K and incubated at 45°C for 1 hour under constant and vigorous agitation followed by 10 minutes' incubation at 95oC. Finally, 1 ml Qiazol was added directly to the beads, vortex and incubated for 10 minutes at room temperature. The RNA extraction was performed using Nucleospin RNA XS purification system (740902.50, Macherey-Nagel).

The RNA eluted from the ODD and EVEN samples were used to prepare cDNA libraries with the TruSeq Small RNA kit (RS-200-0012/24/36, Illumina), as per the manufacturer's suggestions. cDNA libraries were multiplexed, loaded into a V3 flow cell and sequenced in a single-reads mode (50bp) on a MiSeq sequencer (Illumina), obtaining ~4 million reads per samples. Read counts were obtained as described in the miR-seq section method. To evaluate the enrichment of miRNA binding to *Satb2* 3'UTR, at each time of analysis (DIV12 or DIV18) *Satb2*-captured miRNAomes from three biological replicas (DIV12: 3 EVEN and 2 ODD; DIV18: 2 EVEN and 2 ODD) and total miRNAomes (DIV12 and DIV18, n=3) were compared. miRNA reads were normalized as CPM. Aiming to discover miRNAs with high biological relevance, those in the highest quartile of expression were considered for the analysis. The

enrichment of miRNA binding to *Satb2* 3'UTR was evaluated as log_2 miRNA fold change between captured and input miRNAs. The non-parametric NOISeqBIO statistical test of NOISeq R-package was applied with a probability >0.9 (Tarazona et al., 2015).

In Situ Hybridization

miRNA in situ hybridization (ISH) was performed using LNA-modified oligonucletides probes (Exiqon), according to the manufacturer protocol, with minor modifications, Cryosections were collected on slides (J1800AMNZT, Thermo Scientific) and postfixed 15' with 4% paraformaldehyde (PFA) in PBS. Sections were treated with 10ng/µL proteinase K (15'), washed with 2 mg/mL glycine (2x 5'), PBS (2x5'), and postfixed 15' with 4% PFA. Sections were then pre-hybridized (50") in hybridization solution containing: with 50% formamide, 5X sodium saline citrate buffer (SSC) (pH 6), 1% sodium dodecyl sulfate (SDS), 50 g/mL heparin (9041-08-1, ThermoFischer Scientific) and 500 g/mL yeast RNA (10109223001, Sigma Aldrich). Hybridization with the digoxigenin-labeled probes was per-formed overnight at a temperature of approximately 21°C lower than the melting temperature of the probe. miRNA probes (miRNA Detection Probes, 339111, Exiqon) to mmu-miR-541-5p, and control probe with scrambled sequence, were employed. Washes were carried out in 50% formamide, 2XSSC at the hybridization temperature (1x 30') and 1X SSC (2x 15'). Sections were blocked 30' in MABT (1% BSA, A3294-100G, Sigma Aldrich; 150 mM NaCl; 0.1% Tween 20, pH7.5) containing 10% sheep serum (S2263, Sigma Aldrich) and incubated with alkaline phosphatase (AP)-labeled anti-digoxigenin antibody (1:2000; 11093274910, Sigma Aldrich)) in MABT and 1% BSA, overnight at 4°C. Sections were washed 5x5' in MABT and 3x5' in NMNT (100 mM NaCl, 100 mM TrisHCl pH 9.5, 50 mM MgCl, 0.1% Tween-20, 2 mM Tetramisole (L9756-5G, Sigma Aldrich: 500 mg/L). Sections were eventually stained with BM-Purple AP-substrate (L9756-5G, Sigma Aldrich) at RT 0.5'- 2 hours, then blocked by washes with PBS and counter-stained with anti-Satb2 antibody.

MiRNA-mRNA interaction prediction and GO enrichment

miRNA-mRNA *in silico* affinity was predicted as described (Enright et al., 2003), using score >120, energy < -18 kd as thresholds. 3'UTR sequences were obtained from Ensembl resources (Hunt et al., 2018), using Cran Biomart package. MiRNA sequences were obtained from miRBase database (v.22) (Kozomara et al., 2019). Enriched GO terms were obtained using two unranked lists of genes (target versus background) as described (Eden et al., 2009). Analysis results were visualized using Cran ggplot2 packages.

ACKNOWLEDGMENTS

This hard and long work would have been harder and longer if I hadn't had the best advisor a PhD student could possible ask for, Prof. Federico Cremisi. Thank you very much for everything you have taught me, all the care you have for me and all the moments you made me realize a boss can also become a friend, and in my case, family. I treasure every moment we shared and I will have you forever in my heart.

I would like to thank my lab colleagues Marco Terrigno, Keagan Dunville, Edoardo Sozzi, Silvia Galfrè and Giacomo Siano for all the fun and laughter we had throughout these years, cell culture room is always going to bring a smile into my face. Besides them, I must thank Leonardo Lupori, Raffaele Mazziotti and Giuliano Timossi for being more than friends but almost brothers, being there through laugh, pain, tears and desperation moments. I thank my second work family, Prof. Matteo Caleo, Claudia Alia and Marco Salluzzo for embrace me and give me the opportunity of working in their lab and learning so much. I express my sincere gratitude to Antonella Calvello that has been my guardian angel during these years helping me every day and making every problem disappear. Thanks also to Vania Liverani for all the help and support always with a smile and kind eyes.

Of course, I must thank my parents, Magali and José Carlos and my brothers, Phelipe and Phernando and my grandparents, Agostinha e Antonio, for being my true inspiration and the reason why I will never stop pursuing my dreams, no matter what. Thank you for being my great support through distance and rough times. Thank you for being the loving family you are and mostly, for letting me know and feel, that even apart and spread through the world, we are always together. Of course, as part of my family, I must thank my sister Nadia Giordano. Thank you for being always present, for all the good, great, amazing, unforgettable moments and thank you twice for all the not so good moments too. You have been the only constant in my life for these years, since that Monday when we "stopped crying".

Finally, I thank immensely Lorenzo Vatteroni for believing in me more than I believe in myself, for keep pushing me towards the best I can be and for all the amazing moments we still haven't lived. Besides you, I thank you all your family that has become my family and that make me feel loved every day.

DECLARATION OF AUTHORSHIP

I declare that I have composed the thesis and that the work has not be submitted for any other degree or professional qualification. I confirm that the work submitted is my own, except where work which has formed part of jointly-authored publications has been included. My contribution and those of the other authors to this work have been explicitly indicated below. I confirm that appropriate credit has been given within this thesis where reference has been made to the work of others.

I have designed the experiments together with Federico Cremisi[1]. I have performed cell culture, molecular biology, imaging, miR-CATCH, Ago-RIP and gene expression data computation analysis.

Silvia Galfrè[2] and Francesco Morandini[3] performed COTAN and EISA bioinformatics analysis. EISA analysis using RNA from tissue was performed by me.

Paolo Malatesta[4, 5] and Irene Appolloni[4, 5] planned and carried out IUE.

Marco Terrigno[1], Alberto Mercantani[6] and Milena Rizzo[6] performed small RNA-Seq

and Luca Pandolfini[1] performed RNA-Seq.

Keagan Dunville[1] performed hIPSC cultures.

1 - Scuola Normale, Pisa, Italy
2 - Dipartimento di Biologia, Universita` Roma Tor Vergata, Roma, Italy
3 - Dipartimento di Scienze Matematiche, Fisiche e Informatiche, Universita` di Parma, Parma, Italy
4 - Dipartimento di Medicina Sperimentale, Universita` di Genova, Genova, Italy
5 - Ospedale Policlinico San Martino, IRCCS per l'Oncologia, Genova, Italy
6 - Istituto di Fisiologia Clinica CNR, Pisa, Italy

And, my most important gratitude and acknowledge goes to God.
Thank you Lord because without you I wouldn't have anything to thank for.

Thank you for always giving me way more than I ask for and more than I could ever think it would be possible. Thank you for having me under your guidance and your love.

BIBLIOGRAPHY

Aaku-Saraste, E., Hellwig, A., & Huttner, W. B. (1996). Loss of occludin and functional tight junctions, but not ZO-1, during neural tube closure--remodeling of the neuroepithelium prior to neurogenesis. *Developmental biology*, *180*(2), 664–679.

Abhang, P., Gawali, B. & Mehrotra, SC. (2016) Introduction to EEG- and Speech-Based Emotion Recognition, *Academic Press* 1-17.

Agirman, G., Broix, L., & Nguyen, L. (2017). Cerebral cortex development: an outside-in perspective. *FEBS letters*, *591*(24), 3978–3992.

Alcamo, E. A., Chirivella, L., Dautzenberg, M., Dobreva, G., Fariñas, I., Grosschedl, R., & McConnell, S. K. (2008). Satb2 regulates callosal projection neuron identity in the developing cerebral cortex. *Neuron*, *57*(3), 364–377.

Ambrozkiewicz, M. C., Bessa, P., Salazar-Lázaro, A., Salina, V., & Tarabykin, V. (2017). Satb2$^{Cre/+}$ mouse as a tool to investigate cell fate determination in the developing neocortex. *Journal of neuroscience methods*, *291*, 113–121.

Avilion, A. A., Nicolis, S. K., Pevny, L. H., Perez, L., Vivian, N., & Lovell-Badge, R. (2003). Multipotent cell lineages in early mouse development depend on SOX2 function. *Genes & development*, *17*(1), 126–140.

Bayer, S. A., & Altman, J. (1991). Development of the endopiriform nucleus and the claustrum in the rat brain. *Neuroscience*, *45*(2), 391–412.

Beattie, R., & Hippenmeyer, S. (2017). Mechanisms of radial glia progenitor cell lineage progression. *FEBS letters*, *591*(24), 3993–4008.

Bernstein, E., Kim, S. Y., Carmell, M. A., Murchison, E. P., Alcorn, H., Li, M. Z., Mills, A. A., Elledge, S. J., Anderson, K. V., & Hannon, G. J. (2003). Dicer is essential for mouse development. *Nature genetics*, *35*(3), 215–217.

Bertacchi, M., Pandolfini, L., D'Onofrio, M., Brandi, R., & Cremisi, F. (2015). The double inhibition of endogenously produced BMP and Wnt factors synergistically triggers dorsal telencephalic differentiation of mouse ES cells. *Developmental neurobiology*, *75*(1), 66–79.

Bertacchi, M., Pandolfini, L., Murenu, E., Viegi, A., Capsoni, S., Cellerino, A., Messina, A., Casarosa, S., & Cremisi, F. (2013). The positional identity of mouse ES cell-generated neurons is affected by BMP signaling. *Cell and Molecular Life Sciences, 70(6),* 1095–1111.

Bertrand, V., Hudson, C., Caillol, D., Popovici, C., & Lemaire, P. (2003). Neural tissue in ascidian embryos is induced by FGF9/16/20, acting via a combination of maternal GATA and Ets transcription factors. *Cell*, *115*(5), 615–627.

Bhinge, A., Poschmann, J., Namboori, S. C., Tian, X., Jia Hui Loh, S., Traczyk, A., Prabhakar, S., & Stanton, L. W. (2014). MiR-135b is a direct PAX6 target and specifies human neuroectoderm by inhibiting TGF-β/BMP signaling. *EMBO Journal*, *33*(11), 1271–1283.

Bian, S., Hong, J., Li, Q., Schebelle, L., Pollock, A., Knauss, J. L., Garg, V., & Sun, T. (2013). MicroRNA cluster miR-17-92 regulates neural stem cell expansion and transition to intermediate progenitors in the developing mouse neocortex. *Cell reports*, *3*(5), 1398–1406.

Boissart, C., Nissan, X., Giraud-Triboult, K., Peschanski, M., & Benchoua, A. (2012). miR-125 potentiates early neural specification of human embryonic stem cells. *Development (Cambridge, England)*, *139*(7), 1247–1257.

Britanova, O., Akopov, S., Lukyanov, S., Gruss, P., & Tarabykin, V. (2005). Novel transcription factor Satb2 interacts with matrix attachment region DNA elements in a tissue-specific manner and demonstrates cell-type-dependent expression in the developing mouse CNS. *The European journal of neuroscience*, *21*(3), 658–668.

Britanova, O., de Juan Romero, C., Cheung, A., Kwan, K. Y., Schwark, M., Gyorgy, A., Vogel, T., Akopov, S., Mitkovski, M., Agoston, D., Sestan, N., Molnár, Z., & Tarabykin, V. (2008). Satb2 is a postmitotic determinant for upper-layer neuron specification in the neocortex. *Neuron*, *57*(3), 378–392.

Budde, H., Schmitt, S., Fitzner, D., Opitz, L., Salinas-Riester, G., & Simons, M. (2010). Control of oligodendroglial cell number by the miR-17-92 cluster. *Development*, *137*(13), 2127–2132.

Bull, D. (2014) Communicating Pictures - A course in imaging and video coding. *Academic Press* 1st Edition.

Bürglin T. R. (2011). A Handbook of Transcription factors: Homeodomain subtypes and functional diversity. *Sub-cellular biochemistry*, *52*, 95–122.

Campbell, K., & Götz, M. (2002). Radial glia: multi-purpose cells for vertebrate brain development. *Trends in neurosciences*, *25*(5), 235–238.

Cárdenas, A., & Borrell, V. (2019). Molecular and cellular evolution of corticogenesis in amniotes. *Cellular and Molecular Life Sciences*, *77*(8):1435-1460.

Cárdenas, A., Villalba, A., de Juan Romero, C., Picó, E., Kyrousi, C., Tzika, A. C., Tessier-Lavigne, M., Ma, L., Drukker, M., Cappello, S., & Borrell, V. (2018). Evolution of Cortical Neurogenesis in Amniotes Controlled by Robo Signaling Levels. *Cell*, *174*(3), 590–606.e21.

Caubit, X., Gubellini, P., Andrieux, J., Roubertoux, P. L., Metwaly, M., Jacq, B., Fatmi, A., Had-Aissouni, L., Kwan, K. Y., Salin, P., Carlier, M., Liedén, A., Rudd, E., Shinawi, M., Vincent-Delorme, C., Cuisset, J. M., Lemaitre, M. P., Abderrehamane, F., Duban, B., Lemaitre, J-F., Woolf, A.S., Bockenhauer, D., Severac, D., Dubois, E., Zhu Y., Sestan, N., Garratt, A.N., Kerkerian-Le Goff, L. & Fasano, L. (2016). TSHZ3 deletion causes an autism syndrome and defects in cortical projection neurons. *Nature Genetics*, *48*(11), 1359–1369

Caviness, V. S., Takahashi, T., Miyama, S., Nowakowski, R. S., & Delalle, I. (1996). Regulation of normal proliferation in the developing cerebrum potential actions of trophic factors. *Experimental Neurology*, *137*(2), 357–366.

Chambers, S. M., Fasano, C. A., Papapetrou, E. P., Tomishima, M., Sadelain, M., & Studer, L. (2009). Highly efficient neural conversion of human ES and iPS cells by dual inhibition of SMAD signaling. *Nature Biotechnology*, *27*(3), 275–280.

Chekulaeva, M., & Filipowicz, W. (2009). Mechanisms of miRNA-mediated post-transcriptional regulation in animal cells. *Current Opinion in Cell Biology*, *21*(3), 452–460.

Chen, B., Schaevitz, L. R., & McConnell, S. K. (2005). Fezl regulates the differentiation and axon targeting of layer 5 subcortical projection neurons in cerebral cortex. *Proceedings of the National Academy of Sciences of the United States of America*, *102*(47), 17184–17189.

Chen, B., Wang, S. S., Hattox, A. M., Rayburn, H., Nelson, S. B., & McConnell, S. K. (2008). The Fezf2-Ctip2 genetic pathway regulates the fate choice of subcortical projection neurons in the developing cerebral cortex. *Proceedings of the National Academy of Sciences of the United States of America*, *105*(32), 11382–11387.

Chen, P. F., Hsiao, J. S., Sirois, C. L., & Chamberlain, S. J. (2016). RBFOX1 and RBFOX2 are dispensable in iPSCs and iPSC-derived neurons and do not contribute to neural-specific paternal UBE3A silencing. *Scientific Reports*, *6*(25368), 1–13.

Chen, Q. Y., Li, J., Sun, H., Wu, F., Zhu, Y., Kluz, T., Jordan, A., DesMarais, T., Zhang, X., Murphy, A., & Costa, M. (2018). Role of miR-31 and SATB2 in arsenic-induced malignant BEAS-2B cell transformation. *Molecular Carcinogenesis*, *57*(8), 968–977.

Chen, Q. Y., Marais, T. Des, & Costa, M. (2019). Deregulation of SATB2 in carcinogenesis with emphasis on miRNA-mediated control. *Carcinogenesis*, *40*(3), 393–402.

Chou, S. J., & O'Leary, D. D. (2013). Role for Lhx2 in corticogenesis through regulation of progenitor differentiation. *Molecular and cellular neurosciences*, *56*, 1–9.

Chui, A., Qiangqiang, Z., & Song-Hai, S. (2020). Oxidative stress regulates progenitor behavior and cortical neurogenesis *Development*, *147*(5).

Cipriani, S., Journiac, N., Nardelli, J., Verney, C., Delezoide, A. L., Guimiot, F., Gressens, P., & Adle-Biassette, H. (2015). Dynamic Expression Patterns of Progenitor and Neuron Layer Markers in the Developing Human Dentate Gyrus and Fimbria. *Cerebral Cortex*, *27*(1), 358–372.

Coolen, M., & Bally-Cuif, L. (2009). MicroRNAs in brain development and physiology. *Current Opinion in Neurobiology*, *19*(5), 461–470.

Das, R. M., & Storey, K. G. (2014). Apical abscission alters cell polarity and dismantles the primary cilium during neurogenesis. *Science*, *343*(6167), 200–204.

De Belle, I., Cai, S., & Kohwi-Shigematsu, T. (1998). The genomic sequences bound to special AT-rich sequence-binding protein 1 (SATB1) in vivo in Jurkat T cells are tightly associated with the nuclear matrix at the bases of the chromatin loops. *Journal of Cell Biology*, *141*(2), 335–348.

De Chevigny, A., Coré, N., Follert, P., Gaudin, M., Barbry, P., Béclin, C., & Cremer, H. (2012). MiR-7a regulation of Pax6 controls spatial origin of forebrain dopaminergic neurons. *Nature Neuroscience*, *15*(8), 1120–1126.

De León Reyes, N. S., Mederos, S., Varela, I., Weiss, L. A., Perea, G., Galazo, M. J., & Nieto, M. (2019). Transient callosal projections of L4 neurons are eliminated for the acquisition of local connectivity. *Nature Communications*, *10*(1), 1–15.

De Pietri Tonelli, D., Pulvers, J. N., Haffner, C., Murchison, E. P., Hannon, G. J., & Huttner, W. B. (2008). miRNAs are essential for survival and differentiation of newborn neurons but not for expansion of neural progenitors during early neurogenesis in the mouse embryonic neocortex. *Development*, *135*(23), 3911–3921.

De Robertis, E. M., & Kuroda, H. (2004). Dorsal-Ventral Patterning and Neural Induction in Xenopus Embryos. *Annual Review of Cell and Developmental Biology*, *20*(1), 285–308.

Dehay, C., Kennedy, H., & Kosik, K. S. (2015). The Outer Subventricular Zone and Primate-Specific Cortical Complexification. *Neuron*, *85*(4), 683–694.

Didiano, D., & Hobert, O. (2008). Molecular architecture of a miRNA-regulated 3'UTR. *RNA*, *14*, 1297–1317.

Dominici, C., Moreno-Bravo, J. A., Puiggros, S. R., Rappeneau, Q., Rama, N., Vieugue, P., Bernet, A., Mehlen, P., & Chédotal, A. (2017). Floor-plate-derived netrin-1 is dispensable for commissural axon guidance. *Nature*, *545*(7654), 350–354.

Durston, A. J., Timmermans, J. P. M., Hage, W. J., Hendriks, H. F. J., De Vries, N. J., Heideveld, M., & Nieuwkoop, P. D. (1989). Retinoic acid causes an anteroposterior transformation in the developing central nervous system. *Nature*, *340*(6229), 140–144.

Eckler, M. J., Larkin, K. A., McKenna, W. L., Katzman, S., Guo, C., Roque, R., Visel, A., Rubenstein, J. L. R., & Chen, B. (2014). Multiple conserved regulatory domains promote Fezf2 expression in the developing cerebral cortex. *Neural Development*, *9*(6).

Eden, E., Navon, R., Steinfeld, I., Lipson, D., & Yakhini, Z. (2009). GOrilla : a tool for discovery and visualization of enriched GO terms in ranked gene lists. *BMC Bioinformatics 10*(48), 1–7.

Eiraku, M., Watanabe, K., Matsuo-Takasaki, M., Kawada, M., Yonemura, S., Matsumura, M., Wataya, T., Nishiyama, A., Muguruma, K., & Sasai, Y. (2008). Self-Organized Formation of Polarized Cortical Tissues from ESCs and Its Active Manipulation by Extrinsic Signals. *Cell Stem Cell*, *3*(5), 519–532.

Eisenberg, E., & Levanon, E. Y. (2013). Human housekeeping genes, revisited. *Trends in Genetics*, *29*(10), 569–574.

Enright, A. J., John, B., Gaul, U., Tuschl, T., Sander, C., & Marks, D. S. (2003). MicroRNA targets in Drosophila. *Genome Biology*, *5*(1), 1-14.

Fame, R. M., MacDonald, J. L., & Macklis, J. D. (2011). Development, specification, and diversity of callosal projection neurons. *Trends in Neurosciences*, *34*(1), 41–50.

Fang, Z., & Rajewsky, N. (2011). The impact of miRNA target sites in coding sequences and in 3′UTRs. *PLoS ONE*, *6*(3), 1–6.

Fietz, S. A., & Huttner, W. B. (2011). Cortical progenitor expansion, self-renewal and neurogenesis-a polarized perspective. *Current opinion in neurobiology*, *21*(1), 23–35.

Fiore, R., Khudayberdiev, S., Christensen, M., Siegel, G., Flavell, S. W., Kim, T. K., Greenberg, M. E., & Schratt, G. (2009). Mef2-mediated transcription of the miR379-410 cluster regulates activity-dependent dendritogenesis by fine-tuning Pumilio2 protein levels. *The EMBO journal*, *28*(6), 697–710.

FitzPatrick, D. R., Carr, I. M., McLaren, L., Leek, J. P., Wightman, P., Williamson, K., Gautier, P., McGill, N., Hayward, C., Firth, H., Markham, A. F., Fantes, J. A., & Bonthron, D. T. (2003). Identification of SATB2 as the cleft palate gene on 2q32-q33. *Human Molecular Genetics*, *12*(19), 2491–2501.

Florio, M., & Huttner, W. B. (2014). Neural progenitors, neurogenesis and the evolution of the neocortex. *Development*, *141*(11), 2182–2194.

Fothergill, T., Donahoo, A. L. S., Douglass, A., Zalucki, O., Yuan, J., Shu, T., Goodhill, G. J., & Richards, L. J. (2014). Netrin-DCC signaling regulates corpus callosum formation through attraction of pioneering axons and by modulating slit2-mediated repulsion. *Cerebral Cortex*, *24*(5), 1138–1151.

Gaidatzis, D., Burger, L., Florescu, M., & Stadler, M. B. (2015). Analysis of intronic and exonic reads in RNA-seq data characterizes transcriptional and post-transcriptional regulation. *Nature Biotechnology*, *33*, 722–729.

Galfrè, S. G., & Morandin, F. (2021). COTAN : Co-expression Table Analysis for scRNA-seq data. *NAR Genomics and Bioinformatics*, *3*(3), 1-11.

Gao, P., Postiglione, M. P., Krieger, T. G., Hernandez, L., Wang, C., Han, Z., Streicher, C., Papusheva, E., Insolera, R., Chugh, K., Kodish, O., Huang, K., Simons, B. D., Luo, L., Hippenmeyer, S., & Shi, S. H. (2014). Deterministic progenitor behavior and unitary production of neurons in the neocortex. *Cell*, *159*(4), 775–788.

García-Moreno, F., López-Mascaraque, L. and De Carlos, J.A. (2007), Origins and migratory routes of murine Cajal-Retzius cells. *J. Comp. Neurol.*, 500: 419-432.

Gaspard, N., Bouschet, T., Herpoel, A., Naeije, G., van den Ameele, J., & Vanderhaeghen, P. (2009). Generation of cortical neurons from mouse embryonic stem cells. *Nature Protocols*, *4*(10), 1454–1463.

Gaspard, N., Bouschet, T., Hourez, R., Dimidschstein, J., Naeije, G., Van Den Ameele, J., Espuny-Camacho, I., Herpoel, A., Passante, L., Schiffmann, S. N., Gaillard, A., & Vanderhaeghen, P. (2008). An intrinsic mechanism of corticogenesis from embryonic stem cells. *Nature*, *455*(7211), 351–357.

Gaspard, N., Gaillard, A., & Vanderhaeghen, P. (2009). Making cortex in a dish: In vitro corticopoiesis from embryonic stem cells. *Cell Cycle*, *8*(16), 2491–2496.

Geschwind, D. H., & Rakic, P. (2013). Cortical evolution: Judge the brain by its cover. *Neuron*, *80*(3), 633–647.

Götz, M., & Huttner, W. B. (2005). The cell biology of neurogenesis. *Nature reviews. Molecular cell biology*, *6*(10), 777–788.

Greig, L. C., Woodworth, M. B., Galazo, M. J., Padmanabhan, H., & Macklis, J. D. (2013). Molecular logic of neocortical projection neuron specification, development and diversity. *Nature Reviews Neuroscience*, *14*(11), 755–769.

Gunhanlar, N., Shpak, G., van der Kroeg, M., Gouty-Colomer, L. A., Munshi, S. T., Lendemeijer, B., Ghazvini, M., Dupont, C., Hoogendijk, W. J. G., Gribnau, J., de Vrij, F. M. S., & Kushner, S. A. (2018). A simplified protocol for differentiation of electrophysiologically mature neuronal networks from human induced pluripotent stem cells. *Molecular Psychiatry*, *23*(5), 1336–1344.

Guo, H., Ingolia, N. T., Weissman, J. S., & Bartel, D. P. (2010). Mammalian microRNAs predominantly act to decrease target mRNA levels. *Nature*, *466*(7308), 835–840.

Guo, Y., Chen, Y., Ito, H., Watanabe, A., Ge, X., Kodama, T., & Aburatani, H. (2006). Identification and characterization of lin-28 homolog B (LIN28B) in human hepatocellular carcinoma. *Gene*, *384*(1–2), 51–61.

Ha, M., Lu, J., Tian, L., Ramachandran, V., Kasschau, K. D., Chapman, E. J., Carrington, J. C., Chen, X., Wang, X. J., & Chen, Z. J. (2009). Small RNAs serve as a genetic buffer against genomic shock in Arabidopsis interspecific hybrids and allopolyploids. *Proceedings of the National Academy of Sciences of the United States of America*, *106*(42), 17835–17840.

Hanashima, C., Li, S. C., Shen, L., Lai, E., & Fishell, G. (2004). Foxg1 suppresses early cortical cell fate. *Science*, *303*(5654), 56–59.

Harb, K., Magrinelli, E., Nicolas, S., Lukianets, N., Frangeul, L., Pietri, M., Sun, T., Sandoz, G., Grammont F, Jabaudon D, Studer, M. & Alfano, C. (2016). Area-specific development of distinct projection neuron subclasses is regulated by postnatal epigenetic modifications. *eLife*, 1–25.

Hatanaka, Y., Kawasaki, T., Abe, T., Shioi, G., Kohno, T., Hattori, M., Sakakibara, A., Kawaguchi, Y., & Hirata, T. (2019). Semaphorin 6A–Plexin A2/A4 Interactions with Radial Glia Regulate Migration Termination of Superficial Layer Cortical Neurons. *iScience*, *21*, 359–374.

Hevner, R. F., Shi, L., Justice, N., Hsueh, Y. P., Sheng, M., Smiga, S., Bulfone, A., Goffinet, A. M., Campagnoni, A. T., & Rubenstein, J. L. R. (2001). Tbr1 regulates differentiation of the preplate and layer 6. *Neuron*, *29*(2), 353–366.

Houart, C., Caneparo, L., Heisenberg, C. P., Barth, K. A., Take-Uchi, M., & Wilson, S. W. (2002). Establishment of the telencephalon during gastrulation by local antagonism of Wnt signaling. *Neuron*, *35*(2), 255–265.

Huang, Y., Song, N., Lan, W., Hu, L., Su, C.J., Ding, Y.Q, Zhang, L. (2013). Expression of Transcription Factor Satb2 in Adult Mouse Brain. *The Anatomical Record. 296*, 452–461.

Inui, M., Martello, G., & Piccolo, S. (2010). MicroRNA control of signal transduction. *Nature Reviews Molecular Cell Biology*, *11*(4), 252–263.

Jiang, G., Cui, Y., Yu, X., Wu, Z., Ding, G., & Cao, L. (2015). miR-211 suppresses hepatocellular carcinoma by downregulating SATB2. *Oncotarget*, *6*(11), 9457–9466.

Kalebic, N., Gilardi, C., Albert, M., Namba, T., Long, K. R., Kostic, M., Langen, B., & Huttner, W. B. (2018). Human-specific ARHGAP11B induces hallmarks of neocortical expansion in developing ferret neocortex. *ELife*, *7*, 1–25.

Kanellopoulou, C., Muljo, S. A., Kung, A. L., Ganesan, S., Drapkin, R., Jenuwein, T., Livingston, D. M., &

Rajewsky, K. (2005). Dicer-deficient mouse embryonic stem cells are defective in differentiation and centromeric silencing. *Genes and Development*, *19*(4), 489–501.

Kang, H. J., Kawasawa, Y., Cheng, F., Zhu, Y., & Sestan, N. (2011). Spatiotemporal transcriptome of the human brain. *Nature*, *478*(7370), 483–489.

Keene, J. D. (2007). RNA regulons: Coordination of post-transcriptional events. *Nature Reviews: Genetics 8*, 533–543.

Kiecker, C., & Niehrs, C. (2001). A morphogen gradient of Wnt/beta-catenin signaling regulates anteroposterior neural patterning in *Xenopus*. *Development*, *128*(21), 4189–4201.

Kobak, D., & Berens, P. (2019). The art of using t-SNE for single-cell transcriptomics. *Nature Communications 10*(5416), 1-14.

Kolb, B. and Wishaw, I.Q. (1990) Fundamentals of Human Neuropsychology. *W. H. Freeman and Company, New York.*

Kosik, K. S., & Nowakowski, T. (2018). Evolution of New miRNAs and Cerebro-Cortical Development. *Annual Review of Neuroscience*, *41*, 119–137.

Kovach, C., Dixit, R., Li, S., Mattar, P., Wilkinson, G., Elsen, G. E., Kurrasch, D. M., Hevner, R. F., & Schuurmans, C. (2013). Neurog2 Simultaneously Activates and Represses Alternative Gene Expression Programs in the Developing Neocortex. *Cerebral Cortex*, *23*, 1884–1900.

Krützfeldt, J., Rajewsky, N., Braich, R., Rajeev, K. G., Tuschl, T., Manoharan, M., & Stoffel, M. (2005). Silencing of microRNAs in vivo with 'antagomiRs'. *Nature*, *438*(7068), 685–689.

Lancaster, M. A., & Knoblich, J. A. (2012). Spindle orientation in mammalian cerebral cortical development. *Current opinion in neurobiology*, *22*(5), 737–746.

Le Dréau, G., & Martí, E. (2012). Dorsal-ventral patterning of the neural tube: A tale of three signals. *Developmental Neurobiology*, *72*, 1471–1481.

Lee, J. S., Yoo, Y., Lim, B. C., Kim, K. J., Choi, M., & Chae, J. H. (2016). SATB2-associated syndrome presenting with Rett-like phenotypes. *Clinical genetics*, *89*(6), 728–732.

Leivonen, S. K., Sahlberg, K. K., Mäkelä, R., Due, E. U., Kallioniemi, O., Børresen-Dale, A. L., & Perälä, M. (2014). High-throughput screens identify microRNAs essential for HER2 positive breast cancer cell growth. *Molecular Oncology*, *8*(1), 93–104.

Leone, D. P., Heavner, W. E., Ferenczi, E. A., Dobreva, G., Huguenard, J. R., Grosschedl, R., & Mcconnell, S. K. (2015). Satb2 Regulates the Differentiation of Both Callosal and Subcerebral Projection Neurons in the Developing Cerebral Cortex. *Cerebral Cortex*, *25*, 3406–3419.

Leone, D. P., Srinivasan, K., Chen, B., Alcamo, E., & McConnell, S. K. (2008). The determination of projection neuron identity in the developing cerebral cortex. *Current Opinion in Neurobiology*, *18*(1), 28–35.

Lewitus, E., Kelava, I., Kalinka, A. T., Tomancak, P., & Huttner, W. B. (2014). An Adaptive Threshold in Mammalian Neocortical Evolution. *PLoS Biology*, *12*(11).

Li, H., Zhu, Y., Morozov, Y. M., Chen, X., Page, S. C., Rannals, M. D., Maher, B. J., & Rakic, P. (2019). Disruption of TCF4 regulatory networks leads to abnormal cortical development and mental disabilities. *Molecular Psychiatry*, *24*(8), 1235–1246.

Lim, L. P., Lau, N. C., Garrett-Engele, P., Grimson, A., Schelter, J. M., Castle, J., Bartel, D. P., Linsley, P. S., & Johnson, J. M. (2005). Microarray analysis shows that some microRNAs downregulate large numbers of-target mRNAs. *Letters to Nature*, *433*(7027), 769–773.

Liu, J., Liu, W., Yang, L., Wu, Q., Zhang, H., Fang, A., Li, L., Xu, X., Sun, L., Zhang, J., Tang, F., & Wang, X. (2017). The Primate-Specific Gene TMEM14B Marks Outer Radial Glia Cells and Promotes Cortical Expansion and Folding. *Cell Stem Cell*, *21*(5), 635-649.

Liu, Y., Bergmann, T., Mori, Y., Vidal, J. M. P., Pihl, M., Vasistha, N. A., Thomsen, P. D., Seemann, S. E., Gorodkin, J., Hyttel, P., Khodosevich, K., Witter, M. P., & Hall, V. J. (2021). Development of the entorhinal cortex occurs via parallel lamination during neurogenesis. *BioRxiv preprint.*

Lodato, S., & Arlotta, P. (2015). Generating Neuronal Diversity in the Mammalian Cerebral Cortex. *Annu Rev Cell Dev Biol*, *31*, 699–720.

Loo, L., Simon, J. M., Zylka, M. J., Xing, L., Mccoy, E. S., Niehaus, J. K., Guo, J., & Anton, E. S. (2019). Single-cell transcriptomic analysis of mouse neocortical development. *Nature Communications*, *10*(134), 1–11.

Luo, L., Yang, F., Ding, J. ji, Yan, D. li, Wang, D. dan, Yang, S. jin, Ding, L., Li, J., Chen, D., Ma, R., Wu, J. zhong, & Tang, J. hai. (2016). MiR-31 inhibits migration and invasion by targeting SATB2 in triple negative breast cancer. *Gene*, *594*(1), 47–58. 7

Lupo, G., Bertacchi, M., Carucci, N., Augusti-Tocco, G., Biagioni, S., & Cremisi, F. (2014). From pluripotency to forebrain patterning: An in vitro journey astride embryonic stem cells. *Cellular and Molecular Life Sciences*, *71*(15), 2917–2930.

Lupo, G., Harris, W. A., Barsacchi, G., & Vignali, R. (2002). Induction and patterning of the telencephalon in Xenopus laevis. *Development*, *129*(23), 5421–5436.

Luzzati, F. (2015). A hypothesis for the evolution of the upper layers of the neocortex through co-option of the olfactory cortex developmental program. *Frontiers in Neuroscience*, *9*:162, 1–12.

Maaten, L. Van Der, & Hinton, G. (2008). Visualizing Data using t-SNE. J*ournal of Machine Learning Research 9*, 2579–2605.

MacFarlane, L.-A., & R. Murphy, P. (2010). MicroRNA: Biogenesis, Function and Role in Cancer. *Current Genomics*, *11*(7), 537–561.

Malatesta, P., Hartfuss, E., & Götz, M. (2000). Isolation of radial glial cells by fluorescent-activated cell sorting reveals a neural lineage. *Development*, *127*(24), 5253–5263.

Manno, G. La, Soldatov, R., Zeisel, A., Braun, E., Hochgerner, H., Petukhov, V., Lidschreiber, K., Kastriti, M. E., Lönnerberg, P., Furlan, A., Fan, J., Borm, L. E., Liu, Z., Bruggen, D. Van, Guo, J., He, X., Barker, R., Sundström, E., Castelo-branco, G., Cramer, P., Adameyko, I. , Linnarsson, S. & Kharchenko P (2018). RNA velocity of single cells. *Nature*. *560*:494-519.

Marranci, A., Aurizio, R. D., Vencken, S., Mero, S., Rizzo, M., Pitto, L., Pellegrini, M., Chiorino, G., Greene, C. M., Poliseno, L. (2019). Systematic evaluation of the microRNAome through miR-CATCHv2.0 identifies positive and negative regulators of BRAF-X1 mRNA. *RNA Biology*. *6286*.

Mcconnell, S. K. (1995). Constructing the Cerebral Cortex : Neurogenesis and Fate Determination. *Neuron. 15*, 761–768.

McConnell, S. K., & Kaznowski, C. E. (1991). Cell cycle dependence of laminar determination in developing neocortex. *Science*, *254*(5029), 282–285.

McLoughlin, H. S., Fineberg, S. K., Ghosh, L. L., Tecedor, L., & Davidson, B. L. (2012). Dicer is require for proliferation, viability, migration and differentiation in corticoneurogenesis. *Neuroscience*, *223*(319), 285–295.

Mishkin, M. & Ungerleider, L.G. (1982). Contribution of striate inputs to the visuospatial functions of pariet-preoccipital cortex in monkeys. *Behavioural Brain Research*, *6*(1), 57-77.

Miyata T, Kawaguchi A, Okano H, Ogawa M. (2001). Asymmetric inheritance of radial glial fibers by cortical neurons. *Neuron*, *31*(5), 727-41.

Murchison, E. P., Stein, P., Xuan, Z., Pan, H., Zhang, M. Q., Schultz, R. M., & Hannon, G. J. (2007). Critical roles for Dicer in the female germline. *Genes and Development*, *21*(6), 682–693.

Murchison, E. P., Partridge J. F., Tam O. H., Cheloufi S., and Hannon G. J. (2005). Characterization of Dicer-deficient murine embryonic stem cells. *PNAS*, *102*(34), 12135–12140.

Muzio, L., Di benedetto, B., Stoykova, A., Boncinelli, E., Gruss, P., & Mallamaci, A. (2002). Emx2 and Pax6 control regionalization of the pre-neuronogenic cortical primordium. *Cerebral Cortex*, *12*(2), 129–139.

Namba, T., Kibe, Y., Funahashi, Y., Nakamuta, S., Takano, T., Ueno, T., Shimada, A., Kozawa, S., Okamoto, M., Shimoda, Y., Oda, K., Wada, Y., Masuda, T., Sakakibara, A., Igarashi, M., Miyata, T., Faivre-Sarrailh, C., Takeuchi, K., & Kaibuchi, K. (2014). Pioneering axons regulate neuronal polarization in the developing cerebral cortex. *Neuron*, *81*(4), 814–829.

Noctor, S. C., Martinez-Cerdeño, V., Ivic, L., & Kriegstein, A. R. (2004). Cortical neurons arise in symmetric and asymmetric division zones and migrate through specific phases. *Nature Neuroscience*, *7*(2), 136–144.

Noctor, S. C., Martínez-Cerdeño, V., & Kriegstein, A. R. (2008). Distinct behaviors of neural stem and progenitor cells underlie cortical neurogenesis. *The Journal of comparative neurology*, *508*(1), 28–44.

Nomura, T., Yamashita, W., Gotoh, H., & Ono, K. (2018). Species-Specific Mechanisms of Neuron Subtype Specification Reveal Evolutionary Plasticity of Amniote Brain Development. *Cell Reports*, *22*(12), 3142–3151.

Nowakowski, T. J., Rani, N., Golkaram, M., Zhou, H. R., Alvarado, B., Huch, K., West, J. A., Leyrat, A., Pollen, A. A., Kriegstein, A. R., Petzold, L. R., & Kosik, K. S. (2018). Regulation of cell-type-specific transcriptomes by microRNA networks during human brain development. *Nature Neuroscience*, *21*(12), 1784–1792.

Okamoto, M., Namba, T., Shinoda, T., Kondo, T., Watanabe, T., Inoue, Y., Takeuchi, K., Enomoto, Y., Ota, K., Oda, K., Wada, Y., Sagou, K., Saito, K., Sakakibara, A., Kawaguchi, A., Nakajima, K., Adachi, T., Fujimori, T., Ueda, M., Hayashi, S., Kaibuchi, K., Miyata, T. (2013). TAG-1-assisted progenitor elongation streamlines nuclear migration to optimize subapical crowding. *Nature Neuroscience*, *16*(11), 1556–1566.

Otani, T., Marchetto, M. C., Gage, F. H., Simons, B. D., & Livesey, F. J. (2016). 2D and 3D Stem Cell Models of Primate Cortical Development Identify Species-Specific Differences in Progenitor Behavior Contributing to Brain Size. *Cell Stem Cell*, *18*(4), 1-14.

Pandolfini, L., Luzi, E., Bressan, D., Ucciferri, N., Bertacchi, M., Brandi, R., Rocchiccioli, S., Onofrio, M. D., & Cremisi, F. (2016). RISC-mediated control of selected chromatin regulators stabilizes ground state pluripotency of mouse embryonic stem cells. *Genome Biology*, *17*:94 1–22.

Paolino, A., Fenlon, L. R., Kozulin, P., Haines, E., & Lim, J. W. C., Richards J.L., Suárez R. (2020). Differential timing of a conserved transcriptional network underlies divergent cortical projection routes across mammalian brain evolution. *PNAS, 117* (19) 10554-10564.

Paşca, S.P., Portmann, T., Voineagu, I., Yazawa, M., Cord, B., Palmer, T. D., Chikahisa, S., Seiji, N., Bernstein, J. A., Hallmayer, J., Geschwind, D. H., Dolmetsch, R. E., Sciences, B., & Angeles, L. (2012). Using iPS cell-derived neurons to uncover cellular phenotypes associated with Timothy Syndrome. *Nat Med*. *17*(12), 1657–1662.

Pramparo, T., Youn, Y. H., Yingling, J., Hirotsune, S., & Wynshaw-Boris, A. (2010). Novel embryonic neuronal migration and proliferation defects in Dcx mutant mice are exacerbated by Lis1 reduction. *Journal of Neuroscience*, *30*(8), 3002–3012.

Purves, D. (2004). NEUROSCIENCE Third Edition. *Sinauer Associates, Inc*.

Rakic, P. (2009). Evolution of the neocortex: A perspective from developmental biology. *Nature Reviews Neuroscience*, *10*(10), 724–735.

Rehfeld, F., Rohde, A. M., Nguyen, D. T. T., & Wulczyn, F. G. (2015). Lin28 and let-7: Ancient milestones on the road from pluripotency to neurogenesis. *Cell and Tissue Research*, *359*(1), 145–160.

Rocha, S.T., Edwards, C. A., Ito, M., Ogata, T., & Ferguson-smith, A. C. (2008). Genomic imprinting at the mammalian Dlk1-Dio3 domain. *Trends in Genetics* 24(6), 306-316.

Rosa, A., & Brivanlou, A. H. (2011). A regulatory circuitry comprised of miR-302 and the transcription factors OCT4 and NR2F2 regulates human embryonic stem cell differentiation. *EMBO Journal*, *30*(2), 237–248.

Rubenstein, J. L. R. (2011). Annual research review: Development of the cerebral cortex: Implications for neurodevelopmental disorders. *Journal of Child Psychology and Psychiatry*, *52*(4), 339–355.

Salomoni, P., & Calegari, F. (2010). Cell cycle control of mammalian neural stem cells: Putting a speed limit on G1. *Trends in Cell Biology*, *20*(5), 233–243.

Smart, I.H. (1973). Proliferative characteristics of the ependymal layer during the early development of the mouse neocortex: a pilot study based on recording the number, location and plane of cleavage of mitotic figures. *J. Anat.* 116, 67-91.

Sasaki, T., Nishihara, H., Hirakawa, M., Fujimura, K., Tanaka, M., Kokubo, N., Kimura-yoshida, C., Matsuo, I., Sumiyama, K., Saitou, N., Shimogori, T., & Okada, N. (2008). Possible involvement of SINEs in mammalian-specific brain formation. *PNAS*, *105*(11), 4220-4225.

Sauer, F.C. (1935). Mitosis in the neural tube. *The Journal of Comparative Medicine. 62,*(2), 377-405.

Scheuermann R.H. & Garrard W.T. (1999). MARs of antigen receptor and co-receptor genes. *Critical Reviews in Eukaryotic gene expression*, 9(3), 295–310.

Sessa, A., Mao, C. an, Hadjantonakis, A. K., Klein, W. H., & Broccoli, V. (2008). Tbr2 Directs Conversion of Radial Glia into Basal Precursors and Guides Neuronal Amplification by Indirect Neurogenesis in the Developing Neocortex. *Neuron*, *60*(1), 56–69.

Sheehan-Rooney, K., Pálinkášová, B., Eberhart, J. K., & Dixon, M. J. (2010). A cross-species analysis of Satb2

expression suggests deep conservation across vertebrate lineages. *Developmental Dynamics*, *239*(12), 3481–3491.

Shimogori, T., Banuchi, V., Ng, H. Y., Strauss, J. B., & Grove, E. A. (2004). Embryonic signaling centers expressing BMP, WNT and FGF proteins interact to pattern the cerebral cortex. *Development*, *131*(22), 5639–5647.

Shinmyo, Y., Terashita, Y., Dinh Duong, T. A., Horiike, T., Kawasumi, M., Hosomichi, K., Tajima, A., & Kawasaki, H. (2017). Folding of the Cerebral Cortex Requires Cdk5 in Upper-Layer Neurons in Gyrencephalic Mammals. *Cell Reports*, *20*(9), 2131–2143.

Shu, P., Wu, C., Ruan, X., Liu, W., Hou, L., Fu, H., Wang, M., Liu, C., Zeng, Y., Chen, P., Yin, B., Yuan, J., Qiang, B., Peng, X., & Zhong, W. (2019). Opposing Gradients of MicroRNA Expression Temporally Pattern Layer Formation in the Developing Neocortex. *Developmental Cell*, *49*(5), 764-785.

Sidman LR & Rakic P. (1973). Neuronal migration, with special reference to developing human brain: A review. *Brain Research*, *62*(1), 1–35.

Smukler, S. R., Runciman, S. B., Xu, S., & Van Der Kooy, D. (2006). Embryonic stem cells assume a primitive neural stem cell fate in the absence of extrinsic influences. *Journal of Cell Biology*, *172*(1), 79–90.

Srinivasan, K., Leone, D. P., Bateson, R. K., Dobreva, G., Kohwi, Y., Kohwi-Shigematsuc T, Grosschedlb R, and McConnell SK. (2012). A network of genetic repression and derepression specifies projection fates in the developing neocortex. *PNAS. 109*(47), 19071-8.

Srivatsa, S., Parthasarathy, S., Britanova, O., Bormuth, I., Donahoo, A. L., Ackerman, S. L., Richards, L. J., & Tarabykin, V. (2014). Unc5C and DCC act downstream of Ctip2 and Satb2 and contribute to corpus callosum formation. *Nature Communications*, *5 (3708)*, 1–15.

Stappert, L., Roese-Koerner, B., & Brüstle, O. (2014). The role of microRNAs in human neural stem cells, neuronal differentiation and subtype specification. *Cell and Tissue Research*, *359*(1), 47–64.

Stavridis, M. P., & Smith, A. G. (2003). Neural differentiation of mouse embryonic stem cells. *Biochemical Society Transactions*, *31*(1), 45–49.

Stiles, J., & Jernigan, T. L. (2010). The basics of brain development. *Neuropsychology Review*, *20*(4), 327–348.

Striedter, G. F., & Beydler, S. (1997). Distribution of radial glia in the developing telencephalon of chicks. *Journal of Comparative Neurology*, *387*(3), 399–420.

Sun, T., & Hevner, R. F. (2014). Growth and folding of the mammalian cerebral cortex: from molecules to malformations. *Nature Reviews Neuroscience 15*(4), 217–232.

Suter, B., Nowakowski, R. S., Bhide, P. G., & Caviness, V. S. (2007). Navigating neocortical neurogenesis and neuronal specification: a positional information system encoded by neurogenetic gradients. *The Journal of neuroscience : the official journal of the Society for Neuroscience*, *27*(40), 10777–10784.

Tarabykin, V., Stoykova, A., Usman, N., & Gruss, P. (2001). Cortical upper layer neurons derive from the subventricular zone as indicated by *Svet1* gene expression. *Development*, *128*(11), 1983–1993.

Tarazona, S., Furió-Tarí, P., Turrà, D., Di Pietro, A., Nueda, M. J., Ferrer, A., & Conesa, A. (2015). Data quality aware analysis of differential expression in RNA-seq with NOISeq R/Bioc package. *Nucleic Acids Research*, *43*(21), 1–15.

Taverna E. & Huttner, W.B. (2010) Neural Progenitor Nuclei IN Motion, *Neuron. 67*(6), 906-914.

Tashiro, K., Teissier, A., Kobayashi, N., Nakanishi, A., Sasaki, T., Yan, K., Tarabykin, V., Vigier, L., Sumiyama, K., Hirakawa, M., Nishihara, H., Pierani, A., & Okada, N. (2011). A mammalian conserved element derived from SINE displays enhancer properties recapitulating Satb2 expression in early-born callosal projection neurons. *PLoS ONE*, *6*(12), 1-14.

Telley, L., Agirman, G., Prados, J., Amberg, N., Fièvre, S., Oberst, P., Bartolini, G., Vitali, I., Cadilhac, C., Hippenmeyer, S., Nguyen, L., Dayer, A., & Jabaudon, D. (2019). Temporal patterning of apical progenitors and their daughter neurons in the developing neocortex. *Science Neurodevelopment*, *364*(547), 1-7.

Terrigno, M., Bertacchi, M., Pandolfini, L., Baumgart, M., Calvello, M., Cellerino, A., Studer, M., & Cremisi, F. (2018). The microRNA miR-21 Is a Mediator of FGF8 Action on Cortical COUP-TFI Translation. *Stem Cell Reports*, *11*(3), 756–769.

The Boulder Committee. (1970). Embryonic vertebrate central nervous system: revised terminology. *The Anatomical record*, *166*(2), 257–261.

Ton, Q. V., & Kathryn Iovine, M. (2012). Semaphorin3d mediates Cx43-dependent phenotypes during fin regeneration. *Developmental Biology*, *366*(2), 195–203.

Tosches, M. A., Yamawaki, T. M., Naumann, R. K., Jacobi, A. A., Tushev, G., & Laurent, G. (2018). Evolution of pallium, hippocampus, and cortical cell types revealed by single-cell transcriptomics in reptiles. *Science Neurodevelopment*, *360*(6391), 881–888.

Tosches, M. A. & Laurent G (2019) Evolution of neuronal identity in the cerebral cortex. *Current Opinion in Neurobiology*, *56*, 199-208

Tropepe, V., Hitoshi, S., Sirard, C., Mak, T. W., Rossant, J., & Van Der Kooy, D. (2001). Direct neural fate specification from embryonic stem cells: A primitive mammalian neural stem cell stage acquired through a default mechanism. *Neuron*, *30*(1), 65–78.

Van den Ameele, J., Tiberi, L., Vanderhaeghen, P., & Espuny-Camacho, I. (2014). Thinking out of the dish: What to learn about cortical development using pluripotent stem cells. *Trends in Neurosciences*, *37*(6), 334–342.

Visvanathan, J., Lee, S., Lee, B., Lee, J. W., & Lee, S. K. (2007). The microRNA miR-124 antagonizes the anti-neural REST/SCP1 pathway during embryonic CNS development. *Genes and Development*, *21*(7), 744–749.

Watanabe, K., Kamiya, D., Nishiyama, A., Katayama, T., Nozaki, S., Kawasaki, H., Watanabe, Y., Mizuseki, K., & Sasai, Y. (2005). Directed differentiation of telencephalic precursors from embryonic stem cells. *Nature Neuroscience*, *8*(3), 288–296.

Wilsch-Bräuninger, M., Peters, J., Paridaen, J. T., & Huttner, W. B. (2012). Basolateral rather than apical primary cilia on neuroepithelial cells committed to delamination. *Development*, *139*(1), 95–105.

Wilson, S. W., & Rubenstein, J. L. R. (2000). Induction and dorsoventral patterning of the telencephalon. *Neuron*, *28*(3), 641–651.

Xu, L., Du, B., Lu, Q. J., Fan, X. W., Tang, K., Yang, L., & Liao, W. L. (2018). miR-541 suppresses proliferation and invasion of squamous cell lung carcinoma cell lines via directly targeting high-mobility group AT-hook 2. *Cancer Medicine*, *7*(6), 2581–2591.

Xu, N., Papagiannakopoulos, T., Pan, G., Thomson, J. A., & Kosik, K. S. (2009). MicroRNA-145 Regulates OCT4, SOX2, and KLF4 and Represses Pluripotency in Human Embryonic Stem Cells. *Cell*, *137*(4), 647–658.

Yamagishi, S., Hampel, F., Hata, K., Toro, D., Schwark, M., Kvachnina, E., Bastmeyer, M., Yamashita, T., & Tarabykin, V. (2011). FLRT2 and FLRT3 act as repulsive guidance cues for Unc5-positive neurons. *The EMBO Journal*. *30*(14), 2920–2933.

Yang, C., Sun, L., Zhang, L., Zhou, L., Niu, D., Cao, W., Li, Z., Huang, X., Kang, Q., Jia, L., Platik, M., Liu, X., Lai, J., & Cao, D. (2018). SATB2 Shows Different Profiles Between Appendiceal Adenocarcinomas Ex Goblet Cell Carcinoids and Appendiceal/Colorectal Conventional Adenocarcinomas: An Immunohistochemical Study With Comparison to CDX2. *Gastroenterology Research*, *11*(3), 221–230.

Yang, M. H., Yu, J., Chen, N., Wang, X. Y., Liu, X. Y., Wang, S., & Ding, Y. Q. (2013). Elevated microRNA-31 expression regulates colorectal cancer progression by repressing its target gene SATB2. *PLoS ONE*, *8*(12), 1–14.

Yang, T., Huang, H., Shao, Q., Yee, S., Majumder, T. & Liu, G. (2018). miR-92 Suppresses Robo1 Translation to Modulate Slit Sensitivity in Commissural Axon Guidance. *Cell Reports*, *24*(10), 2694-2708.

Yang, W. J., Yang, D. D., Na, S., Sandusky, G. E., Zhang, Q., & Zhao, G. (2005). Dicer is required for embryonic angiogenesis during mouse development. *Journal of Biological Chemistry*, *280*(10), 9330–9335.

Yao, J., Mu, Y., & Gage, F. H. (2012). Neural stem cells: Mechanisms and modeling. *Protein and Cell*, *3*(4), 251–261.

Yoo, A. S., Staahl, B. T., Chen, L., & Crabtree, G. R. (2009). MicroRNA-mediated switching of chromatin-remodelling complexes in neural development. *Nature*, 460 (642-646)). *Nature*, *460*, 642-646.

Yoo, A. S., Sun, A. X., Li, L., Shcheglovitov, A., Portmann, T., Li, Y., Lee-Messer, C., Dolmetsch, R. E., Tsien, R. W., & Crabtree, G. R. (2011). MicroRNA-mediated conversion of human fibroblasts to neurons. *Nature*, *476*(7359), 228–231.

Yuzwa, S. A., Borrett, M. J., Innes, B. T., Kaplan, D. R., Voronova, A., Ketela, T., Kaplan, D. R., Bader, G. D. & Miller, F. D. (2017). Developmental Emergence of Adult Neural Stem Cells as Revealed by Single-Cell Transcriptional Profiling. *CellReports*, *21*(13), 3970–3986.

Zhang, Q., Huang, Y., Zhang, L., Ding, Y. Q., & Song, N. N. (2019). Loss of satb2 in the cortex and hippocampus leads to abnormal behaviors in mice. *Frontiers in Molecular Neuroscience*, *12*(33), 1–12.

Zhang, Y., Fan, M., Zhang, X., Huang, F., Wu, K., Zhang, J., Liu, J., Huang, Z., Luo, H., Tao, L., & Zhang, H. (2014). Cellular microRNAs up-regulate transcription via interaction with promoter TATA-box motifs. *Rna*, *20*(12), 1878–1889.

Zhang, Z., Zheng, F., You, Y., Ma, Y., Lu, T., Yue, W., & Zhang, D. (2016). Growth arrest specific gene 7 is associated with schizophrenia and regulates neuronal migration and morphogenesis. *Molecular Brain*, *9*(54), 1–13.

Zhao, C., Sun, G. Q., Li, S., Lang, M. F., Yang, S., Li, W., & Shi, Y. (2010). MicroRNA let-7b regulates neural stem cell proliferation and differentiation by targeting nuclear receptor TLX signaling. *Proceedings of the National Academy of Sciences of the United States of America*, *107*(5), 1876–1881.